Large Eddy Simulation of Hydrogen Sonic Jet

Mohammadamin Afroosheh

A Thesis

in

the Department

of

Mechanical and Industrial Engineering

Presented in Partial Fulfillment of the Requirements
for the Degree of Master of Applied Science (Mechanical Engineering) at

Concordia University

Montreal, Quebec, Canada

February 2014

CONCORDIA UNIVERSITY

School of Graduate Studies

This is to certify that the thesis prepared

By: **Mohammadamin Afroosheh**

Entitled: **Large Eddy Simulation of Hydrogen Sonic Jet**

and submitted in partial fulfillment of the requirements for the degree of

MASTER OF APPLIED SCIENCE (Mechanical Engineering)

complies with the regulations of the University and meets the accepted standards with respect to originality and quality.

Signed by the final examining committee:

Dr. Onur Kuzgunkaya	*Chair*
Dr. S. Samuel Li	*Examiner*
Dr. Ali Dolatabadi	*Examiner*
Dr. Marius Paraschivoiu	*Supervisor*

Approved by _____
Chair of Department or Graduate Program Director

mm/dd/yy _____
Dean of Faculty

ABSTRACT

LARGE EDDY SIMULATION OF HYDROGEN SONIC JET

Mohammadamin Afroosheh

This dissertation is investigating the turbulence behavior of highly under expanded hydrogen jet based on a 3D Navier-Stokes parallel solver and an extra transport equation for the hydrogen concentration. The solver uses an implicit conservative scheme on unstructured tetrahedral. The discretization exploits finite volumes and finite element with a second order of accurate flux calculation and time discretization. This work presents the extension of the code to simulate hydrogen jets based on Large Eddy Simulation (LES) model for turbulence while considering the real gas behavior. The developed code is equipped with a dynamic wiggle detector to reduce the contribution of the upwinding part in the flux calculation because upwind methodology adds undesired artificial viscosity to the solution.

For validation, the developed code is used to simulate a subsonic hydrogen jet. Considering similar studies among literature, good agreement is observed. Afterward, this tool is employed to numerically investigate a 70 MPa hydrogen jet release into ambient air. The turbulence effects in the principal and lateral jet direction are studied. During these simulations, the performance and stability of the developed numerical tool for high pressure ratio is reported.

ACKNOWLEDGMENTS

I wish to express my sincere gratitude to my supervisor *Dr. Marius Paraschivoiu* for all his support, patience and valuable advice throughout this research and also my friend, *Matin Komeili* for all his faithful aide.

Table of Contents

List of Figures

List of Tables

List of Symbols

C	Concentration
C_p	Constant pressure specific heat capacity
C_v	Constant volume specific heat capacity
C_s	Smagorinsky constant
D	Diameter of the release area
D_f	Diffusion coefficient
e	Total specific energy
F^{conv}	Convective flux
F^{diff}	Diffusive flux
G	Filter function
h	Total specific enthalpy
I	Identity matrix
J	Diffusion flux
P	Pressure
Pr	Prandtl number
$\mathrm{Pr_t}$	Turbulence Prandtl number
Q	Subgrid scale heat flux
R	Specific ideal gas constant
Re	Reynolds number
S	Rate-of-strain tensor
T	Temperature
t	Time
v	Velocity
X	Position vector
x	x-direction of Cartesian coordinate
y	y-direction of Cartesian coordinate
z	z-direction of Cartesian coordinate
β	Parameters to adjust the gradients in MUSCL scheme
γ	Parameters to adjust the upwinding in MUSCL scheme
γ_g	Specific heat ratio
Δ	Filter width
Δt	Time step
Δx	x-direction mesh size
Δy	y-direction mesh size
Δz	z-direction mesh size
δ	Partial derivative operator
δ_s	Viscous sub-layer thickness
ε	Intensity of the local wiggle
ζ	Piecewise linear finite element basis function
η	Characteristic test function

μ	Molecular viscosity coefficient
ρ	Density
σ	Molecular viscous stress tensor
τ	Subgrid scale stress tensor
ϕ	Conservative variables
ψ	Test function
$\vec{\nabla}$	Gradient vector operator
$\forall$	Volume

Subscripts

-	Spatially filtered quantity
~	Spatially Favre-filtered quantity
*	Non-dimensional quantity
$\rightarrow$	Vector quantity
T	Transpose

Abbreviations

CFD	Computational Fluid Dynamics
CFL	Courant Friedrichs Lewy
CNG	Compressed Natural Gas
DNS	Direct Numerical Simulation
GMRES	Generalized Minimal Residual
ILES	Implicit Large Eddy Simulations
LES	Large Eddy Simulations
MPI	Message Passing Interface
MUSCL	Monotone Upwind Scheme for Conservation Laws
PIV	Particle Image Velocimetry
RANS	Reynolds Averaged Navier-Stokes
RNG	Re-Normalisation Group
SGS	Sub-Grid Scale

Chapter 1

INTRODUCTION

1.1 Motivation

Fossil fuel is a key energy resource for industries. Indiscriminate use of this valuable natural resource in recent decays causes environmental pollution and rapid diminution of this resource. Combustion products of fossil fuels lead to greenhouses gas that have destructive effects on the environment. Enforcement of international treaties like Kyoto protocol shows the depth of this disaster. On the other hand, this fuel is produced over many years and their quick formation is close to impossible. These two issues advocate the use a clean and renewable energy replacement.

One of the best options for alternative fuel is hydrogen, which is a clean and available gas leading to a single combustion product which is water vapour. Hydrogen can be produced in different ways: from costly methods like electrolysis of water to more affordable ways like decomposition of natural gas. Today, the most economical way to

produce hydrogen is produced from natural gas. Moreover, hydrogen has some unique features that make it a good candidate for replacing fossil fuels. It can be ignited with a small amount of energy and it is combustible in a wide range of concentration.

Besides these positive sides, replacing hydrogen is facing a serious problem. In comparison with other gas fuels like CNG, hydrogen has a small energy per volume; hence, for typical applications such as automobile fuel, huge volume of hydrogen is required. As an example, in a typical cylinder, pressurized at 20.78 MPa, feeling with hydrogen or CNG the energy content are equivalent to 1.87 or 9.44 of gasoline, respectively [1]. A common way to overcome this problem is by storing hydrogen gas in higher pressure reservoirs. This method is more common for the automobile industry. In particular, Honda FCX (2006 FCX concept) has a tank with capacity up to 156.6 litres of hydrogen at a pressure of 350 atmospheres [2] and BMW hydrogen 7 has a 170 litre cylinder that can store compressed hydrogen at 700 bar [3].

1.2 Pressurized Jet Structure

Releasing hydrogen in air can cause a combustible cloud that can be detonative if the hydrogen concentration reaches 4-77% [4]. Fig (1.1) illustrates a simulation of high pressure hydrogen jet in the first microseconds of release into atmospheric environment. When high pressure hydrogen releases to an atmospheric environment, due to huge pressure ratio between the reservoir and the atmosphere, the flow in the exit tube reaches a sonic condition and is chocked. In this case, the flowrate will be constant. The front of

the jet propagates at a supersonic speed and a shock wave is formed. This shock wave will propagate in the atmospheric environment, ahead of the hydrogen jet, and will compress the air. This moving shock is known as the lead shock. The compressed air, which was affected by lead shock, will increase to a very high temperature. The temperature decreases across the interface in the hydrogen cloud. Behind this region, a strong shock wave is located that is known as the Mach disk. Again behind this expansion, in the supersonic regime, the temperature will be less. In lateral direction, there will be more diffusion in

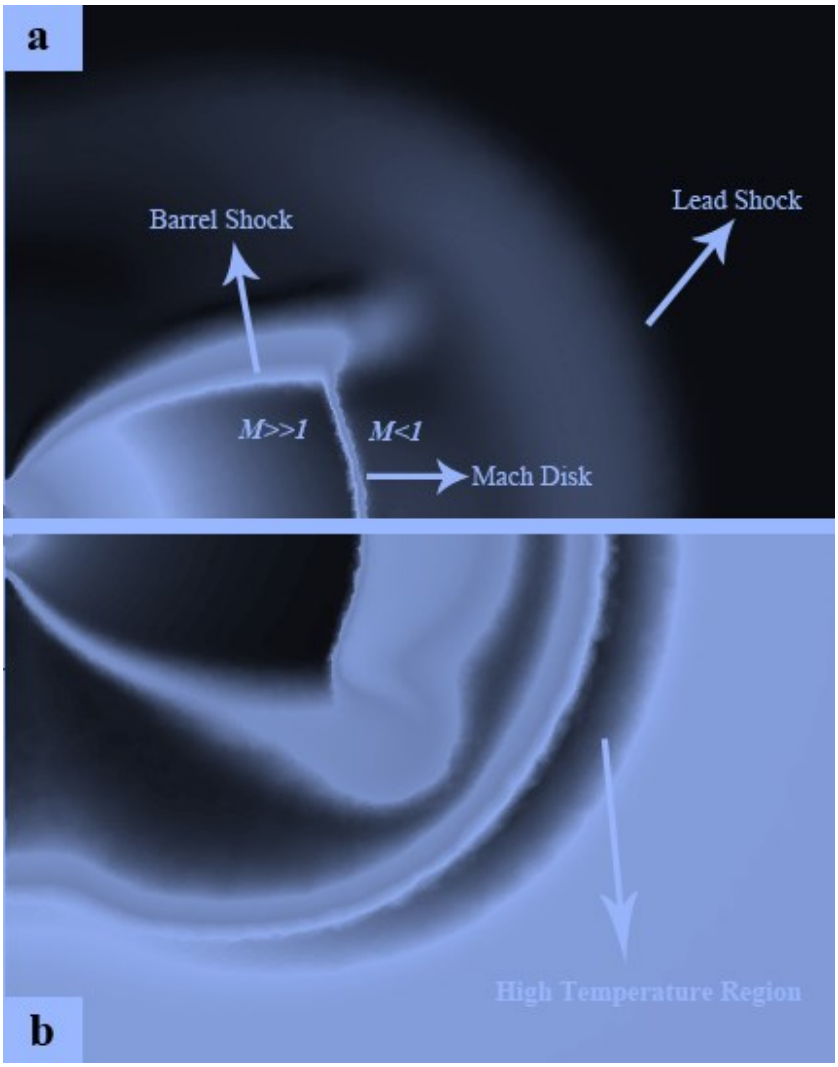

Fig (1. 1): High pressure jet structure

a) Mach number
b) temperature contours

comparison to principal direction. A barrel shock is formed there which reduced the temperature.

As it was mentioned before, the hydrogen cloud is very detonable within a wide range of hydrogen concentrations. Reviewing Hydrogen Accidental Database declare that about 60% of accidental hydrogen released ignited for no apparent reasons [5]. The high temperature caused by the release hydrogen jet may lead to spontaneous. In the literatures, the diffusion ignition is known as a spontaneous ignition, which was first proposed by Wolanski and Wojciki [6]. Therefore, there are some concerns about high pressure storage that can lead to this under-expanded hydrogen jet.

Many researches have studied the behaviour of pressurized hydrogen after its sudden release. These researches can be divided into two major groups: laboratory experiments and numerical simulations. Although laboratory experiments bring invaluable information, it is difficult and expensive to explore all interesting scenarios with this approach. Hence, Computational Fluid Dynamics (CFD) is well known as a key tool for this type of work. Nevertheless, it is important to understand the accuracy and the limitation of CFD for simulation hydrogen release.

1.3 Numerical Studies

Rapid development in computers abilities boost the capabilities of computer aided engineering based on Computational Fluid Dynamics (CFD) to address more sophisticated

engineering problems. Employing CFD has undeniable advantages. By way of illustration, CFD can provide detailed view of the field with very complex geometry which is not affordable in experiments. Beside all advantages, CFD has limitations. Numerical simulations always approximate the physics, either by approximations in the numerical methods, simplifying the problem or models in the equations. In hydrogen jet problems, some simplifications are applied to ease the work. These simplifications are generally negligible and have a very small influence on the final solution. But some simplifications like assuming hydrogen as an ideal gas lead to inaccurate results for high pressure ratios, which was proved before by Khaksarfard et al. [7]. One common assumption is modeling the flow as an inviscid one in the near field of release. For the near field zone of release a high pressure jet, because of very high speeds of the flow, this assumption is acceptable. Away from exit area, the viscous effects appear and this assumption is not trustable any more. To simulate the viscosity, which leads to turbulent flows, additional modelling of turbulence with methods such as RANS, DNS, ILES and LES is needed. Among them LES seems to be very promising as it provided the best combination between accuracy and computational cost.

In LES, the kinetic energy spectrum is divided into a resolved part which contains large eddies, and an unresolved part which contains a model of the remaining eddies. It is assumed that the large eddies are conducting momentum, energy and scalars in the flow. Hence, the main idea would be to solve large scale eddies in the flow and model the small scales.

Large eddies are subjected to history and non-equilibrium effects, and strongly contingent on geometry and boundary conditions, while, small eddies are less flow depended which makes their modeling easier [8]. Theoretically, since LES can solve more sophisticated features of turbulent flow, and also, it solves the most energetic eddies, it is computationally a good compromise between the physics and the computation cost. Furthermore, since there is an energy cascade for small scales eddies from solving large eddies, LES is expected to be quite accurate for free shear flows like jet problem [8].

1.4 Literature Review

There is a variety of previous studies about hydrogen jet in the literature based on analytical, experimental and computational studies. Although experiments in this matter are expensive, a limited number of experimental studies have been undertaken, including the experiments by Shirvill et al. [9]. They have done some experiments with jet of 13 MPa of hydrogen from a 3 mm diameter circular orifice. Similarly, Ganci et al. [10] made some experimental studies of releasing 1 MPa hydrogen jet from 11 mm orifice in a pipeline. They studied the wind direction on the cloud shaping and also compare with CFD modeling where a good agreement was reported. Merilo et al. [11] did an experimental study around hydrogen release in an ordinary one-car garage. The garage had a size of 2.72 m high, 3.64 m wide, and 6.10 m long and they tested with natural and mechanical ventilation. As a part of their test, a car was parked inside the garage to capture blast effects. In their test, the peak pressure captured by sensors is just about 30 kPa. Addressing many of the challenges of studying supersonic hydrogen jets, Faris and Byer [12] and Dillman et al. [13] did such

studies. Their experiments provided insight about supersonic jet flows. They used interferometric measurements and tomography to measure supersonic free jet flow properties. Note that most of the work was at low pressure.

High pressure jet release is an interesting subject with two main objectives; understanding near exit flow behavior and its effect on spontaneous ignition and hydrogen cloud modeling and dispersion. Bragin and Molkov [14] modeled hydrogen release from a 93.7 bar hydrogen reservoir with LES. They assumed a tube with a non-inertial rupture disc separating the two different zones. The same method that was used by Dryer et al. [15], Mogi et al. [16] and Golub et al. [17] to initially separate the pressurized hydrogen and air in their experiments was modeled. The problem was simulated with FLUENT 6.3.26 and they considered a detailed 21-step chemical reaction mechanism of hydrogen combustion in air. They concluded that the initial jet formation stage is a weighty factor for formation of final jet flame. Their comparison between the LES model and experimental data showed that LES can be used for pressure release problems. Similarly, Wen et al. [18], used implicit large eddy simulation (ILES) approach with the 5th-order weighted essentially non-oscillatory (WENO) scheme to study the release of hydrogen from instrumental line. They mostly focused on rupture time of rupture disc and spontaneous ignition. They modeled hydrogen with 50, 100 and 150 bar and concluded that the rupture process generate reflected shock waves that cause turbulent mixing in the contact area. They found that the initial flame forms inside the tube which does not survive, except at two locations: in front of under-expanded jet and in the recirculation zone near exit. Xu et al. [19] performed the same study. They simulated spontaneous ignition of pressurized hydrogen release by assuming hydrogen at 40, 70 and 100 bar from a tube of

1 cm of diameter. Their study showed that with sufficient length of tube and proper pressure ratio, spontaneous ignition of hydrogen through molecular diffusion occurs inside the tube. They mentioned that turbulence plays an important role for hydrogen-air mixing in contact surface and led the initial laminar flame to transit into a stable turbulent flame. In their follow-up work, Xu et al. [5] declared that turbulence diffusion at the lateral surface is important in the mixing process. They concentrated on spontaneous ignition of sudden released hydrogen jet from 1-cm-diameter orifice with maximum 250 bar of pressure, using multi-component mixture of ideal gases approach to calculate molecular transportations. In this study it was confirmed that turbulent diffusion evolves initially from a laminar flame to a final turbulent one, although low local temperature does not permit formation of any combustion. The flame thickness was very thin initially in their simulation and it extends to downstream. It should be emphasized that in all these studies the pressure ratio considered did not exceed 300 while, as it was mentioned earlier, cars with 700 bar pressurized tank (pressure ratio of 700) are becoming the norm.

For very high pressure released jet the inviscid flow assumption is almost always used while considering turbulence behaviour of the jet is examined for lower pressuers. Velikorodny and Kudriakov [20] tried to simulate realise of 30 bar pressurized helium in air with LES model. They also did the simulation with one component, i.e. air in air jet. Ideal gas modeling was assumed in this study while 30-bar was considered to be insufficient for real gas effects. Their simulations predict the position and diameter of the Mach disk and characteristics of subsonic and potential cores in acceptance agreement with experimental data. Rona and Zhang [21] simulated a jet flow with Mach number of 2 considering k-ω turbulence model. They showed the effect of shear layer instabilities on

formation of shock wave. They concluded that unsteady shocks and bow shock appears within the core of the jet. Péneau et al. [22] simulated the release of pressurized hydrogen, as an ideal gas in atmosphere with pressure ratio of about 42, employing FLUENT commercial code. Considering hydrogen in hydrogen and hydrogen in air jets, they showed that in H_2-in-air jet, a protuberance appears in the shock wave. Also, the flow features such as dynamics and stability of the jet is affected by vortex generation in early time of release. Coaxial jet of helium and air was studied by Culter et al. [23] considering the k-ω turbulence model. The supersonic flow (M=1.8) in their simulation was modeled by one-third MUSCL method and second order central viscous fluxes. While there was some deviation from their simulation and experimental data, a correction was done by adding lateral diffusion of turbulent kinetic energy. Zbikowski et al. [24] applied LES turbulence model with renormalization group (RNG) model for subgrid scale (SGS) to simulate a 2D jet of hydrogen. Their results were verified by Zel'dovichvon Neumann-Doring (ZND) theory and showed the ability of applied numerical method in small cell size for modeling this phenomena.

Employing barriers is one the most common way to reduce damages of jet flames. Houf et al. [25] reported doing a set of numerical simulation and experiments in this case to provide a guide of configuration and position of vertical barriers with 3D RANS CFD Code. They choose RNG k-ε turbulence model for their turbulence simulation using 20% inlet turbulence intensity, considering hydrogen as an ideal gas. First order upwind differencing scheme was employed for discretizing convection terms. They simulated both compressible and incompressible release of hydrogen in air. Their free jet results constants in good agreement (within 5%) with experimental data with this set up. Comparably, high

pressure hydrogen jet flames of bonfire test were simulated in Zheng et al. [26]. They assumed firing test of a 41.3 MPa pressurized composite storage tank and model it with a 3D numerical method. Their simulation is based on the species transfer model and they use k-ω turbulence model. Their study showed that the barrier walls can greatly reduce the damage of flame to surrounding and a 45 degree barrier has better protection than 60 or 90 degree one. They validated their numerical results with experimental results of Sandia National Laboratories [27].

Considering safety concerns on labs motivate Heitsch et al. [28] to do a study to predict the distribution of hydrogen cloud which released in a laboratory. They assumed two different scenarios in their work; firstly, leaks from a constant pressure pipeline and secondly, release when the pressure inside the vessel drops gradually. ANSYS CFX version 10 was applied in this study and hydrogen was assumed to be an ideal gas while the maximum pressure did not reached more than 20 MPa. Since the flow had supersonic character, SST (k–ù shear stress transport) turbulence model with standard parameters was selected. Venetsanos et al [29] considered more possible scenario of safety issues in their simulations. They considered a sudden release of hydrogen and natural gas from a gaseous system which was typically installed in city busses. In their simulations, hydrogen was stored at a pressure of 70 MPa and natural gas had 20 MPa. They considered real gas behaviour while Fanno flow was assumed.

Meantime, some researches study the buoyance diffusion of hydrogen release. Vudumu and Koylu [30] modeled an unsteady hydrogen flow in the absence of momentum forces. A simple vertical cylinder was considered to investigate the mixing pattern of flow

for a short time. They used FLUENT 6.3 for their work and they assume laminar incompressible flow analysis. Applying second order implicit scheme with a segregated solver which is suitable for low speed incompressible flows, it was concluded that for closed top containers the propagation speed of hydrogen in axial direction is two time faster than for an open top configuration. Similarly, El-Amin and Kanayama [31] analysed the far region of hydrogen jet, near the top wall by using boundary layer theory.

As noted earlier, inviscid modeling of high pressure hydrogen release is found in the literature. Radulescu and Law [32] did a comprehensive study about initial transient of highly under expanded jet. They considered pressure ratio up to 700. This study delivered good details about the formation of shock wave in sonic jet flow. Liu et al. [33] simulated the flow of up to 70 MPa while Radulescu et al. [32] simulated a 100 MPa jet. Most of these studies used asymmetrical condition which does not have capabilities for turbulence flow. Han and Chang [34] simulated a 2D release of up to 400-bar hydrogen jet into air applying k-ε model of turbulence and ignored effect of buoyancy forces while using FLUENT commercial code. They validated their simulation with experimental results and good agreement was reported.

As mentioned above, many researchers like, Péneau et al. [22] employed ideal gas law in their simulation. They simulated release from a 10 MPa tank by using FLUENT. The ideal gas assumption with such pressure ratio provides acceptable results. Mohamed et al. [35] and Khaksarfard et al. [7] showed that for pressures higher than 10 MPa the real gas model is mandatory. They compared Beattie-Bridgeman and Abel-Noble equation of states and recommend Abel-Noble equation of state since Beattie-Bridgeman cause

instability in simulation. Similarly, Abel-Noble equation of state was employed in a Cheng et al [36] study. They concluded that for a 400 bar released pressure, in first 10 sec the mass flow rate is 30% more for ideal gas in comparison with real gas assumption.

In summary, although there are a large number of different studies for under-expanded jets, only a few of them can handle very high pressure ratio jets, i.e. pressure ratio of 700 which will be common in the automotive industry for hydrogen compressed reservoirs. Note that many commercial codes like FLUENT and ANSYS CFX could not handle this high pressures. In addition, all studies based on the LES turbulent simulation of hydrogen jet consider low pressure ratios. The lack of high pressure turbulent jet simulations encouraged me to extend an in-house code and to perform the first LES study with such pressure ratio.

Regarding the numerical methods, upwind method add some artificial dissipation to the applied numerical method, it is more numerically stable in comparison to central method. Doubtless this artificial term reduce the accuracy of the results. Some researchers reduce this numerical error while keep the simulation stable. Andersson et al. [37] simulated a compressible jet by applying a 3^{rd} order upwinding method. They reduced the upwinding term by factor of 1/8 and guaranteed stability.

The 2^{nd} order Roe-MUSCL method ($\beta\gamma$ scheme) is the most common method for calculating fluxes. In this method, the upwinding term can be adjusted by a ratio factor (γ) which is multiplied to this part while a coefficient (β) is employed to estimate the control volume boundaries' values. Different values of these two factors can bring different dissipative and dispersive errors. Indubitably randomness is inseparable part of a turbulent

flow and a major part of turbulent energy is coming from random motion. Furthermore, central scheme could generate random fluctuations when the grid resolution is not too high, like what is using in the LES simulation. Hence, exchanging from upwind to central scheme by reducing γ, improves the turbulent simulation with more randomness. The goal is to use the lowest possible contribution of upwinding term to minimize the dissipative error while maintaining stability. The basic idea is to control this parameter based on the simulation such as a dynamics method which is based on a wiggle detection technics. Ciardi et al [38] presented a new method to adjust the contribution of upwinding term by detecting wiggles along three consecutive edges which are not collinear necessarily. Although in their method there was no need for several simulations to optimise the contribution coefficient of upwinding term, the energy captured in smallest scales were damped. Tajallipour [39] introduced a self-adapting upwinding based on wiggle detection method. This method which is compatible for Roe-MUSCL scheme, reduce the numerical dissipation of low order flux calculations. In this method, if the sign of a primitive variable gradient changes twice on an arbitrary edge, a wiggle is presumed to be present on that edge and the scheme should get closer to upwind method to have more stable scheme. There is a limit to allow some wiggles to exist. In this study, this method is employed to have better understanding about turbulence in the flow.

1.5 Objective

As it was mentioned previously, the lack of investigation based on LES for large pressure ratios (i.e. pressure ratio of 700) is the main motivation of this study. The objective of this work is to develop an in-house code to investigate the behaviour of real gas high pressure hydrogen jet from sudden release by considering turbulence facts. The specific objectives are:

1. A 3D in-house code using unstructured mesh and LES is extended to model hydrogen into air jet.
2. Validate the new code with results in the literature.
3. To study the effect of turbulence on the near exit turbulent jet in the first micro seconds at high reservoir pressures.
4. Compare with the inviscid simulations.

After developing the code, validation of the code will be considered by simulating the same test case as Chernyavsky et al. [40]. In chapter 4, the difference in the jet structure between turbulent and inviscid simulation will be discussed.

Chapter 2

GOVERNING EQUATIONS and NUMERICAL METHOD

The applied numerical method in this dissertation is a mixed finite volume – finite element method. For the temporal term, a second order implicit scheme is applied. Convective fluxes are discretized with the 2nd order Roe-MUSCL ($\beta\gamma$ scheme) while a 2nd order finite element method is used for diffusive fluxes. Subgrid scale terms are modeled by the Smagorinsky model. The Iterative GMRES solver is used for solving system of equations. The MPI parallel programming is employed to parallelize the simulation.

2.1 Governing Equations

For flow simulation a compressible medium, the equation governing conservation of mass, momentum and energy must be solved. These equations should be filtered for turbulence modeling. Filtering an arbitrary function like f is defined as a convolution integral:

$$\bar{f}(\vec{x},t) = \iiint G\,(\vec{x}-\xi,\Delta) f\left(\vec{\xi},t\right) d^3\xi \tag{2.1}$$

Which Δ is filter width, associated with mesh size as $\Delta = (\Delta x \Delta y \Delta z)^{1/3}$. In addition to velocity and pressure fluctuations, density and temperature fluctuations must take into account for compressible flow. Hence, instead of time averaging, Favre averaging operation is employed:

$$\tilde{f}(\vec{x},t) = \frac{\overline{\rho f}}{\bar{\rho}} \tag{2.2}$$

This filtering decomposes the various flow properties in terms of convectional mean and fluctuating part. Applying this averaging operation, Favre averaged mean conservation equations are derived as [22], [39] and [40]:

$$\frac{\partial \bar{\rho}}{\partial t} + \vec{\nabla}.\left(\bar{\rho}\vec{\tilde{v}}\right) = 0 \tag{2.3.1}$$

$$\frac{\partial \bar{\rho}\vec{\tilde{v}}}{\partial t} + \vec{\nabla}.\left(\bar{\rho}\vec{\tilde{v}}\vec{\tilde{v}}\right) = -\vec{\nabla}\bar{P} + \vec{\nabla}.(\vec{\tau} + \vec{\tilde{\sigma}}) \tag{2.3.2}$$

$$\frac{\partial \bar{\rho}\tilde{e}}{\partial t} + \vec{\nabla}.\left((\bar{\rho}\tilde{e} + \bar{P})\vec{\tilde{v}}\right) = \vec{\nabla}.\left(\vec{Q} + \frac{\mu\, C_p}{\mathrm{Pr}}\vec{\nabla}\bar{T} - \bar{\rho}\sum_j \bar{h}_j \overrightarrow{J_j} \;+ \left(\vec{\tau} + \vec{\tilde{\sigma}}\right).\vec{\tilde{v}}\right) \tag{2.3.3}$$

Using this notation, $\tilde{e}$ represents filtered total specific energy which is the summation of internal energy and kinetic energy.

$$\tilde{e} = \tilde{\imath} + \frac{1}{2}\left(\vec{\tilde{v}}.\vec{\tilde{v}}\right) \tag{2.4}$$

Also, $\bar{h}$ represents filtered total enthalpy of each species:

$$\bar{h} = \tilde{e} + \frac{\bar{P}}{\bar{\rho}} \tag{2.5}$$

An equation of state must specified to close this set of equations. Abel-Noble equation of states for real gas modeling is employed:

$$\bar{P} = \frac{\bar{\rho} R \bar{T}}{1 - b\bar{\rho}} \quad , \quad b = 0.00775 \ {}^{m^3}/_{Kg} \tag{2.6}$$

$$\begin{Bmatrix} & R[\frac{J}{Kg\ K}] \\ Air & 287.097 \\ H_2 & 4124.18 \end{Bmatrix}$$

Assuming Newtonian fluid, tensor of molecular viscous forces in (2.3.3) can be represented by the Boussinesq relation

$$\vec{\tilde{\sigma}} = \mu \left[\left(\vec{\nabla}.\vec{\tilde{v}} + \vec{\nabla}.\vec{\tilde{v}}^T \right) - \frac{2}{3} \vec{\nabla}.\vec{\tilde{v}} I \right] \tag{2.7}$$

In equation (2.3) and (2.7), μ represents molecular viscosity modeled by the Sutherland equation as

$$\mu = \mu_{ref} \left(\frac{\tilde{T}}{T_{ref}} \right)^{\frac{3}{2}} \frac{T_{ref} + T_0}{\tilde{T} + T_0} \tag{2.8}$$

$$\begin{Bmatrix} & \mu_{ref}[\frac{Kg}{ms}] & T_{ref}[K] & T_0[K] \\ Air & 1.716 \times 10^{-5} & 273.15 & 110.4 \\ H_2 & 8.411 \times 10^{-6} & 273.15 & 96.67 \end{Bmatrix}$$

Compressible extension of the Smagorinsky subgrid scale model for the eddy viscosity and heat flux, which is based on the local derivatives of the velocity field and the local grid size, is

$$\vec{\tau} = \mu_{SGS} \left[\left(\vec{\nabla}.\vec{\tilde{v}} + \vec{\nabla}.\vec{\tilde{v}}^T \right) - \frac{2}{3} \vec{\nabla}.\vec{\tilde{v}} I \right] \quad , \quad \vec{Q} = \mu_{SGS} \frac{C_p}{\mathrm{Pr}_t} \vec{\nabla} \bar{T} \tag{2.9}$$

$$\mu_{SGS} = \bar{\rho} C_s \Delta_{\mathrm{LES}}^2 \left| \tilde{S} \right| \quad , \quad \Delta_{LES} = (\forall_\omega)^{\frac{1}{3}} \quad , \quad \tilde{S} = \sqrt{\tilde{S}_{ij} \tilde{S}_{ij}} \quad , \quad \tilde{S}_{ij} = \frac{\partial \tilde{u}_i}{\partial x_j} + \frac{\partial \tilde{u}_j}{\partial x_i}$$

Smagorinsky subgrid model's constant (C_s) is chosen to be equal to 0.001. While there are two species, air and hydrogen, considered in this work, a transport equation is solved separately to determine the concentration:

$$\frac{\partial C}{\partial t} + \vec{\nabla}.\left(C\vec{v}\right) = \vec{\nabla}.\vec{J} \quad , \quad \vec{J} = D_f\,\vec{\nabla}C \tag{2.10}$$

Where C, D_f and $\vec{J}$ are concentration, diffusion coefficient of species and the diffusion flux, respectively. C is zero for pure hydrogen and one is used for air. The diffusion coefficient for hydrogen in air at normal temperature and pressure condition is 6.1×10^{-5} m^2/s [42].

Although ratio of specific heats ($\gamma_g = C_p/C_v$) is the same for hydrogen and air, R and the coefficients of Sutherland equation are different. In this case, simple linear averaging with respect to concentration is applied.

$$R = CR_{air} + (1 - C)R_{H_2} \tag{2.11}$$

$$\mu_{ref} = C\mu_{ref}{}_{air} + (1 - C)\mu_{ref}{}_{H_2} \tag{2.12}$$

$$T_0 = CT_{0_{air}} + (1 - C)T_{0_{H_2}} \tag{2.13}$$

In brief, re-writing the governing equations in vector form

$$\frac{\partial \vec{\phi}}{\partial t} + \vec{\nabla}.\left(\vec{F}^{conv} + \vec{F}^{diff}\right) = 0 \tag{2.14}$$

$$\vec{\phi} = \begin{bmatrix} \bar{\rho} \\ \bar{\rho}\vec{\tilde{v}}^T \\ \bar{\rho}\tilde{e} \end{bmatrix} \quad , \quad \vec{F}^{conv} = \begin{bmatrix} \bar{\rho}\vec{\tilde{v}} \\ \vec{\nabla}.\left(\bar{\rho}\vec{\tilde{v}}\vec{\tilde{v}}\right) + \vec{\nabla}\bar{P} \\ \vec{\nabla}.\left(\bar{\rho}\tilde{e} + \bar{P}\right)\vec{\tilde{v}} \end{bmatrix} \quad , \quad \vec{F}^{diff} = \begin{bmatrix} 0 \\ -\vec{\nabla}.\left(\mu + \mu_{SGS}\right)\left[\left(\vec{\nabla}.\vec{\tilde{v}} + \vec{\nabla}.\vec{\tilde{v}}^T\right) - \frac{2}{3}\vec{\nabla}.\vec{\tilde{v}}I\right] \\ -\vec{\nabla}.\left[\left(\frac{\mu}{\mathrm{Pr}} + \frac{\mu_{SGS}}{\mathrm{Pr}_t}\right)C_p\vec{\nabla}\tilde{T} + \left(\mu + \mu_{SGS}\right)\left(\left(\vec{\nabla}.\vec{\tilde{v}} + \vec{\nabla}.\vec{\tilde{v}}^T\right) - \frac{2}{3}\vec{\nabla}.\vec{\tilde{v}}I\right).\vec{\tilde{v}} - \bar{\rho}\sum_j h_j\vec{\tilde{J}_j}\right] \end{bmatrix}$$

For inviscid flow modeling, in (2.14) $\vec{F}^{diff}$ and right-hand–side of (2.10) will be zero. Also Pr and Pr_t are assumed constant and equal to 0.72 and 0.9, respectively.

Before discretizing the governing equations, it should be considered that in this simulation it is assumed that the thermodynamic properties will not be changed and homogenously distributed in domain. No heat transfer to the ambient and no phase change is considered.

2.2 Numerical method

A mixed finite element – finite volume scheme on an unstructured tetrahedral mesh is considering to apply for the simulation of hydrogen release. As specified by this scheme, the finite element technique is used for diffusive fluxes, while for convective fluxes, a finite volume integration is applied. It should mentioned that for transport equation the same methodology is employed considering the second order of accuracy in flux calculations.

2.2.1 Spatial Discretization

To numerically solve equation set (2.14), the weak formulation is carried out by multiplying this equation by a test function Ψ and integrating over the whole domain,

$$\iiint_{\Omega} \left[\frac{\partial \vec{\phi}}{\partial t} + \vec{\nabla}.\left(\vec{F}^{conv} + \vec{F}^{diff}\right)\right] \Psi d\forall = 0 \qquad (2.15)$$

Discretizing the domain to finite non-overlapping cells, allows to write equation (2.14) for each cell. For any arbitrary cell ω_i, considering characteristic function ζ_i for

convective flux and a piecewise linear finite element basis function η_i for diffusion flux, (2.15) is written as:

$$\int_{\omega_i} \left[\frac{\partial \vec{\phi}}{\partial t} + \vec{\nabla}.\vec{F}^{conv}\right] \zeta_i d\forall + \int_{\sum \omega_i} \left[\vec{\nabla}.\vec{F}^{diff}\right] \eta_i d\forall = 0 \tag{2.16}$$

Subsequently, applying Green's theorem to the convective fluxes and integration by parts to diffusive fluxes, discretized equation can be written as:

$$\int_{\omega_i} \frac{\partial \vec{\phi}}{\partial t} d\forall + \oint_{\partial \omega_i} \left[\vec{F}^{conv}.\hat{n}\right] d\Lambda + \int_{\sum \omega_i} \left[\vec{F}^{diff}.\left(\vec{\nabla}.\eta_i\right)\right] d\forall = 0 \tag{2.17}$$

Where $\hat{n}$ is outward unit vector of the face $\partial\omega_i$ on cell ω_i.

2.2.1.1 Convective Flux Discretization

In this work, Roe-MUSCL method is used to calculate the convective fluxes. To achieve second order of accuracy, it is assumed that the flow field variables changes linearly over the cell. It consists of an averaging term between two nodes plus an upwinding component. This scheme can be written as

$$\vec{F}^{conv}.\hat{n}_{nm} = \frac{\vec{F}^{conv}(\phi_{nm}) + \vec{F}^{conv}(\phi_{mn})}{2}.\hat{n}_{nm} - |\partial\omega_{nm}|\frac{\phi_{nm} - \phi_{mn}}{2} \tag{2.18}$$

In this notation, *n* and *m* are the two neighboring nodes which have common cell surface as $\partial\omega_{nm}$ with normal unit vector of $\hat{n}_{nm}$. To calculate ϕ_{nm} , ϕ_{mn} :

$$\phi_{nm} = \phi_n - \frac{1}{2}\mathcal{L}(\Delta\phi, \Delta\phi^{right})$$
$$\phi_{mn} = \phi_m + \frac{1}{2}\mathcal{L}(\Delta\phi, \Delta\phi^{left}) \tag{2.19}$$

In which $\mathcal{L}$ is the limiter function. To control undesired oscillations in discontinuities, Van Leer-Van Albada limiter is applied:

$$\mathcal{L}(x,y) = \begin{cases} 0 & xy < 0 \\ \dfrac{(x^2+\vartheta)y + (y^2+\vartheta)x}{x^2+y^2+\vartheta} & xy \geq 0 \end{cases} \tag{2.20}$$

ϑ has a small positive value which is taken 10^{-16} in this simulation. In (2.19), $\Delta\phi^{left}, \Delta\phi^{right}$ and $\Delta\phi$ are:

$$\Delta\phi^{left} = (1-\beta)\Delta\phi + \beta\vec{\nabla}\phi^{mm'}.\hat{n}_{mn}$$
$$\Delta\phi^{right} = (1-\beta)\Delta\phi + \beta\vec{\nabla}\phi^{nn'}.\hat{n}_{mn} \tag{2.21}$$
$$\Delta\phi = \phi_n - \phi_m$$

As recommended by Tajalipour [39], the factor β is taken 1/3 to minimize both dissipative and dispersive errors. $\vec{\nabla}\phi^{nm}$ and $\vec{\nabla}\phi^{nn'}$ are left and right hand gradients computing with respect to upstream and downstream neighbouring cells.

2.2.1.2 Self-adaptive upwinding method

Averaging method applied in the preceding part, brings some dissipation to the numerical solution. Although this behavior is suitable for Euler and laminar flow to make the scheme stable, it is too dissipative for the LES simulation. To overcome this issue, a

self-adaptive coefficient, γ, is defined for upwinding part of (2.18) to reduce this dissipation while keep the method stable [39]. Hence, (2.18) can rewrite as,

$$\vec{F}^{conv}.\hat{n}_{nm} = \frac{\vec{F}^{conv}(\phi_{nm}) + \vec{F}^{conv}(\phi_{mn})}{2}.\hat{n}_{nm} - \gamma\left\{|\partial\omega_{nm}|\frac{\phi_{nm} - \phi_{mn}}{2}\right\} \qquad (2.22)$$

Where γ can adapted between 0 and 1. $\gamma = 0$ represents central differencing while $\gamma = 1$ forces full Roe-MUSCL method. The smallest possible value for γ should be chosen to have a stable suitable turbulence modeling. To adjust upwinding coefficient Tajallipour [39] proposed adjusting the value based on a wiggle detection scheme. This method based on the concept that a wiggle exists along an edge if the gradient changes its sign at least twice. To get better result for the LES modeling, instead of using the value of primitive variables on nodes, Tajallipour [39] suggested to use gradient of primitive variables on adjacent edges. To explain this concept, consider edge E_{ij} between two nodes *i* and *j*, with a primitive variable like *q* ($q \in [\rho \quad \vec{v} \quad P]$) on each node. For the arbitrary edge $E_{ij,}$

$$\vec{\Delta}q.\hat{n}_{ij} = \frac{q_j - q_i}{|\overrightarrow{X_j} - \overrightarrow{X_i}|} \qquad (2.23)$$

Which $\vec{X}$ presents position vector. Mathematically speaking, a wiggle exist if the following condition is satisfies:

$$\left(\vec{\Delta}q^{left}.\hat{n}_{ij}\right)\left(\vec{\Delta}q.\hat{n}_{ij}\right) < \varepsilon \leq 0 \quad \textbf{AND} \quad \left(\vec{\Delta}q^{right}.\hat{n}_{ij}\right)\left(\vec{\Delta}q.\hat{n}_{ij}\right) < \varepsilon \leq 0 \qquad (2.24)$$

If a wiggle is detected, upwinding coefficient increases to get closer to full upwind method. Otherwise, it decreases to benefit from a central scheme. This changes are:

$$\begin{aligned} &\text{Increment:} \quad \varepsilon - \min\left[\left(\vec{\Delta}q^{left}.\hat{n}_{ij}\right)\left(\vec{\Delta}q.\hat{n}_{ij}\right) \quad , \quad \left(\vec{\Delta}q^{right}.\hat{n}_{ij}\right)\left(\vec{\Delta}q.\hat{n}_{ij}\right)\right] \\ &\text{Decrement:} \quad \max\left[\left(\vec{\Delta}q^{left}.\hat{n}_{ij}\right)\left(\vec{\Delta}q.\hat{n}_{ij}\right) \quad , \quad \left(\vec{\Delta}q^{right}.\hat{n}_{ij}\right)\left(\vec{\Delta}q.\hat{n}_{ij}\right)\right] - \varepsilon \end{aligned} \tag{2.25}$$

A very small negative value for ε should be picked to capture some energy in the highest scales for the LES model. This small value helps to adjust the amount of energy in the smallest scales of grid. In this study ε is set to be -0.0001.

2.2.2 Temporal Discretization

For temporal discretization, (2.17) can rewrite as:

$$\int_{\omega_i} \frac{\partial \vec{\phi}}{\partial t} d\forall = \mathfrak{F}(\phi) \tag{2.26}$$

To have accurate and stable scheme, a second order implicit discretization applied. Assuming constant ϕ in each cell, an implicit form of (2.26) will become

$$\omega_i \frac{\partial \phi}{\partial t}\Big]^n = \mathfrak{F}(\phi)]^{n+1} \tag{2.27}$$

Applying Taylor expansion to linearizing (2.27) and using chain rule, will deliver second order backward finite difference discretization as

$$\left[\alpha \frac{\omega_i}{\Delta t} - (\alpha + \theta)\frac{\partial \mathfrak{F}(\phi)]^{n+1}}{\partial \phi]^n}\right]\Delta\phi]^n = \mathfrak{F}(\phi)]^n + \left[\lambda \frac{\omega_i}{\Delta t} - 2\lambda \frac{\partial \mathfrak{F}(\phi)]^{n+1}}{\partial \phi]^n}\right]\Delta\phi]^n \tag{2.28}$$

where

$$\tau = \frac{\Delta t^n}{\Delta t^{n-1}} \quad , \quad \alpha = \frac{1+2\tau}{1+\tau} \quad , \quad \lambda = \frac{\tau^2}{1+\tau} \quad , \quad \theta = \frac{\tau}{1+\tau}$$

2.3 Stability Concerns

As previously mentioned, higher order accuracy and high pressure ratio for this specific problem lead to stability problem and this is the main reason that common commercial software do not converge. To overcome this problem, some extra conditions should be applied. To guarantee the stability of the simulation, regions with shocks with high gradient in the Mach number require full upwind method ($\gamma = 1$). Similarly, in a small zone near the exit area, the simulation is highly sensitive to the geometric discontinuity of the corner; therefore in this region of the size (2D×2D×D) the flux calculation is switches to first order of accuracy. For a first order method, it is assumed that the flow variables remain constant in each cell. Concurrently, in this region, the full upwind simulation is considered.

For inviscid simulation because of presence of stronger shock wave, the above conditions are not sufficient to guarantee stability. In this case, while high Mach number gradient recognized in computational domain, a limiter switches the accuracy to the first order.

2.4 Boundary Conditions

In this study, the boundary conditions employed are: adiabatic no-slip / slip wall and non-reflecting pressure outlet. For the no-slip wall the zero velocity condition (normal and tangent direction) is imposed to set a realistic condition for a viscous flow while for the inviscid simulation, only zero velocity condition in the normal direction is enforced.

To satisfy adiabatic condition walls, the temperature gradient is set to be zero across the wall.

For non-reflecting boundary condition, flux calculations are done considering the superposition of waves from interior domain and incoming waves coming from virtual outside node. Only the characteristic wave move toward the domain is considered to provide desirable condition, particularly stopping shock wave from reflecting back inside the domain. Concurrently, pressure is set according to the physical domain and the remaining primitive variables come from numerical solution for this boundary.

2.4.1 Boundary Condition Discussion

From basic fluid mechanics, without shear stress, there will be no fluid deformation and the behaviour of the flow is described by the bulk motion. However, when a viscous fluid flows over a static solid surface, the velocity gradients are set up by no-slip condition over the surface on the zone which is known as boundary layer. Experimental studies state that viscous flow has a logarithmic distribution of velocity near the wall, which is known as law of the wall [40]. For a flat plate, flow with higher Reynolds number has smaller boundary layer near for the same distance downstream from the start of the boundary layer.

In this study, during LES simulation which the problem be will defined on chapter 4, it was realized that the no-slip wall condition did not allow the flow to reach a sonic uniform one inside release exit. Fig (2.1) illustrated the Mach number profile in the middle of release area for viscous flow after 25 microsecond of release. Note that after 15 microsecond the velocity profile gets its final shape and remains the same. The mesh

density is the reason for not having the fully developed flow in the release tube. For LES a fine mesh is required in particular in the boundary layer. Nevertheless this will significantly increase the overall number of elements and make the simulation very expensive.

As seen in Fig (2.1), there is an improvement by applying super fine mesh, the flow profile inside release area with no-slip wall condition is better but not yet desirable because it has not reach the sonic flow and it has a big gradient. On the other hand, calculating viscous sub-layer thickness base on Table (4.2), $\frac{\delta_s}{D} = 2.2 \times 10^{-6}$, declare that there is a small viscous effected zone beside the interior walls and a super fine mesh is required to capture this layer. Therefore, it was decided to set the interior wall as slip boundary condition to overcome this problem. The influence of this case, in long simulation, was distinguishable. Fig (2.2) to Fig (2.6) show the field distribution of density, pressure, Mach number, concentration and temperature at six different times for the LES simulation of 70 MPa hydrogen release with two different boundary conditions for interior walls, i.e. slip wall condition and no-slip wall condition, release from a 5mm orifice. Following, the development of density, pressure, Mach number, concentration and temperature on centerline are illustrated on Fig (2.7) to Fig (2.11). It should be mentioned that in both cases the simulation setup are as Table (4. 2).

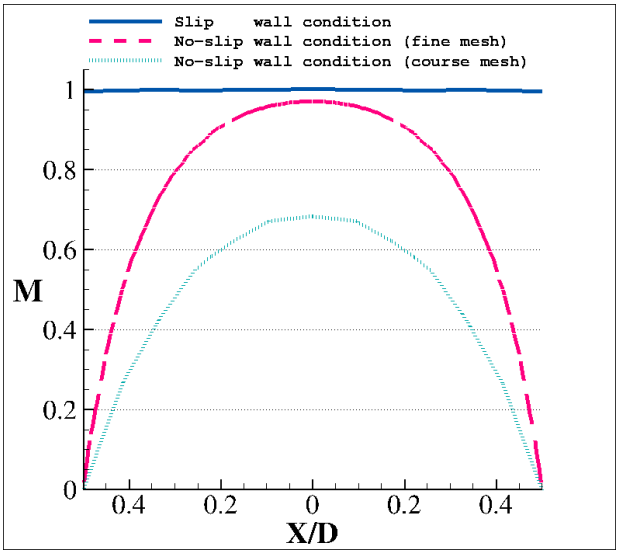

Fig (2. 1): Mach number profile in middle of release area after 25 microsecond of hydrogen release from a 5 mm orifice, LES simulation

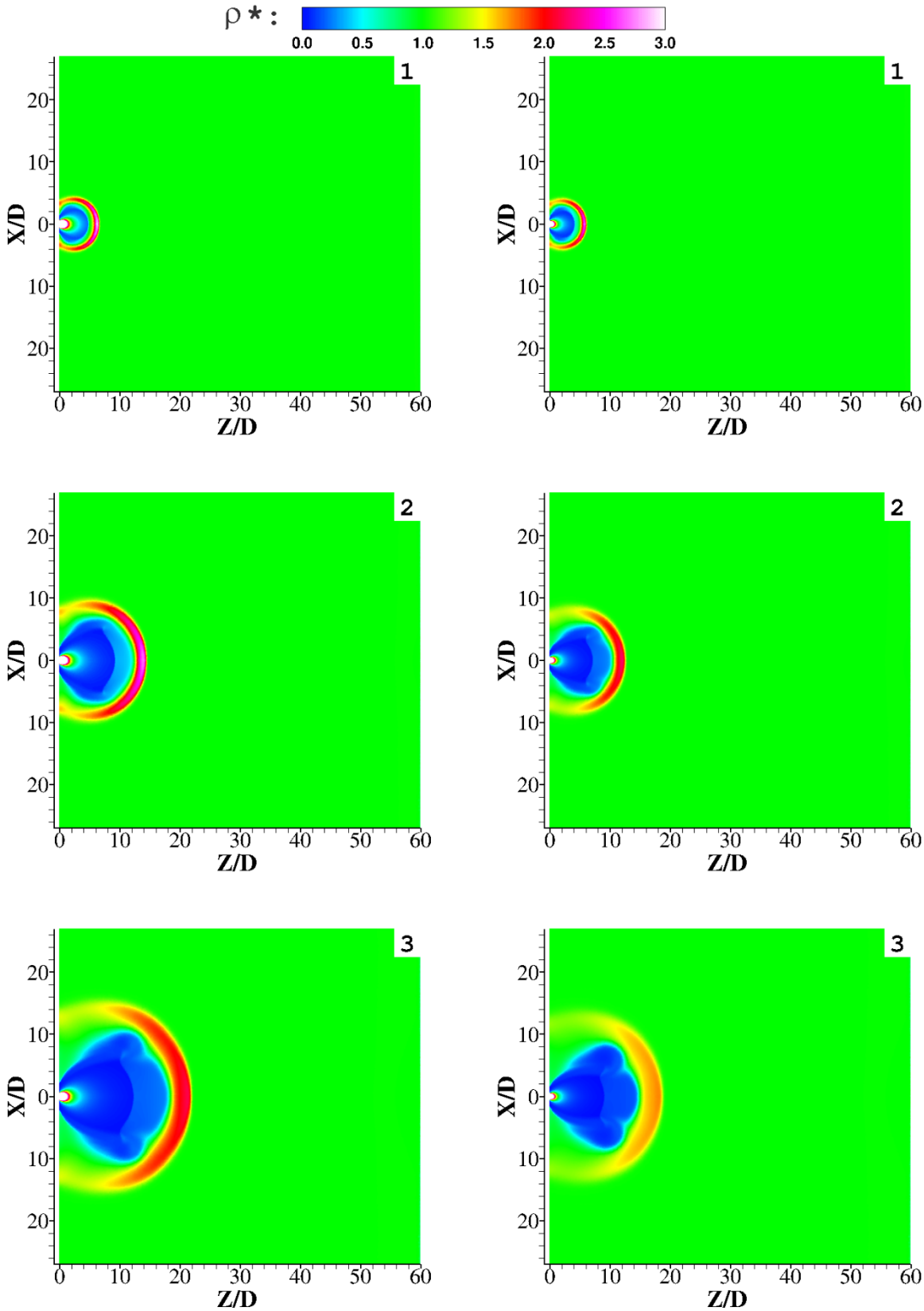

Fig (2. 2): ρ* of hydrogen jet (70 MPa) release from 5mm orifice: slip wall (left) and no-slip wall (right) 1) 25, 2) 70, 3)125, 4)160, 5)200 and 6) 250 microsecond

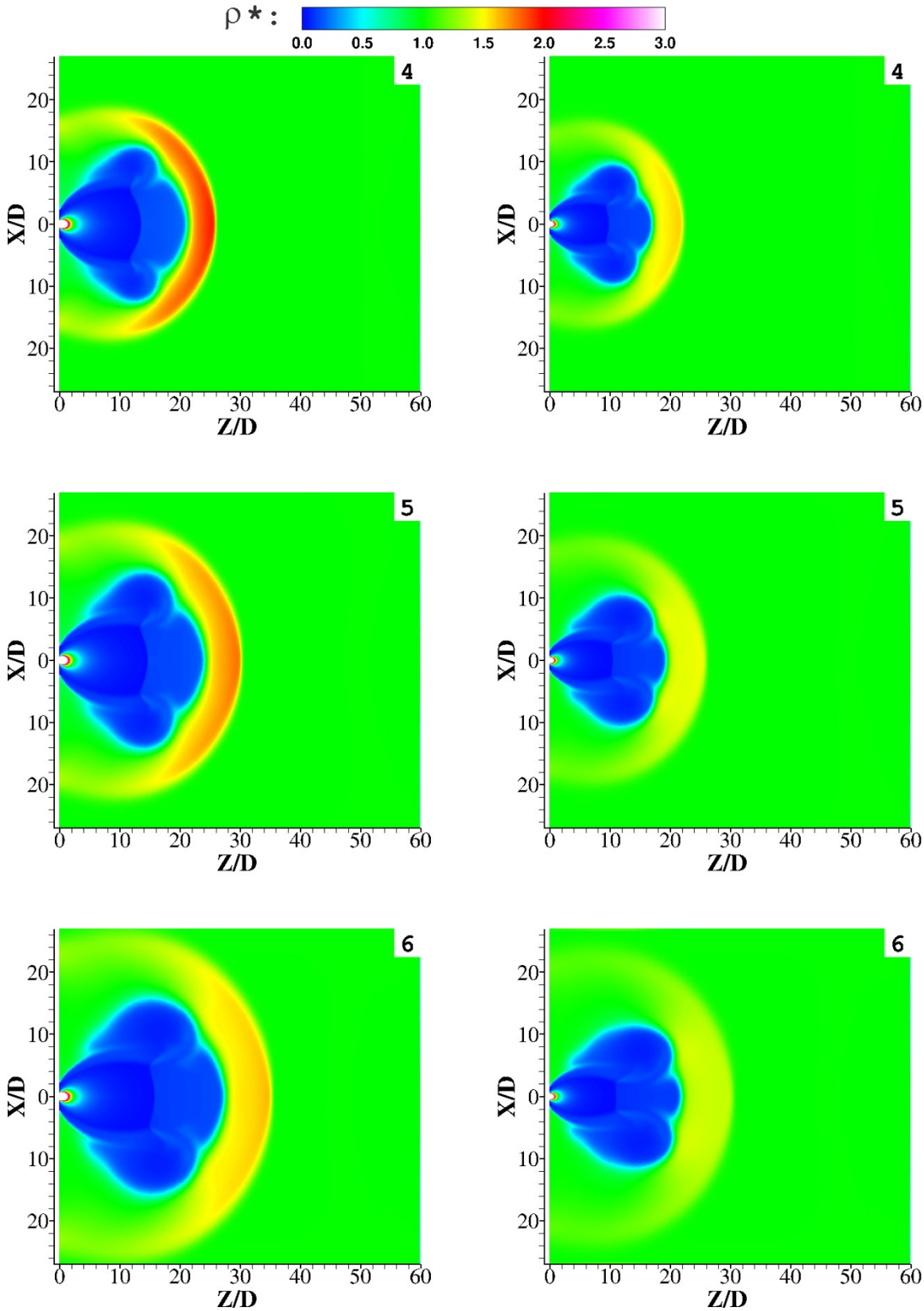

Fig (2. 2): ρ* of hydrogen jet (70 MPa) release from 5mm orifice: slip wall (left) and no-slip wall (right) 1) 25, 2) 70, 3)125, 4)160, 5)200 and 6) 250 microsecond **(continue)**

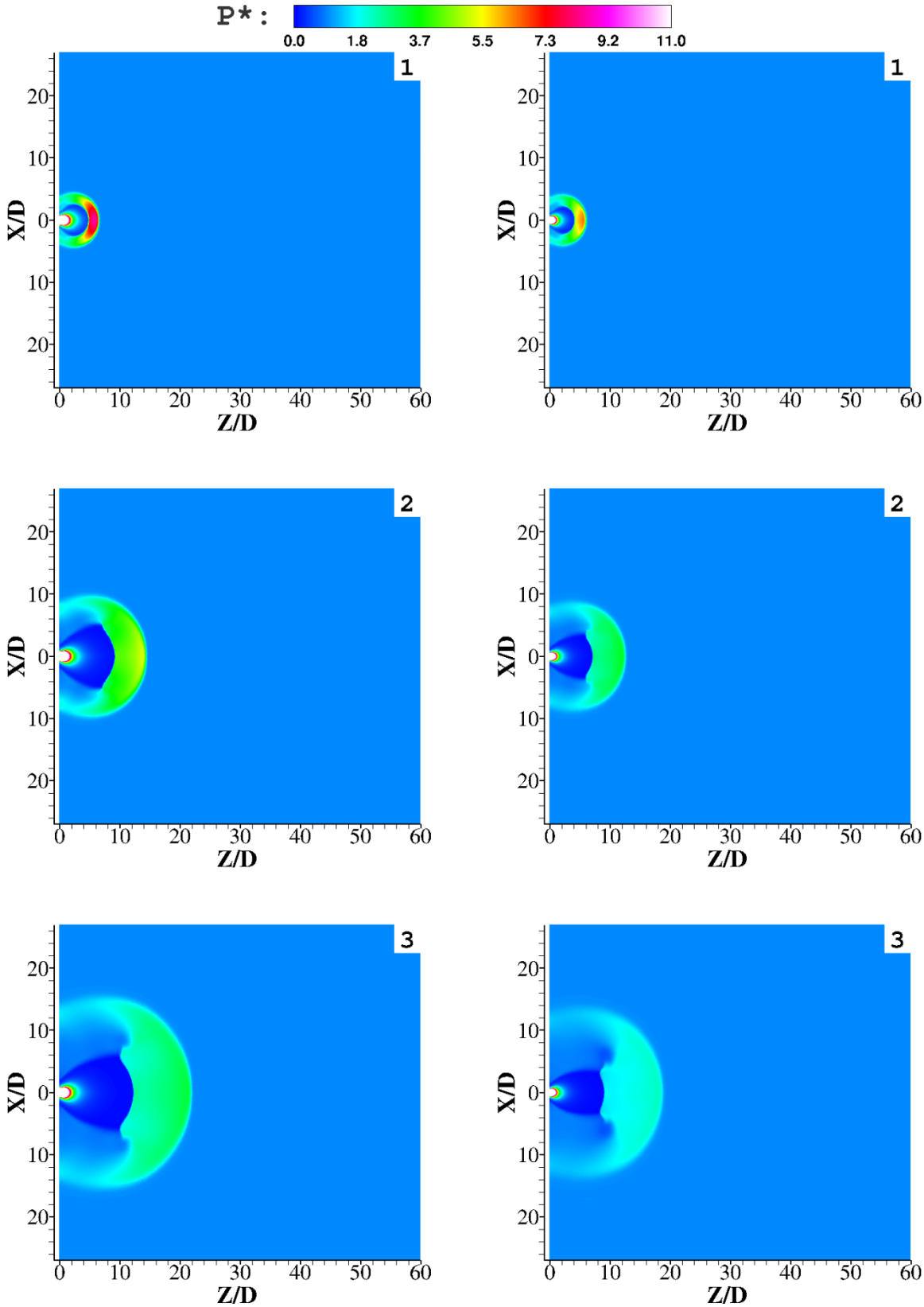

Fig (2. 3): P* of hydrogen jet (70 MPa) release from 5mm orifice: slip wall (left) and no-slip wall (right)

1) 25, 2) 70, 3)125, 4)160, 5)200 and 6) 250 microsecond

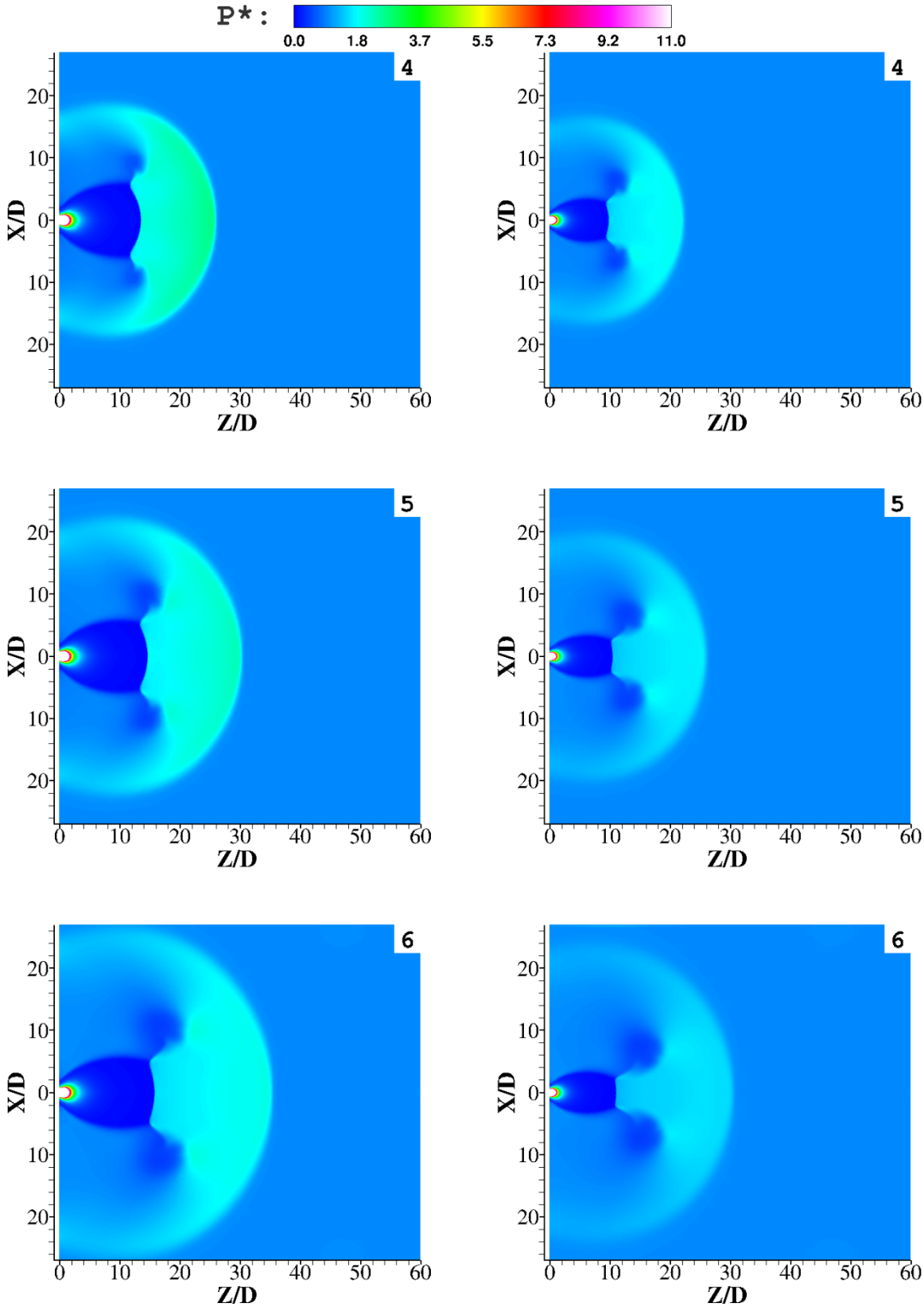

Fig (2. 3): P* of hydrogen jet (70 MPa) release from 5mm orifice: slip wall (left) and no-slip wall (right)

1) 25, 2) 70, 3)125, 4)160, 5)200 and 6) 250 microsecond **(continue)**

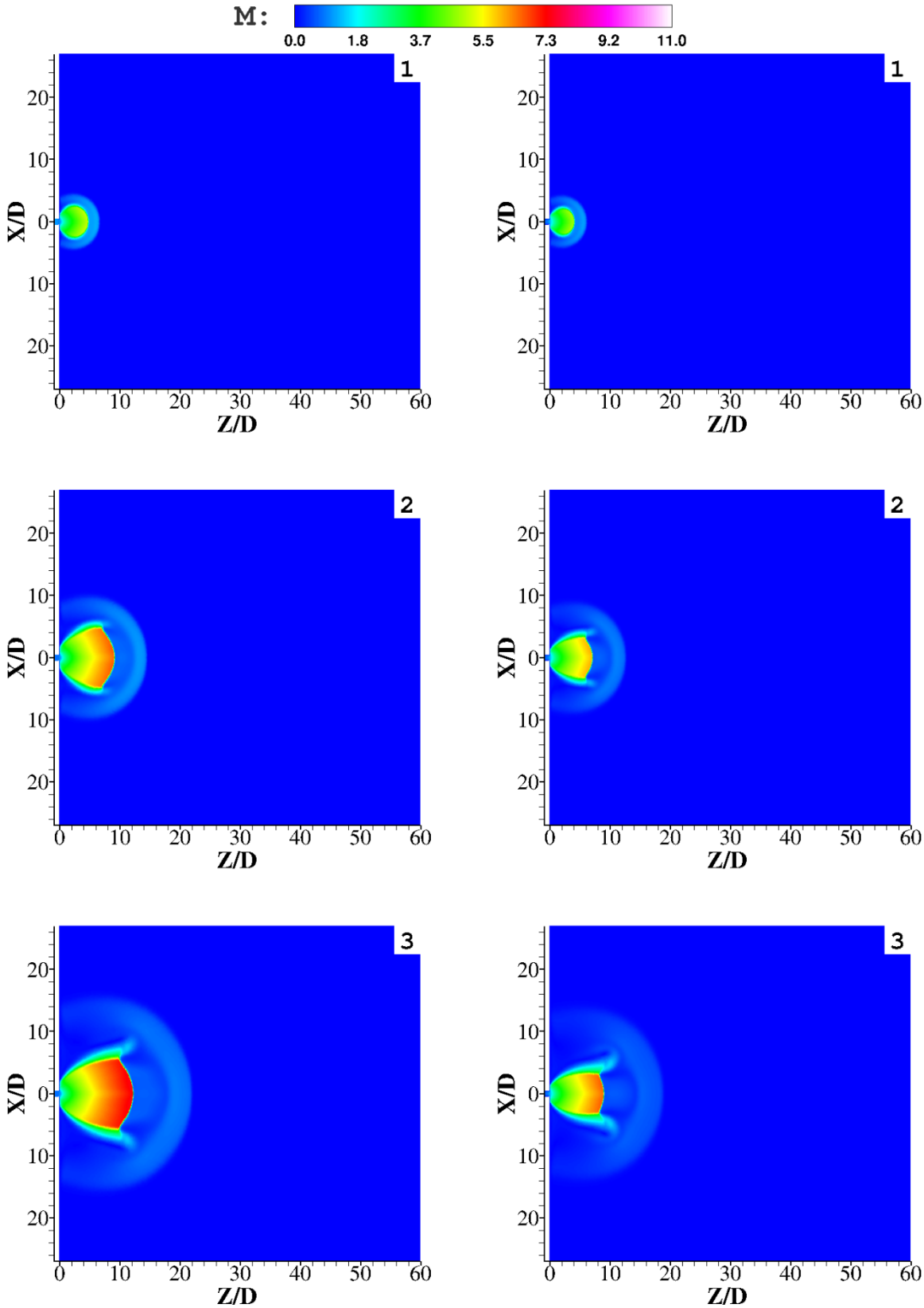

Fig (2. 4): Mach number of hydrogen jet (70 MPa) release from 5mm orifice: slip wall (left) and no-slip wall (right) 1) 25, 2) 70, 3)125, 4)160, 5)200 and 6) 250 microsecond

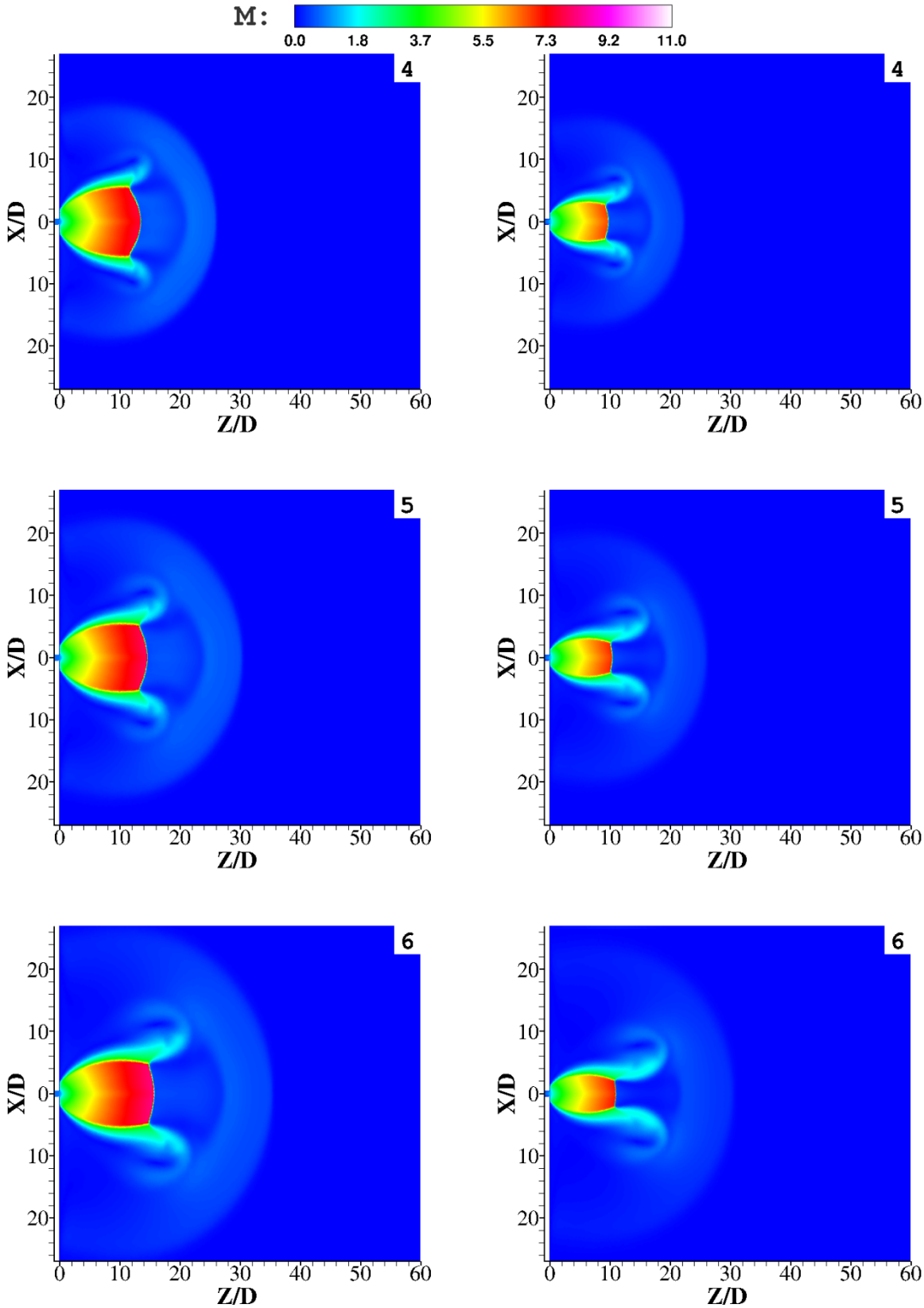

Fig (2. 4): Mach number of hydrogen jet (70 MPa) release from 5mm orifice: slip wall (left) and no-slip wall (right) 1) 25, 2) 70, 3)125, 4)160, 5)200 and 6) 250 microsecond **(continue)**

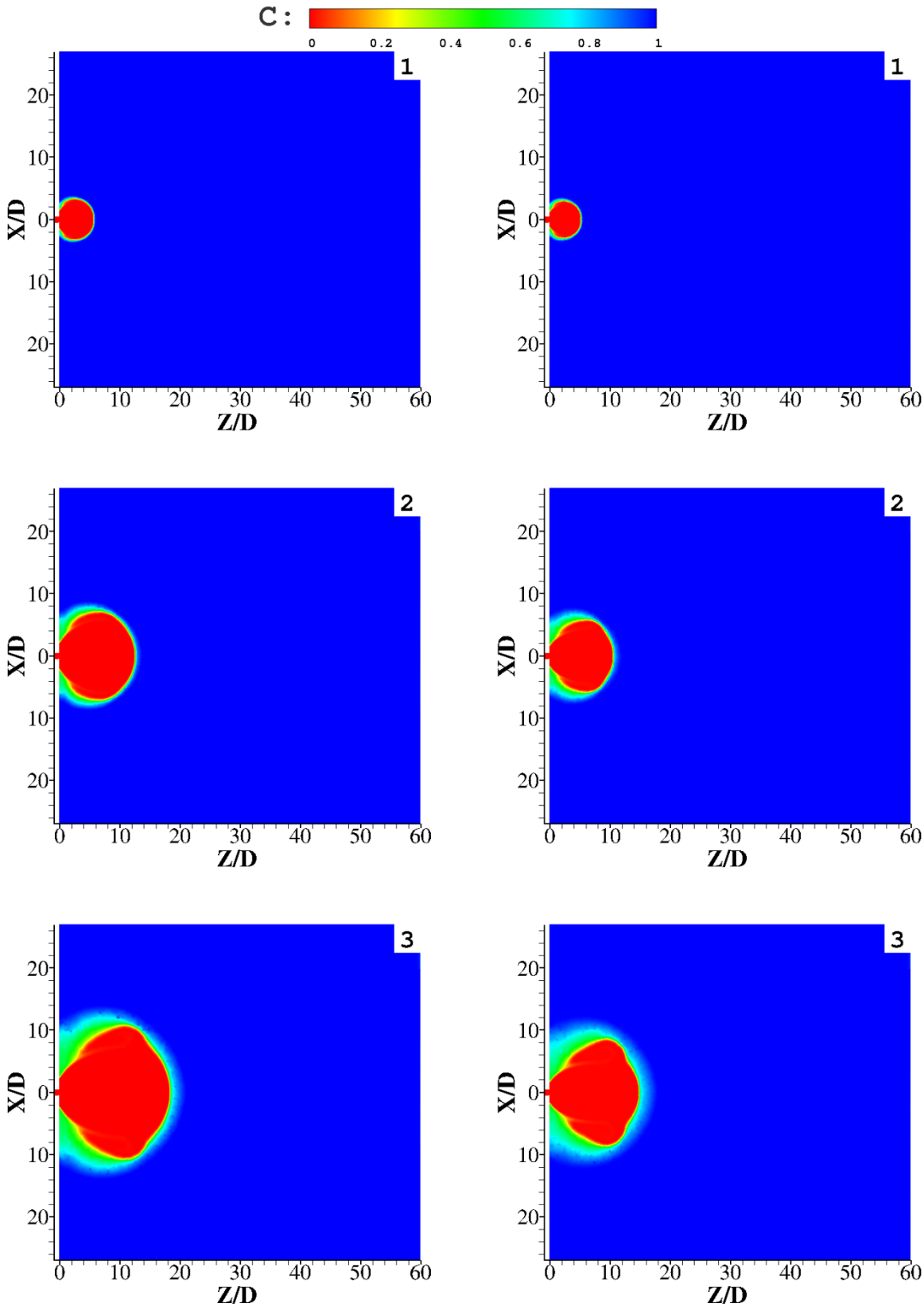

Fig (2. 5): Concentration of hydrogen jet (70 MPa) release from 5mm orifice: slip wall (left) and no-slip wall (right) 1) 25, 2) 70, 3)125, 4)160, 5)200 and 6) 250 microsecond

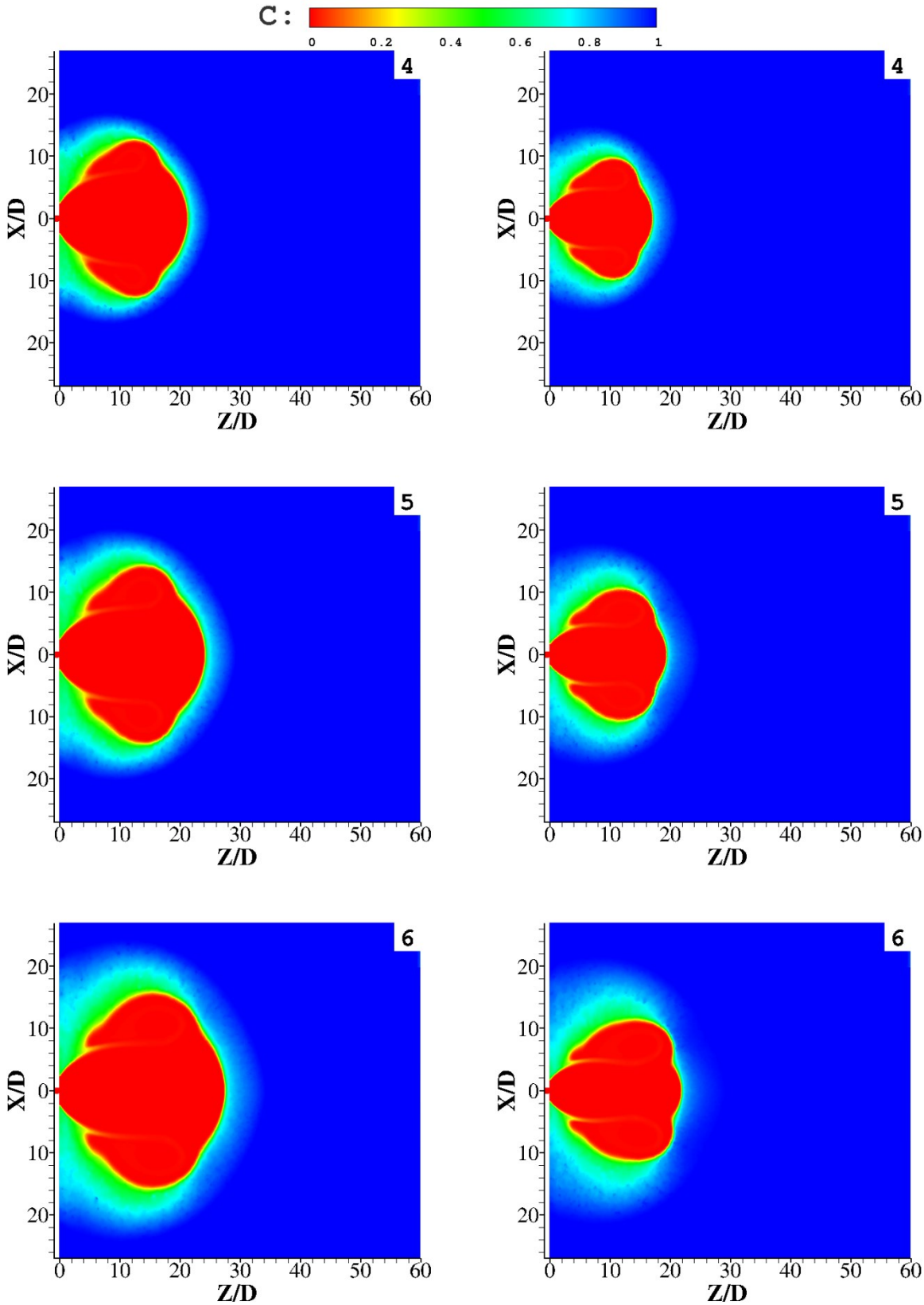

Fig (2. 5): Concentration of hydrogen jet (70 MPa) release from 5mm orifice: slip wall (left) and no-slip wall (right) 1) 25, 2) 70, 3)125, 4)160, 5)200 and 6) 250 microsecond **(continue)**

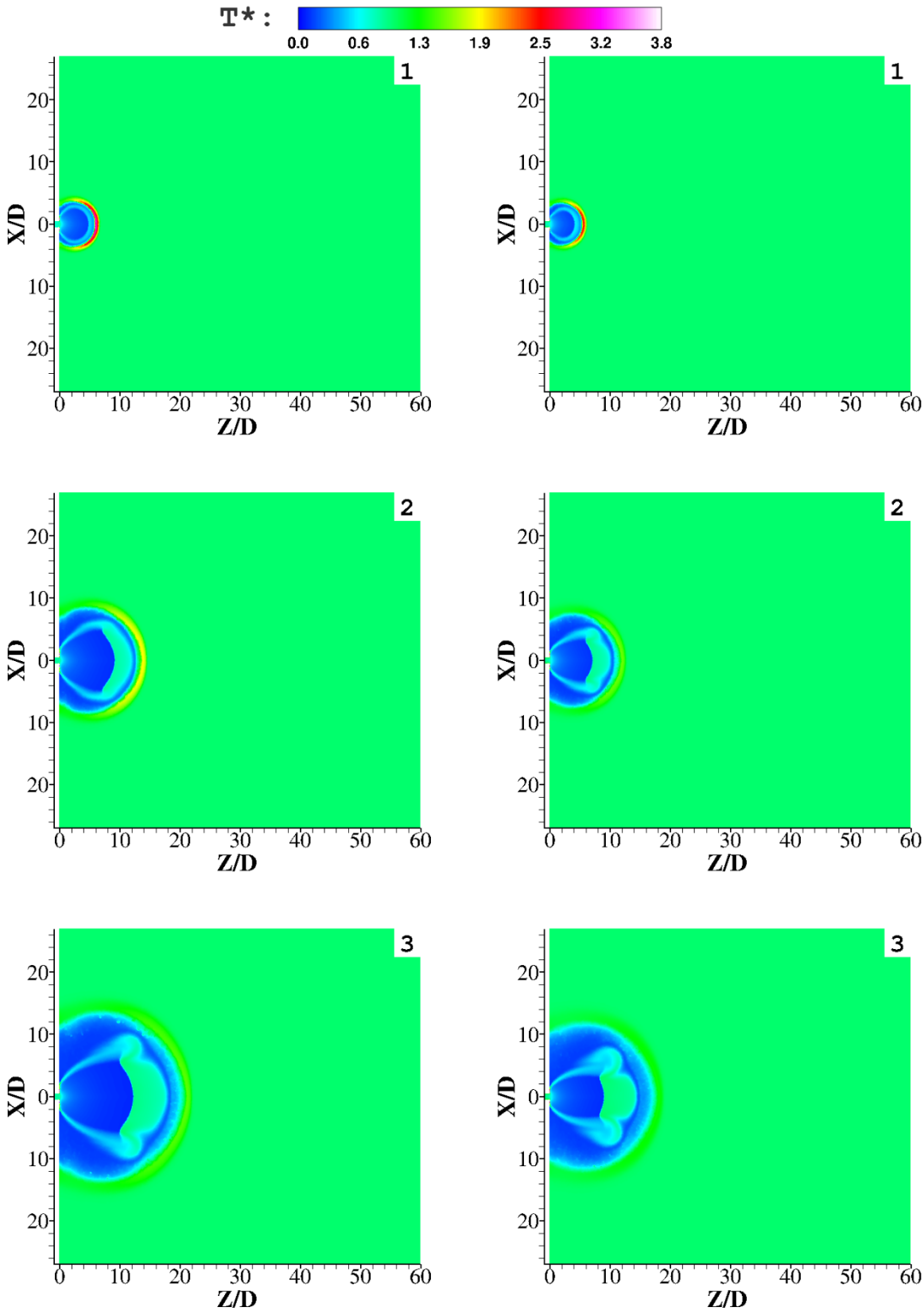

Fig (2. 6): T* of hydrogen jet (70 MPa) release from 5mm orifice: slip wall (left) and no-slip wall (right) 1) 25, 2) 70, 3)125, 4)160, 5)200 and 6) 250 microsecond

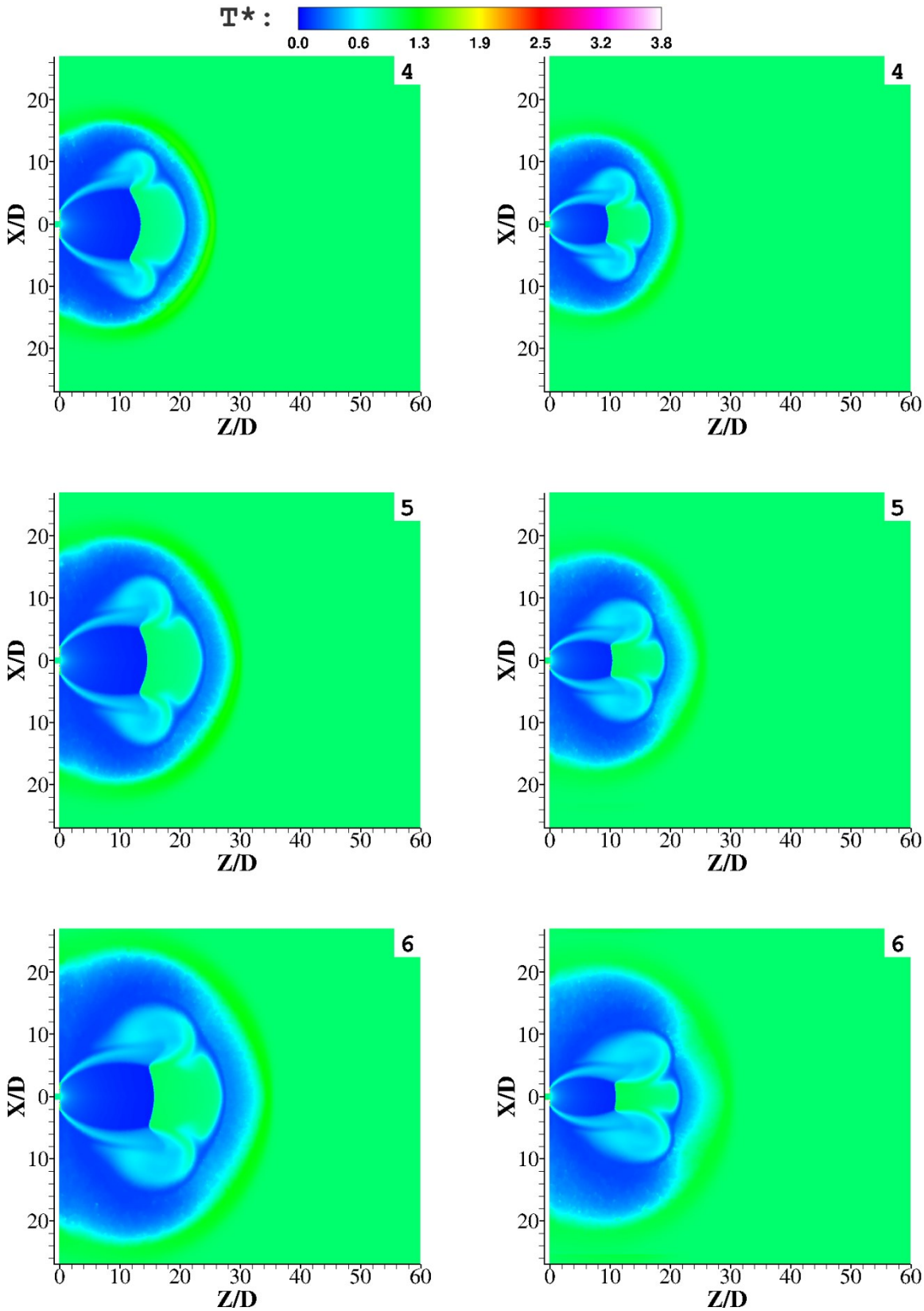

Fig (2. 6): T* of hydrogen jet (70 MPa) release from 5mm orifice: slip wall (left) and no-slip wall (right)

1) 25, 2) 70, 3)125, 4)160, 5)200 and 6) 250 microsecond **(continue)**

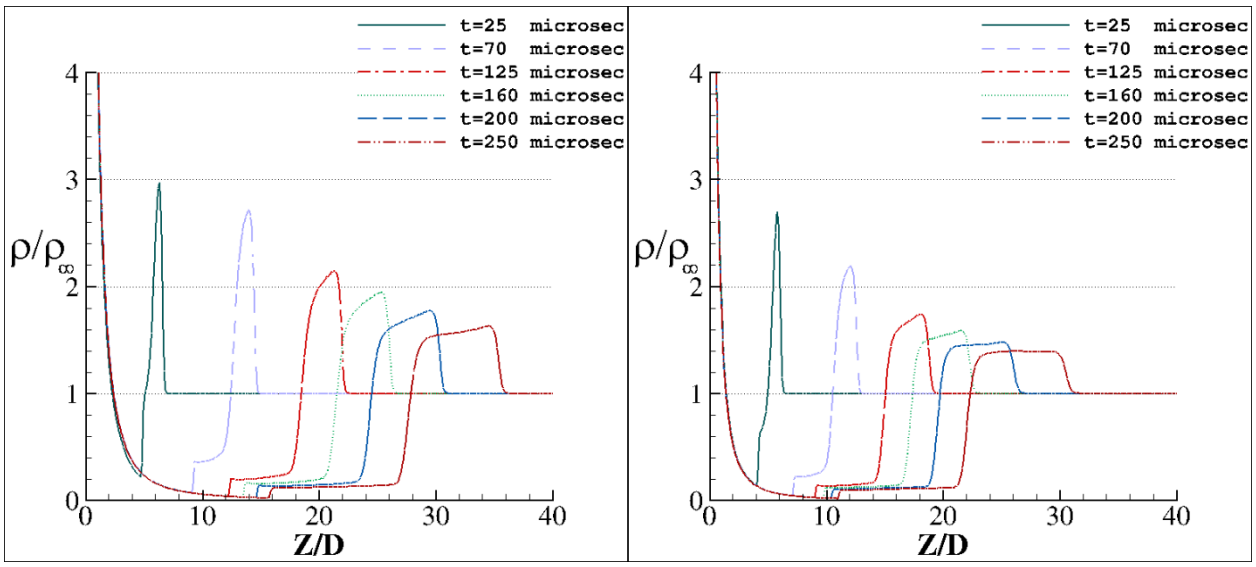

Fig (2. 7): ρ* along centerline, 70 MPa hydrogen jet release from 5mm orifice: slip wall (left) and no-slip wall (right) LES simulation

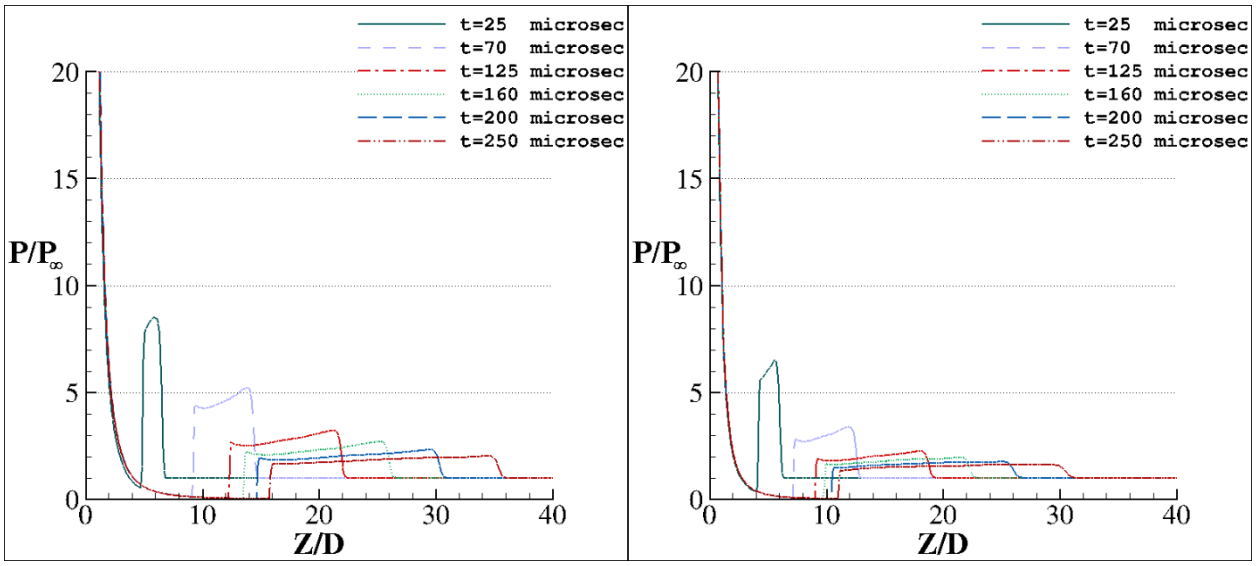

Fig (2. 8): P* along centerline, 70 MPa hydrogen jet release from 5mm orifice: slip wall (left) and no-slip wall (right) LES simulation

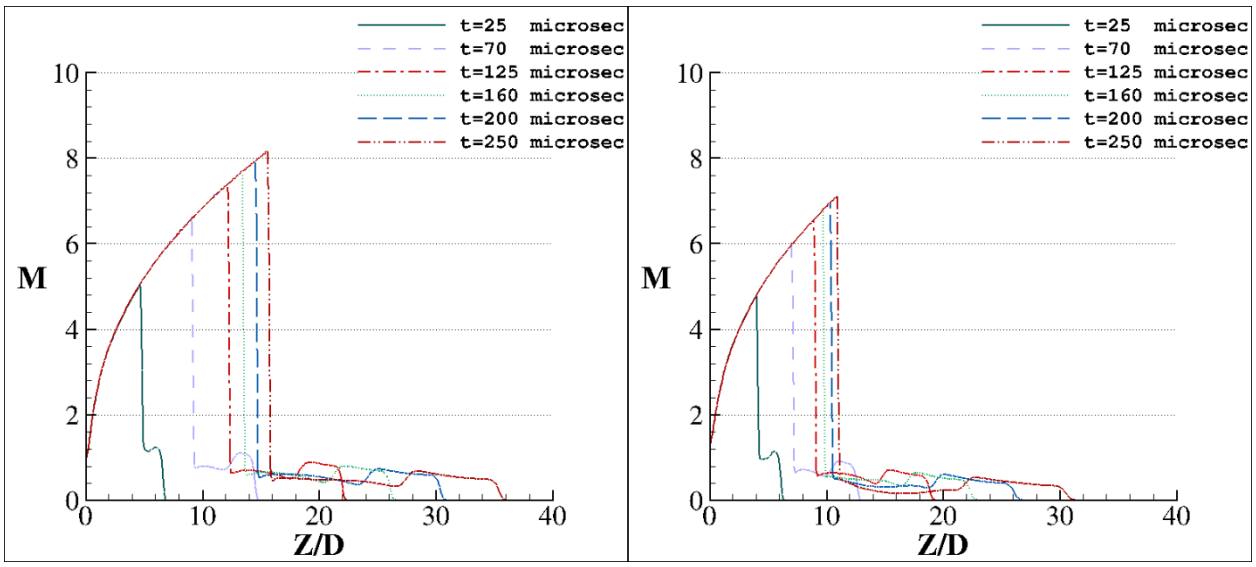

Fig (2. 9): Mach number along centerline, 70 MPa hydrogen jet release from 5mm orifice: slip wall (left) and no-slip wall (right) LES simulation

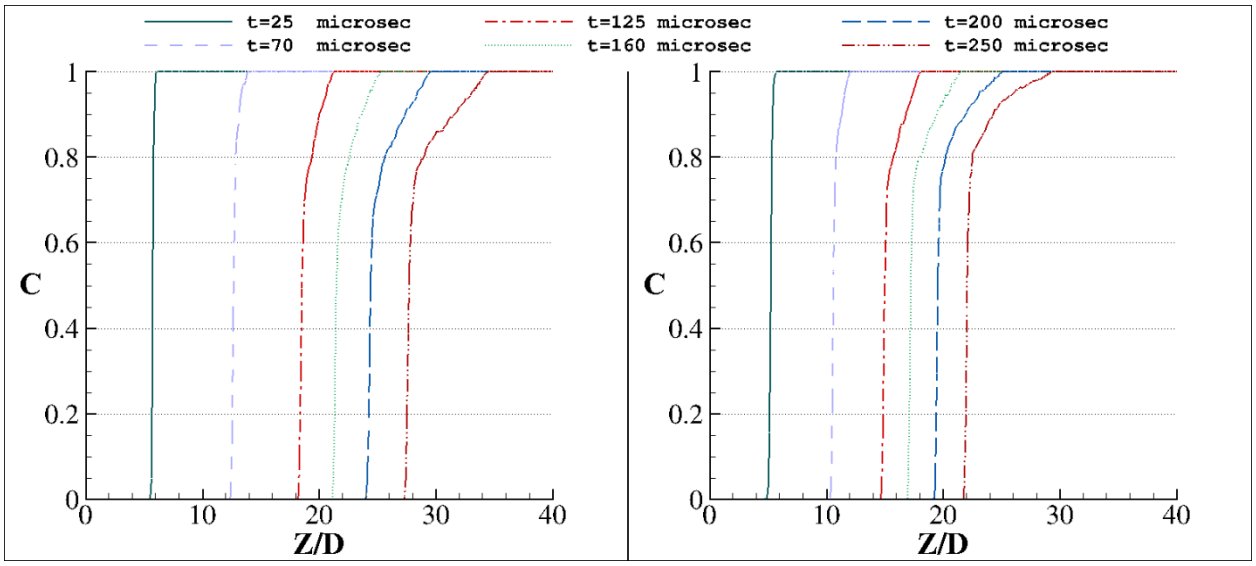

Fig (2. 10): Concentration along centerline, 70 MPa hydrogen jet release from 5mm orifice: slip wall (left) and no-slip wall (right) LES simulation

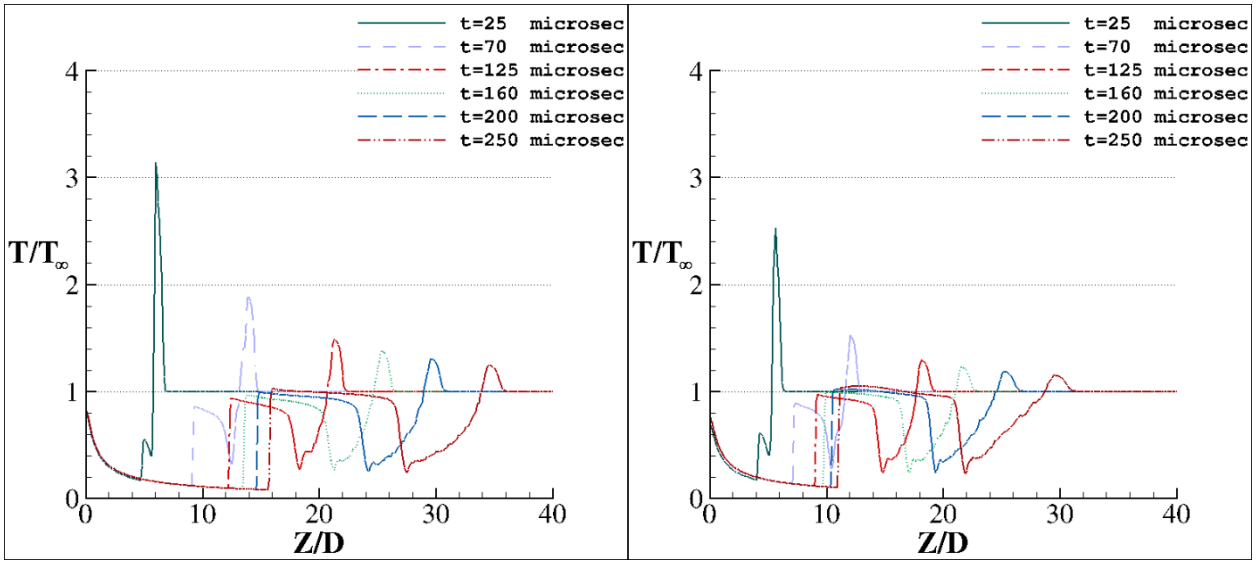

Fig (2. 11): T* along centerline, 70 MPa hydrogen jet release from 5mm orifice: slip wall (left) and no-slip wall (right) LES simulation

It is clear that the slip wall condition leads to a bigger cloud shaped with stronger lead shock and Mack disk. In other words, the peak value of density, pressure and Mach number in the domain has bigger value with slip-wall condition. Furthermore, this stronger shock explore faster. Considering the Mach number study, this results is expected. Studying the shape and position of concentration, it is evidence that hydrogen cloud explore faster and develops a bigger hydrogen cloud.

The maximum temperature inside the domain is increased by changing the boundary condition. For example, after 25 microsecond of release, the maximum temperature reaches 3 times more than ambient temperature while with no-slip wall condition this value reduced to 2.5. The concentration of hydrogen and the temperature in computational domain are key parameters for studying possibility of auto ignition.

Chapter 3

NUMERICAL VALIDATION

The goal of this study is to understand the viscous behaviour of highly under expanded hydrogen jet. In this chapter, the extended code based on the numerical method explained in chapter 2 is validated by simulating a subsonic turbulent jet to study the dynamics of the flow in transient time and compare it with the work of Chernyavsky et al. [40], qualitatively. The main idea of this validation is to see if the extended code is capable to capture randomness.

3.1 Reference Problem Definition

Chernyavsky et al. [40] studied a subsonic turbulent jet venting into the atmosphere considering buoyancy forces and turbulence effects. They investigated the dynamic features of this flow and mixing processes during the transient process. Their study contained two parts. In the first part, the authors simulated the release of helium jet with flow parameters corresponding closely to hydrogen jet release considering the LES

simulation for turbulence model. Comparing their numerical results with PIV measurements, the buoyancy effects did not allow them to capture the exact self-similarity of turbulent jet but the centerline mass fraction evolution showed expected behaviour. In the next part of their study, which is considered for comparison here, the LES results of low speed hydrogen jet were presented for early time in the transient phase. Employing a research code, they tried to keep the Mach number around 0.3 at the entrance. Regarding to hydrogen concentration in near exit zone (<4D) during jet penetration, strong vortex ring were observed which lead to an increment of 25-30% of radial flammable region. Hence, hydrogen concentration increased by 30-40% above the flammability threshold in this direction.

3.2 Validation Simulation

In this section, a transient low pressure subsonic jet development is simulated to study the vortex rings and hydrogen radial penetration. It should note that since the

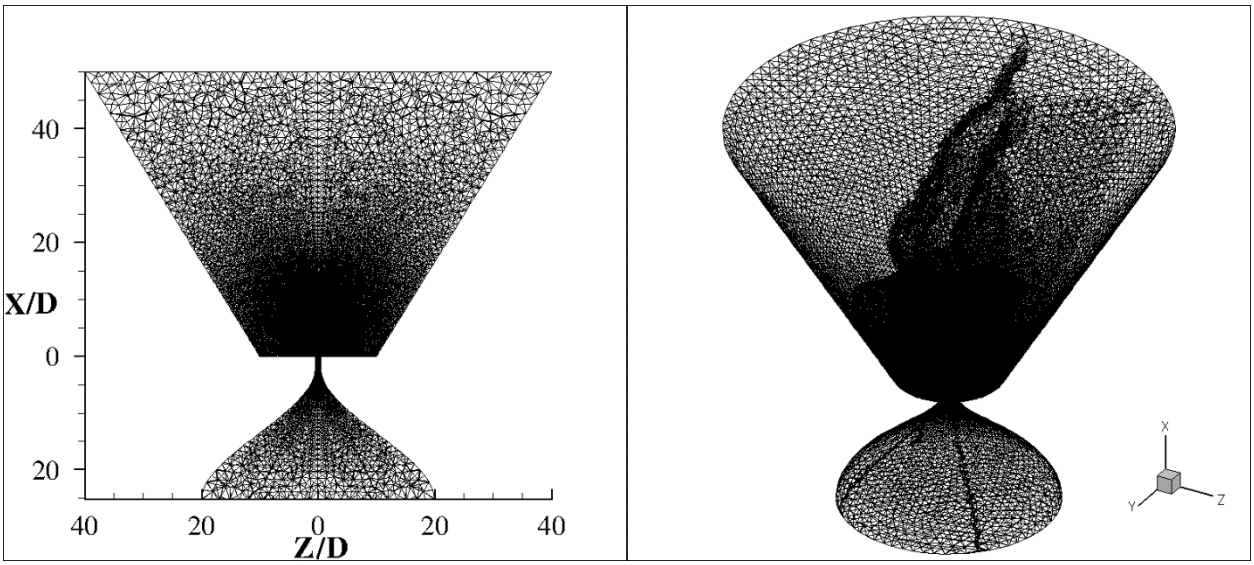

Fig (3. 1): 2D and 3D view of the computational domain for subsonic turbulent jet

numerical methodology here and in reference [40] are different, only qualitative results are considered for validation. The computational domain consists of a hydrogen reservoir and the atmosphere (Fig (3.1)). The release area is considered as an orifice of 5 mm diameter and length of 10 mm. The initial contact surface is 5 mm away from expansion exit. The main computation domain is a frustum with a base diameter of 20D, outer diameter of 80D and a height of 50D. Base on static condition in the reservoir, the pressure inside the reservoir is calculated to have Mach number around 0.3 in throat. The reservoir should be

Simulation	LES simulation – low pressure jet
D (mm)	5
$P_{reservoir}$ ***(Pa)***	113,134
P_{∞} ***(Pa)***	101,325
ρ_{∞} ***(Kg/m^3)***	1.1658
T_{∞} ***(K)***	300
Re_{throat}	11,881
Number of nodes	5,489,557
Number of cells	32,727,004
Maximum cell volume (m^3)	2.63×10^{-12}
Minimum cell volume (m^3)	9.73×10^{-14}
Number of CPU	144
Initial time step (sec)	4.40×10^{-10}
Maximum CFL	50
Elapsed time (hour)	120

Table (3. 1): Computational setup for subsonic turbulent jet simulation

big enough to guarantee static condition inside the reservoir for long time simulation. Table (3.1) reports computational data of this simulation. The applied boundary conditions is no-slip wall inside the reservoir and pressure outlet boundary condition in the far field. (Fig (3.2)). Calculating viscous sub-layer thickness for the case based on Table (3.1), $\frac{\delta_s}{D} = 1.1 \times 10^{-2}$, and also presented results later shows that the employed mesh is satisfactory for capturing this zone. Hence, no-slip wall condition is applied for this low-pressure jet.

To have a good understanding about the position and the shape of the hydrogen cloud as well as turbulence effects, temporal changes of hydrogen concentration for two reference points are monitored at all time steps. These reference nodes are chosen based on Chernyavsky et al. [40] work.

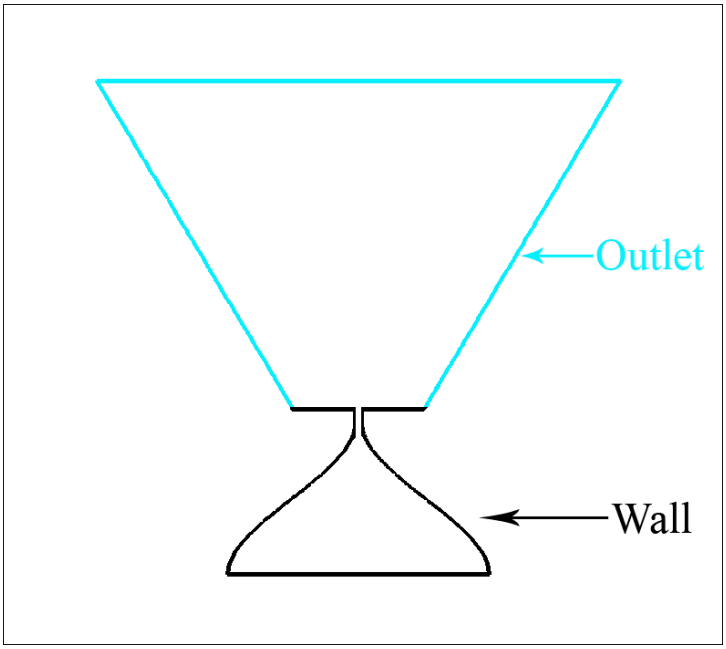

Fig (3. 2): Applied boundary condition for subsonic turbulent jet simulation

3.3 Validation Results

Following, the distribution of concentration and relative density (ρ/ρ_∞), at six different time step are presented in Fig (3.3) and Fig (3.4). Commencing by the hydrogen release in the atmosphere, it generates large scale vortices that transport hydrogen. For early time, this phenomenon is more recognizable in the near field (<4D). Although the cloud has a symmetry shape in early time, wiggles start to deform the cloud after a while. The turbulence and unsteadiness of the flow is clearly captured with our methodology without adding any instability or randomness to the simulation.

In Fig (3.5) the mass fraction at two different downstream reference points during initial jet formation up to 1.46 millisecond is reported and compared with the same graph from [40]. It should be mentioned that in our simulation, concentration is zero in hydrogen side and one in air side. To comfort comparison, in Fig (3.5.c) the reverse value for concentration is illustrated, which is $C' = 0.5-(C-0.5)$. Although the graphs are not exactly the same, the behaviour of turbulence flow is very close. Observing Fig (3.5), the hydrogen cloud reached the reference points almost at the same time for both simulations. To be specific, the hydrogen cloud reached point Y=D/2 and X=2D at 0.25 millisecond but after a short time it started to leave that point. The similar comportment is observed at 0.4 millisecond for Y=D and X=4D.

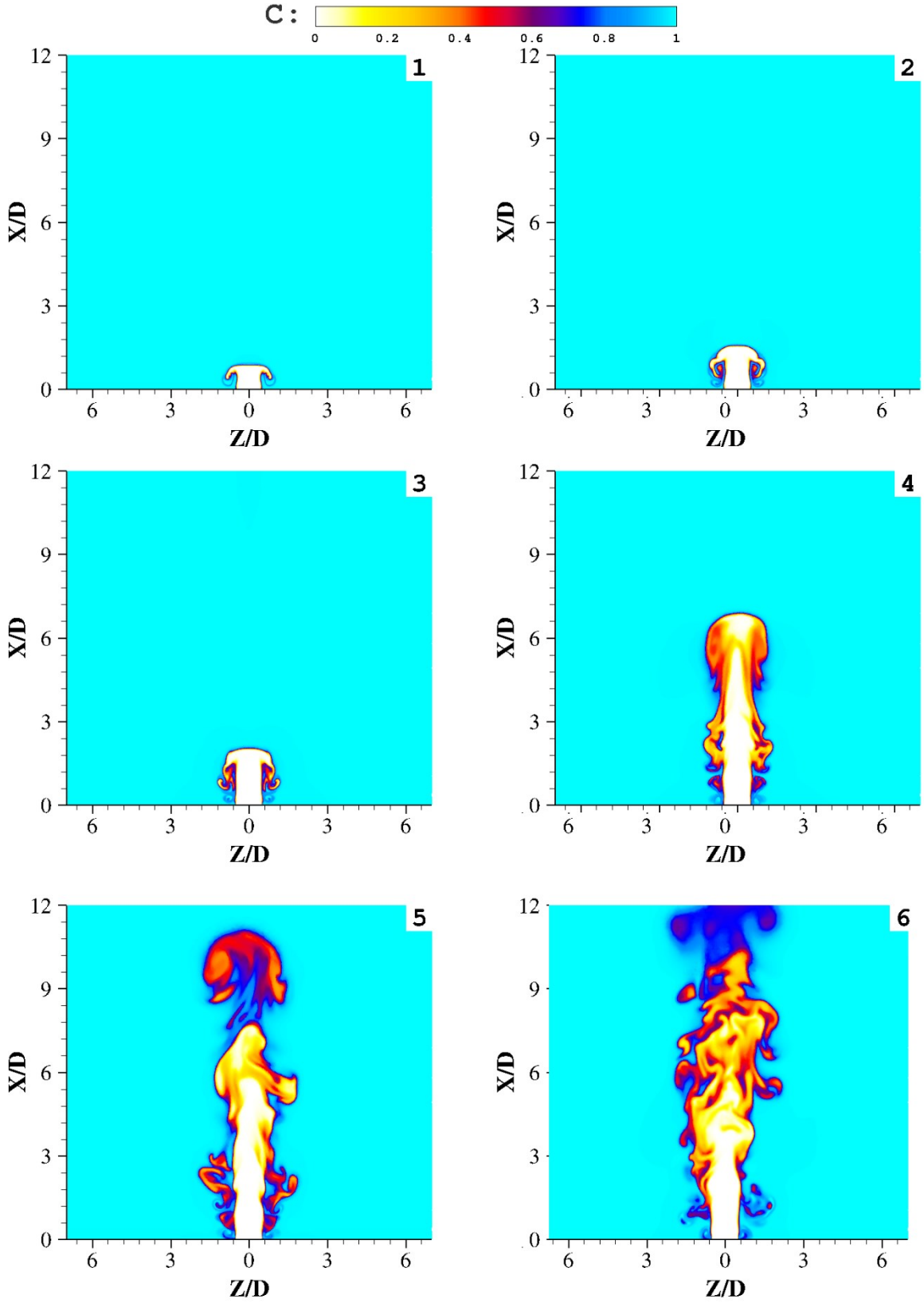

Fig (3. 3): Concentration of a subsonic hydrogen jet release from a 5 mm orifice
1) 0.17, 2) 0.23, 3) 0.27, 4) 0.60, 5) 1.01 and 6) 1.23 millisecond

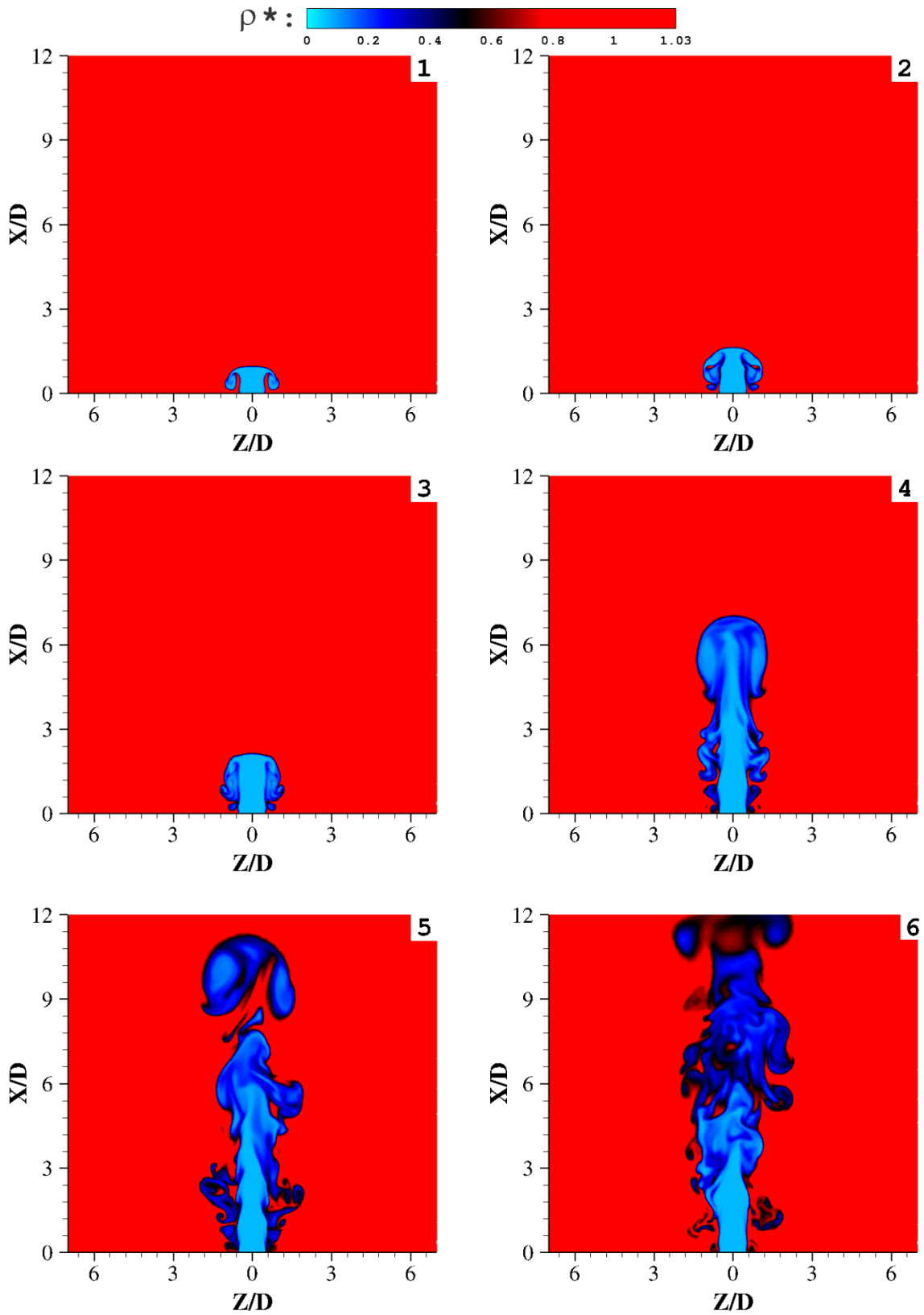

Fig (3. 4): Relative density (ρ/ρ_∞) of a subsonic hydrogen jet release from a 5 mm orifice 1) 0.17, 2) 0.23, 3) 0.27, 4) 0.60, 5) 1.01 and 6) 1.23 millisecond

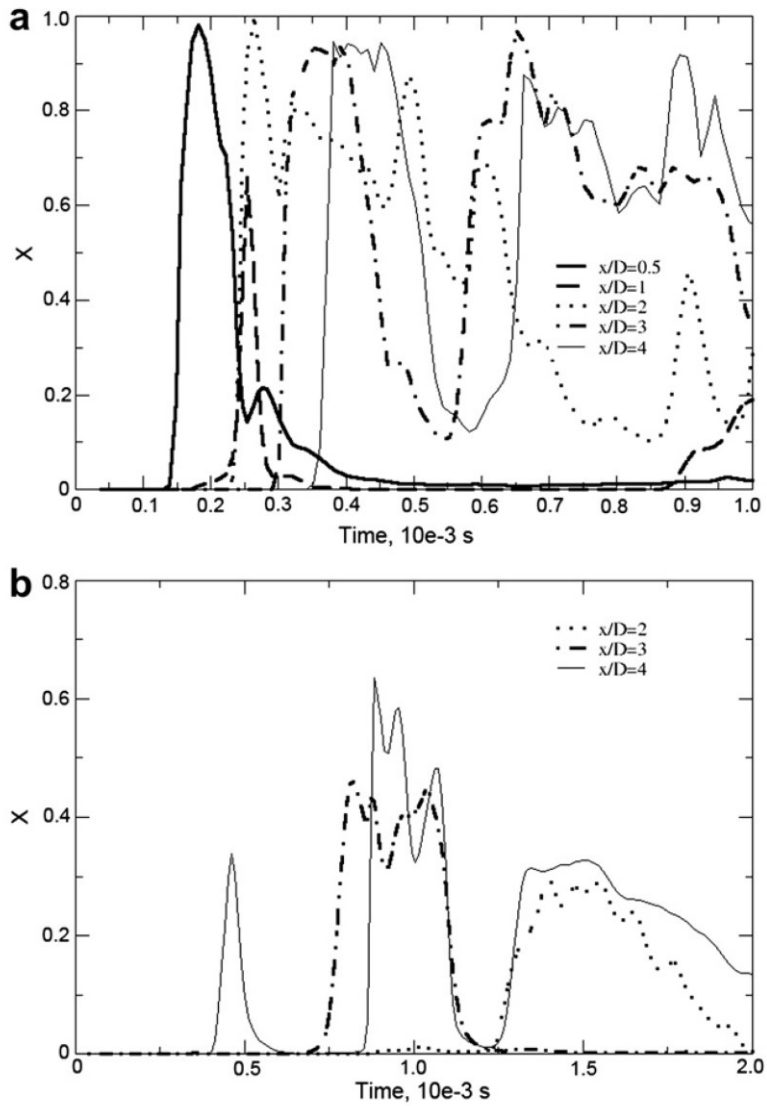

Fig (3. 5): Temporal mass fraction changes at different reference points during initial development of a jet from a 5 mm orifice

a) along line Y=D/2, [40]

b) along line Y=D, [40]

c) validation simulation

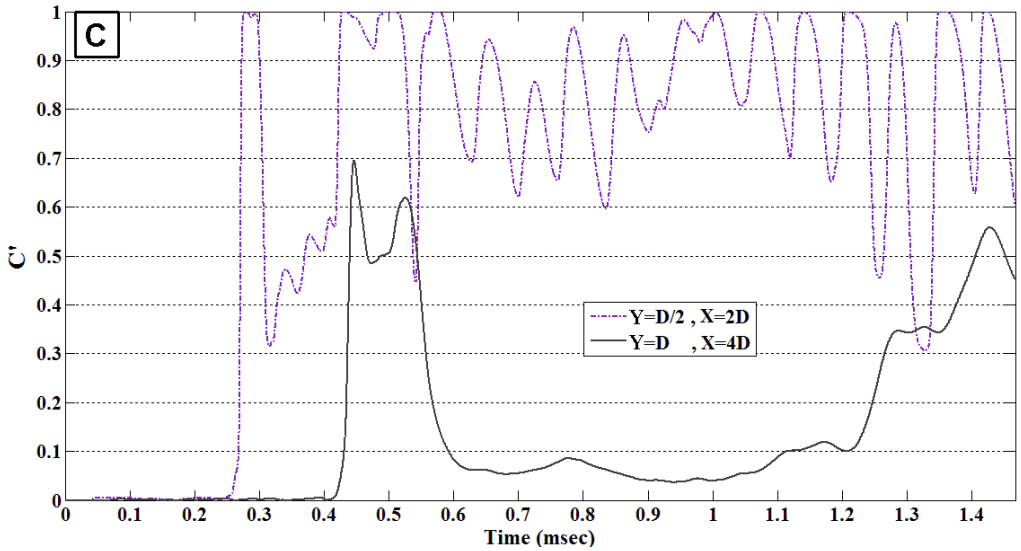

3.4 Conclusion

In this chapter, the transient behaviour of subsonic hydrogen jet was investigated to validate numerical methodology. In this simulation, real gas behaviour was considered for simulation and gravitational force was not considered while second order of accuracy was considered for flux calculation. These are the main differences with study of Chernyavsky et al. [40]. The turbulence behaviour of flow was captured clearly in early millisecond from release by the LES itself without adding any randomness to the simulation. Qualitative comparison showed that the applied LES method has acceptable agreement with literature [40]. The instabilities and radial vortexes were shaped and forced the cloud to expand in the radial direction.

Chapter 4

NUMERICAL SIMULATION

4.1 Problem Definition

The developed in-house code is employed to simulate high pressure release of hydrogen with turbulence effects. The results here corresponds to the release of hydrogen jet via a 1 mm and 5 mm circular orifice from reservoir pressurized with 70 MPa. To have better understanding, the same flow condition is simulated assuming inviscid flow for 5 mm orifice case. The results of these simulations will be compared in this section.

4.1.1 Computational Domain and Grid

The computational domain which is illustrated in Fig (4.1) and Fig (4.2) contains two zones: a high pressure reservoir and a low pressure atmosphere. The ambient part is modeled by a cylinder with size of 60D length and 80D diameter. For the LES simulation, a fine mesh is mandatory. On the other hand, the computational cost is proportional to the size of the mesh. Hence, for both simulations the number of nodes is kept around 11 million

to overcome memory problem while having a fine mesh. It should be mentioned that previously Khaksarfard [43] showed that for inviscid simulation with same conditions, considering 2 million nodes has satisfactory results. Table (4.1) shows the exact number of nodes and cells for each case.

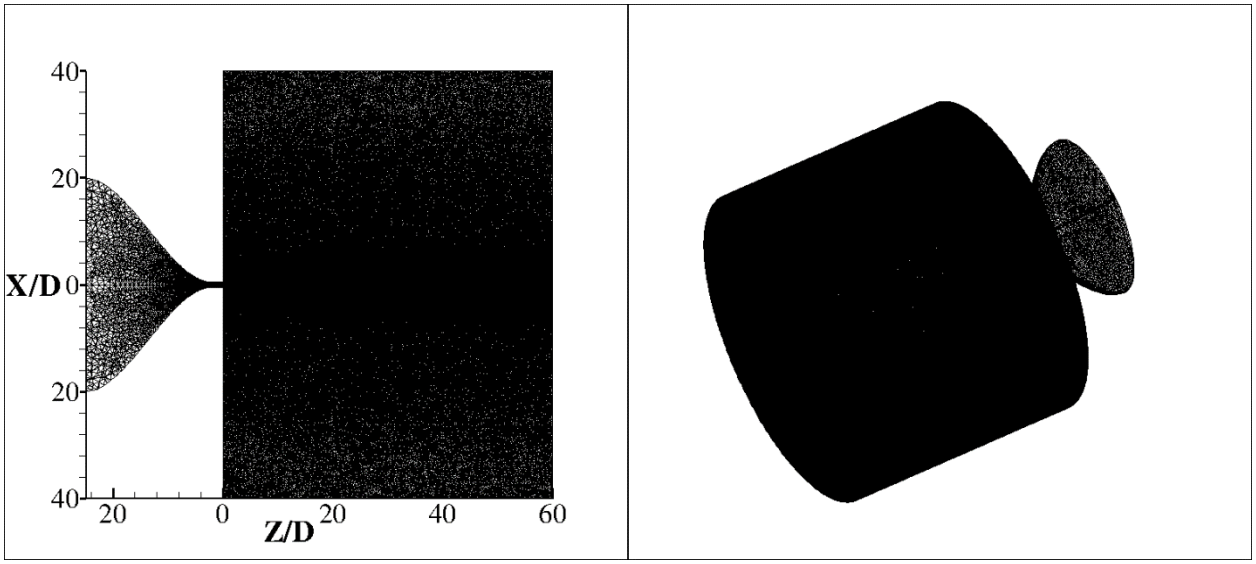

Fig (4. 1): 2D and 3D view of 5 mm orifice case

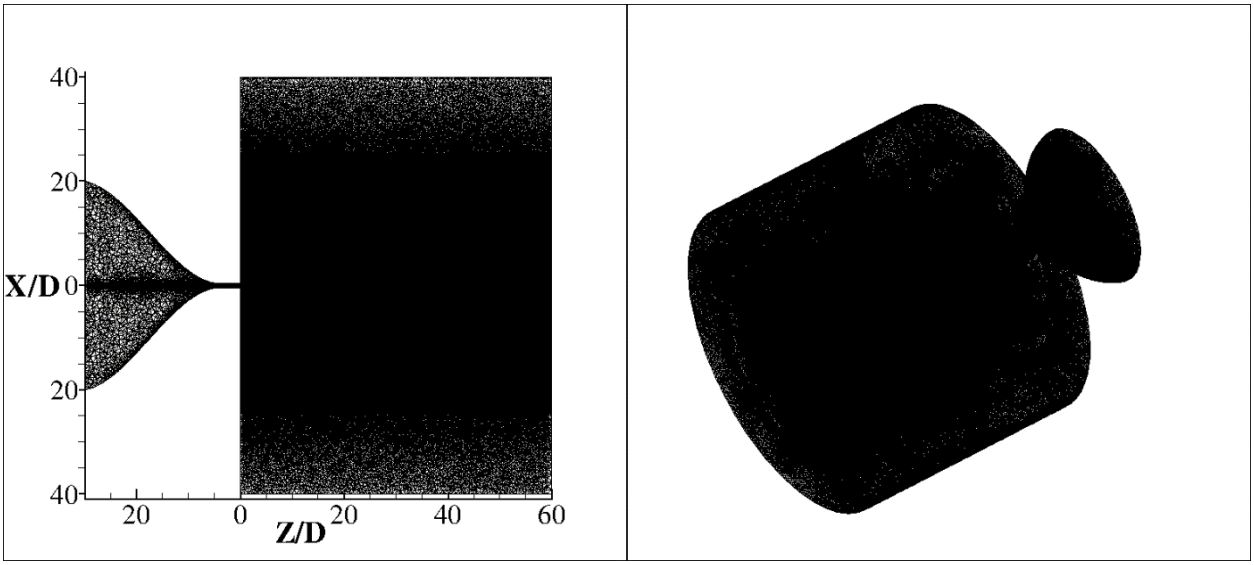

Fig (4. 2): 2D and 3D view of 1 mm orifice case

Orifice size	*Number of nodes*	*Number of cells*	*Minimum cell volume (m^3)*	*Maximum cell volume (m^3)*
5mm	10,903,960	64,922,116	1.10×10^{-11}	7.56×10^{-10}
1mm	11,706,269	69,907,768	4.82×10^{-14}	2.79×10^{-12}

Table (4. 1): Mesh data for sonic turbulent jet simulation

In this simulation, two boundary conditions are employed: wall condition and pressure outlet condition. While simulating viscous flow, the no-slip wall condition inside the reservoir did not allow the flow to develop completely and reach sonic condition, it was decided to choose slip wall condition inside the reservoir and the release area, while the outside wall has no-slip condition. This problem was discussed in Chapter 2. Fig (4.3) shows applied boundary conditions.

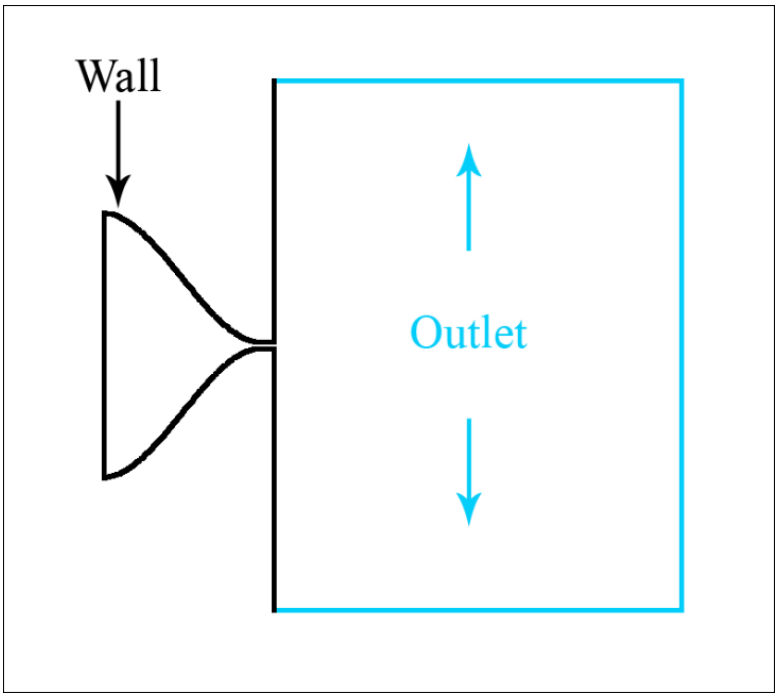

Fig (4. 3): Applied boundary condition for sonic turbulent jet simulation

4.1.2 Numerical Setup

The fluid in the reservoir side is hydrogen while air occupied the atmosphere side. For all simulations, the initial contact surface is at 5 mm away from the exit. It is assumed that all thermodynamic properties are distributed homogeneously and hydrogen and air are real gases. Initially, the flow in all domains is at rest with a temperature of 300 K. Two different orifice size for a 70 MPa reservoir are examined to investigate turbulence flow regime. All the computational conditions are listed in Table (4.2).

	Case 1	*Case 2*	*Case 3*
Simulation	Inviscid flow	Viscous flow	Viscous flow
D (mm)	5		1
$P_{reservoir}$ ***(Pa)***	70×10^6		
P_∞ ***(Pa)***	101,325		
ρ_∞ ***(Kg/m^3)***	1.1658		
T_∞ ***(K)***	300		
Re_{throat}	1.39×10^7		2.78×10^6
Number of CPU	144		
Initial time step (sec)	3.61×10^{-10}		7.38×10^{-11}
Maximum CFL	50	30	15
Elapsed time (hour)	70	100	120

Table (4. 2): Computational setup for sonic turbulent jet simulation

In this table, Re_{throat} is calculated based on the choked condition at the throat and stagnation condition inside reservoir, considering steady state condition.

4.2 Numerical Results

In following as usual practice in fluid dynamics, the following non-dimensional quantities are used for data presentation and analysis:

$$\rho^* = \frac{\rho}{\rho_\infty} \quad , \quad P^* = \frac{P}{P_\infty} \quad , \quad T^* = \frac{T}{T_\infty} \tag{4.1}$$

Where subscript ∞ indicates ambient initial properties, as it was shown in Table (4. 2).

4.2.1 Part one: 5 mm orifice

The distribution of density, pressure, Mach number, concentration and temperature are presented at six different times in Fig (4.4) to Fig (4.8). In these figures, the LES and inviscid flow simulation are compared. To have better insight, value of density, pressure, Mach number, concentration and temperature on centerline are presented at six different times in Fig (4.9) to Fig (4.13).

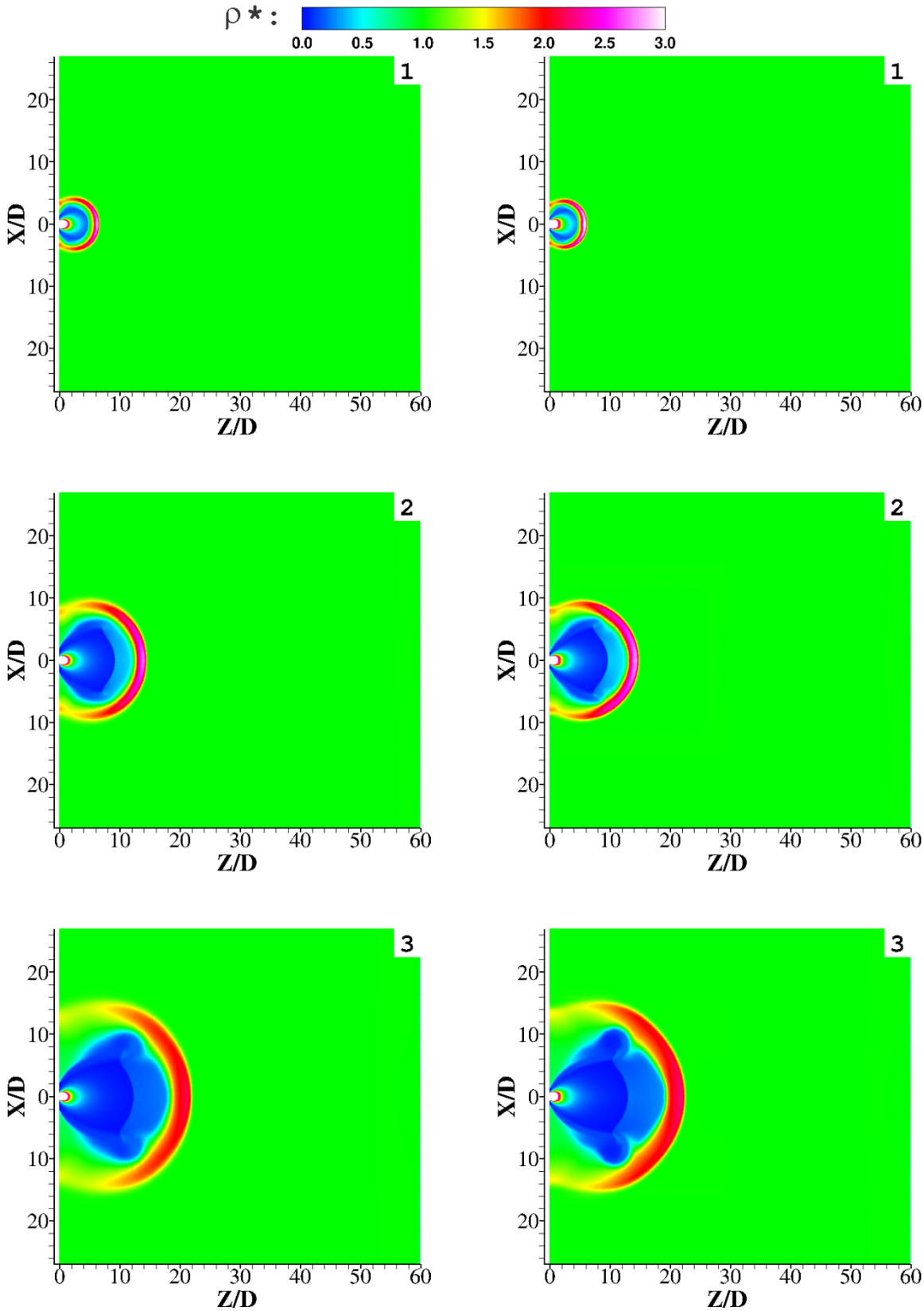

Fig (4. 4): ρ* of hydrogen jet (70 MPa) release from 5mm orifice: LES (left) and inviscid (right) 1) 25, 2) 70, 3)125, 4)160, 5)200 and 6) 250 microsecond

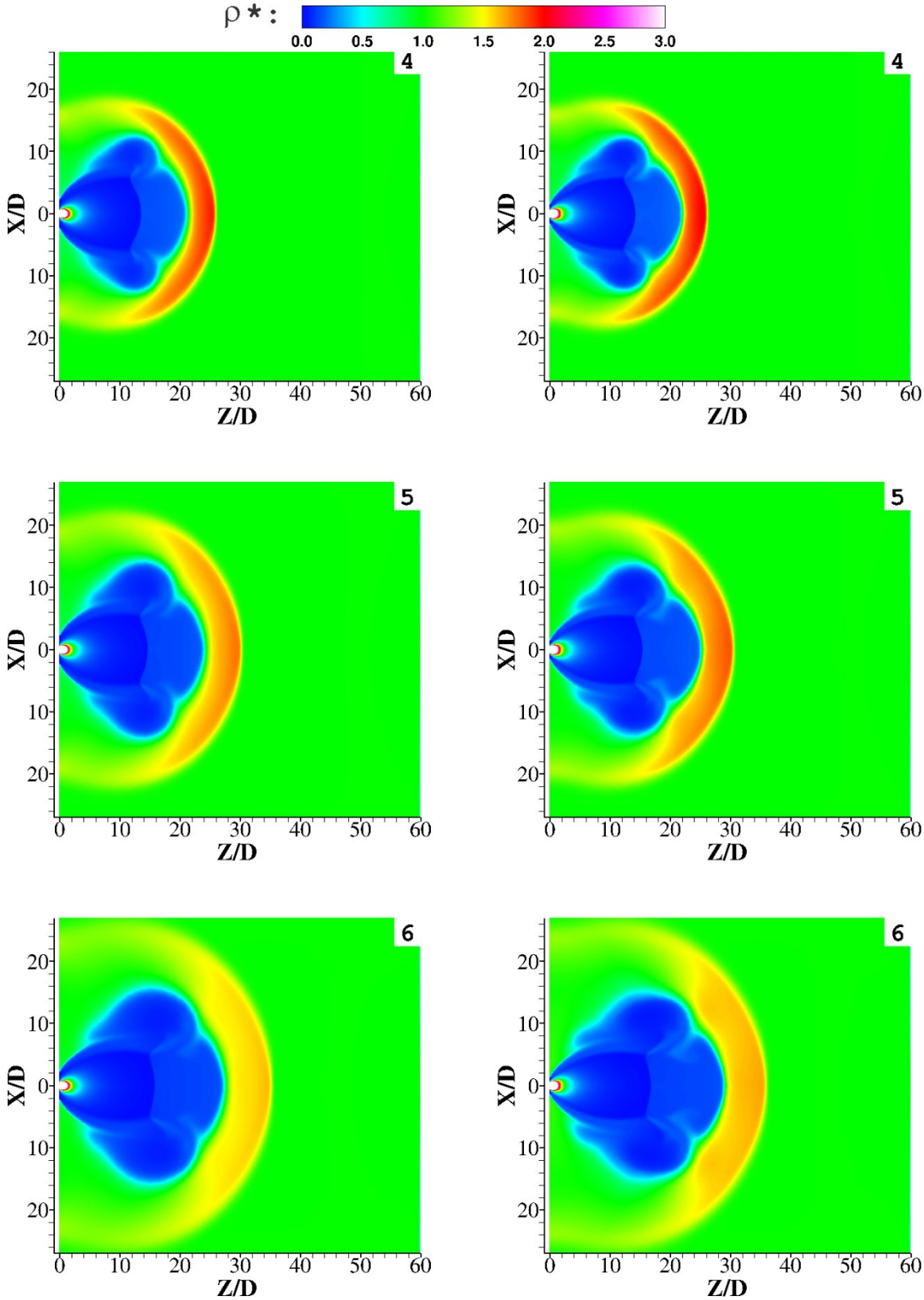

Fig (4.4): ρ* of hydrogen jet (70 MPa) release from 5mm orifice: LES (left) and inviscid (right)

1) 25, 2) 70, 3)125, 4)160, 5)200 and 6) 250 microsecond **(continue)**

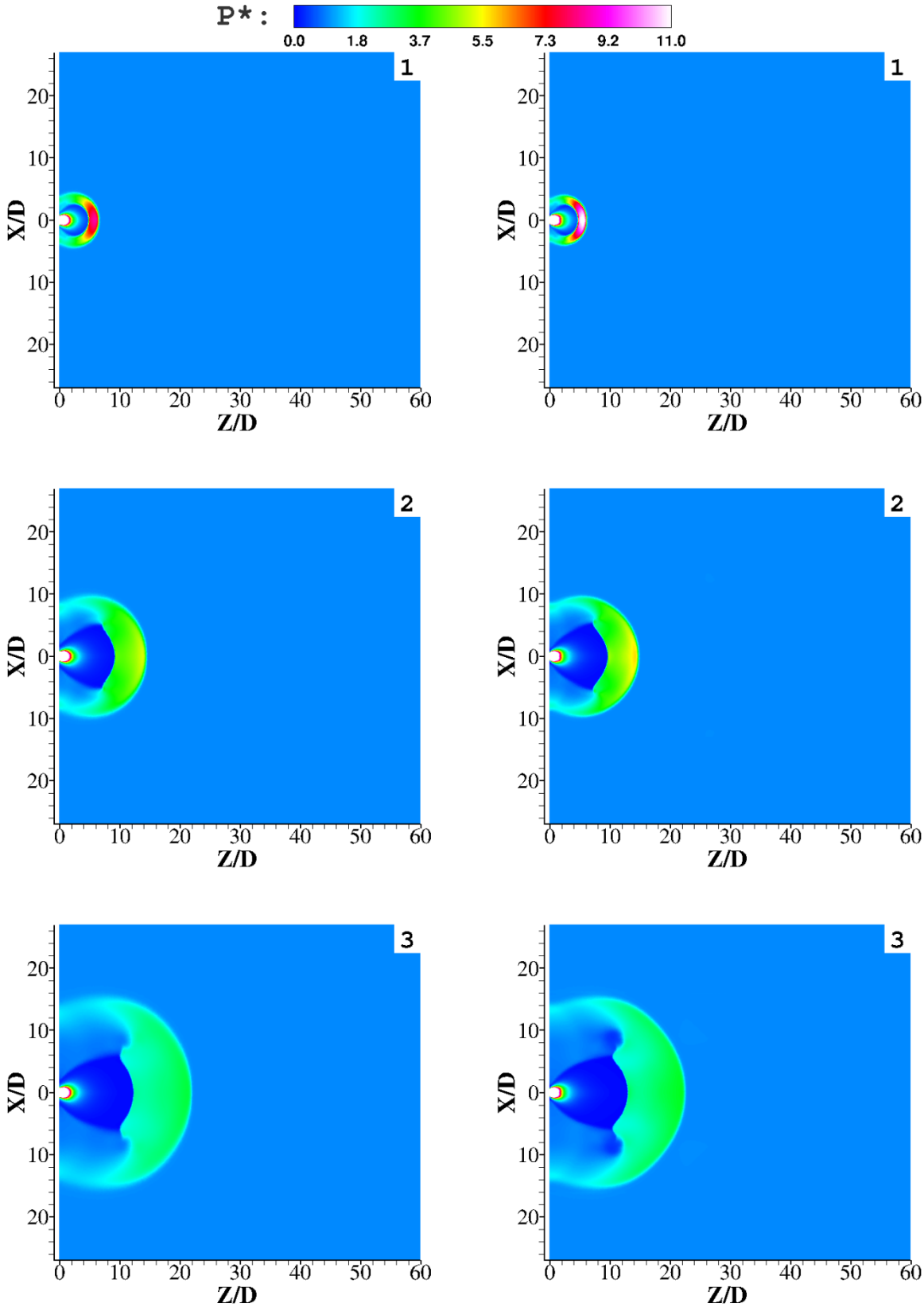

Fig (4. 5): P* of hydrogen jet (70 MPa) release from 5mm orifice: LES (left) and inviscid (right) 1) 25, 2) 70, 3)125, 4)160, 5)200 and 6) 250 microsecond

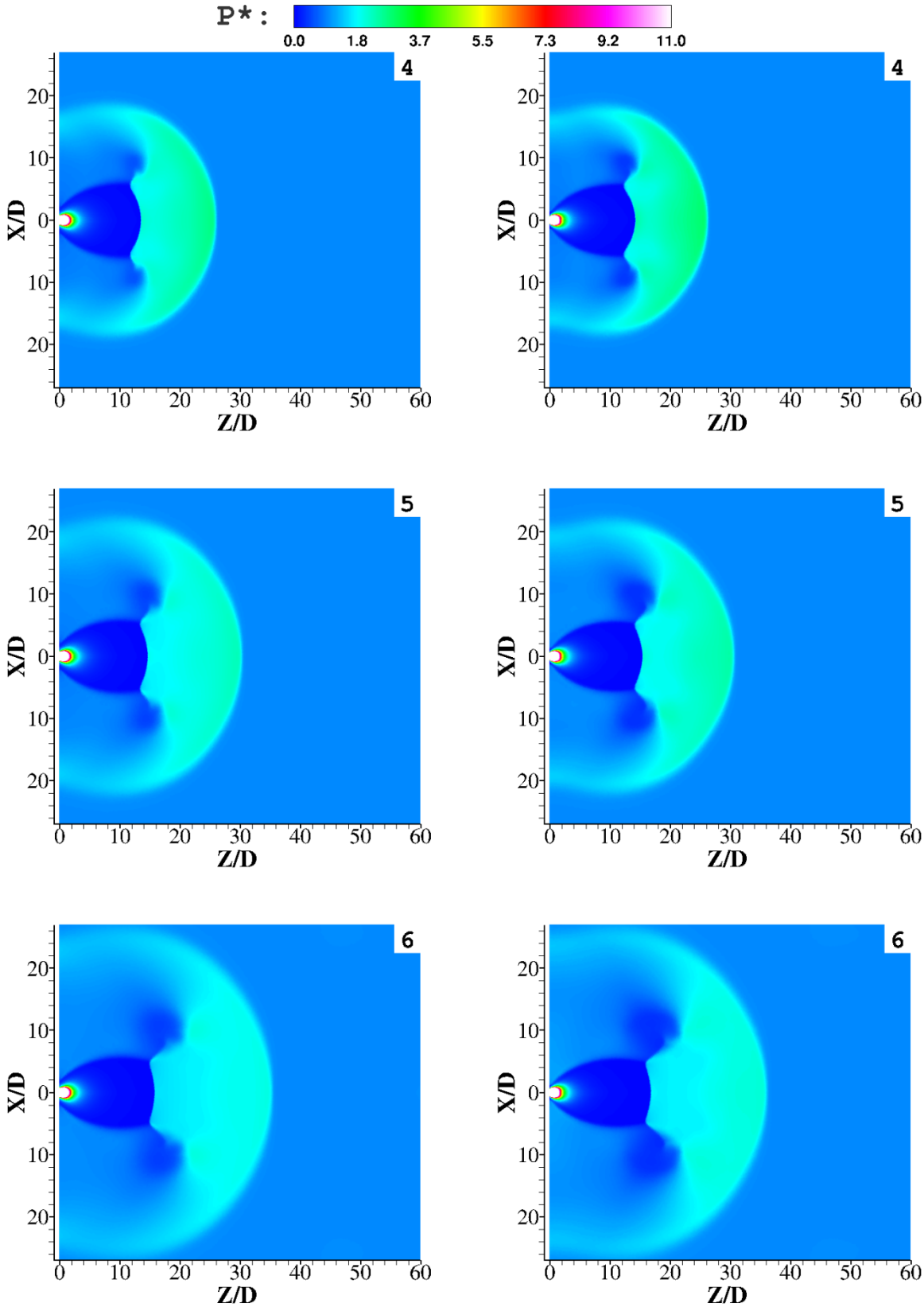

Fig (4.5): P* of hydrogen jet (70 MPa) release from 5mm orifice: LES (left) and inviscid (right) 1) 25, 2) 70, 3)125, 4)160, 5)200 and 6) 250 microsecond **(continue)**

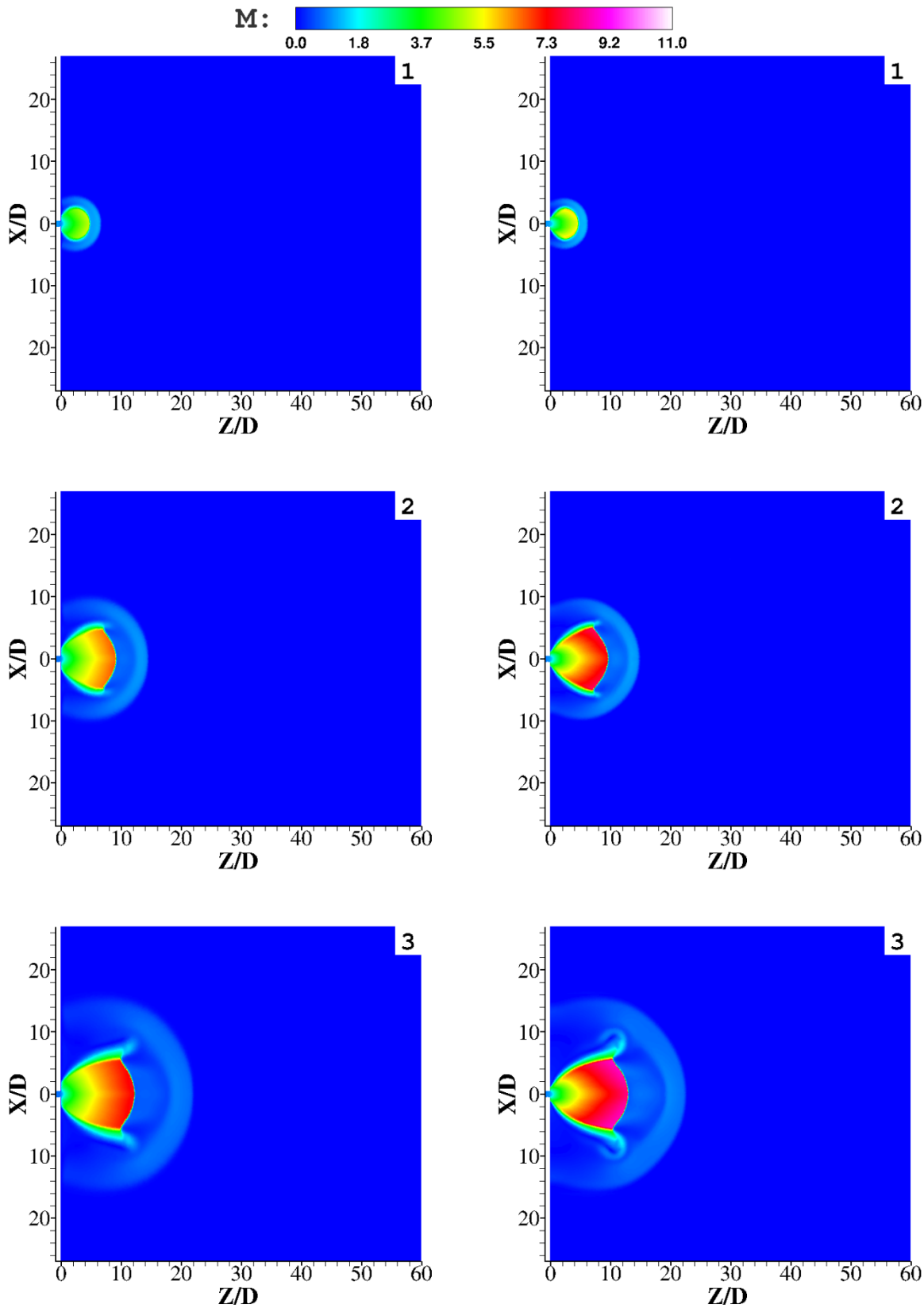

Fig (4. 6): Mach number of hydrogen jet (70 MPa) release from 5mm orifice: LES (left) and inviscid (right) 1) 25, 2) 70, 3)125, 4)160, 5)200 and 6) 250 microsecond

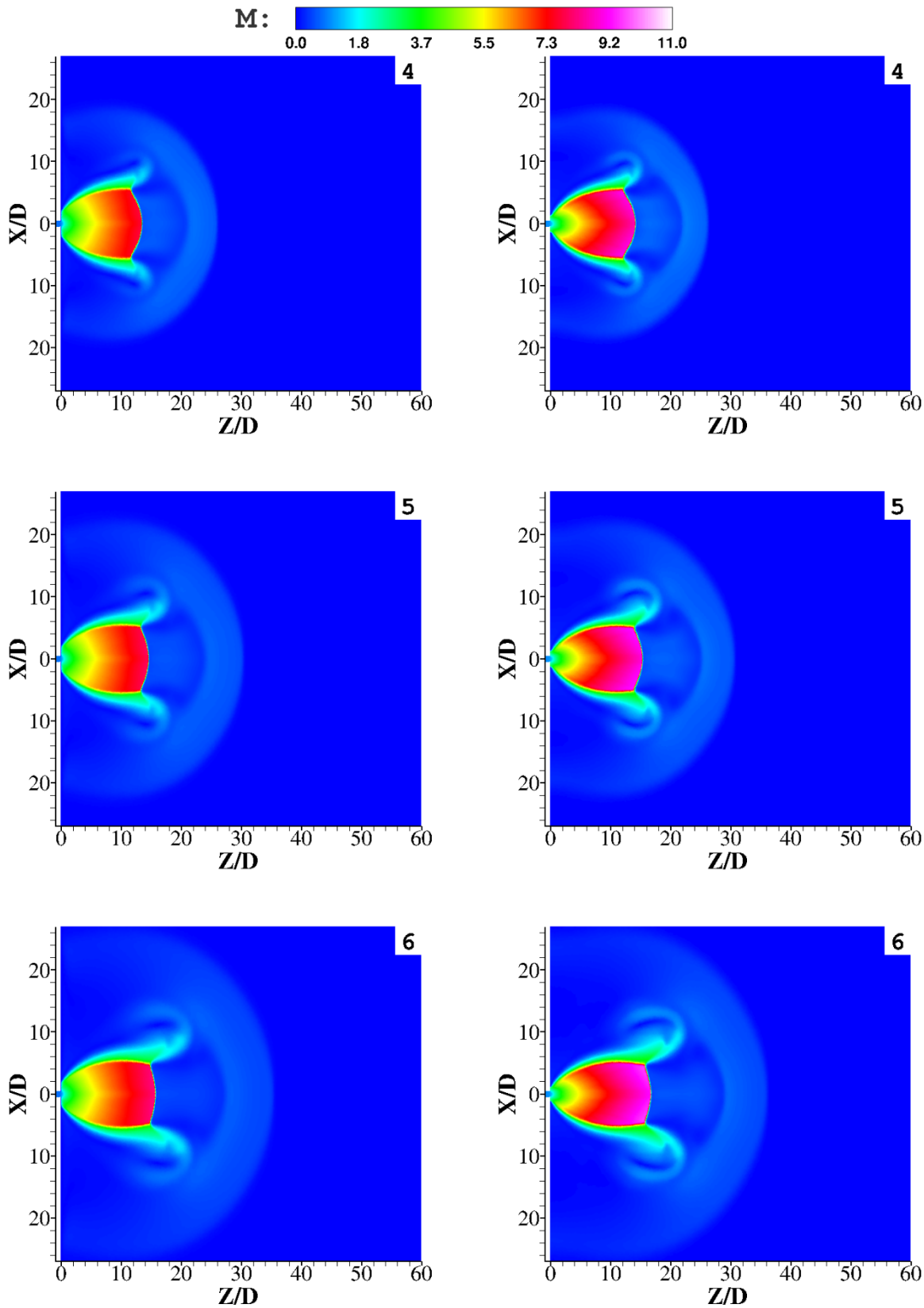

Fig (4.6): Mach number of hydrogen jet (70 MPa) release from 5mm orifice: LES (left) and inviscid (right) 1) 25, 2) 70, 3)125, 4)160, 5)200 and 6) 250 microsecond **(continue)**

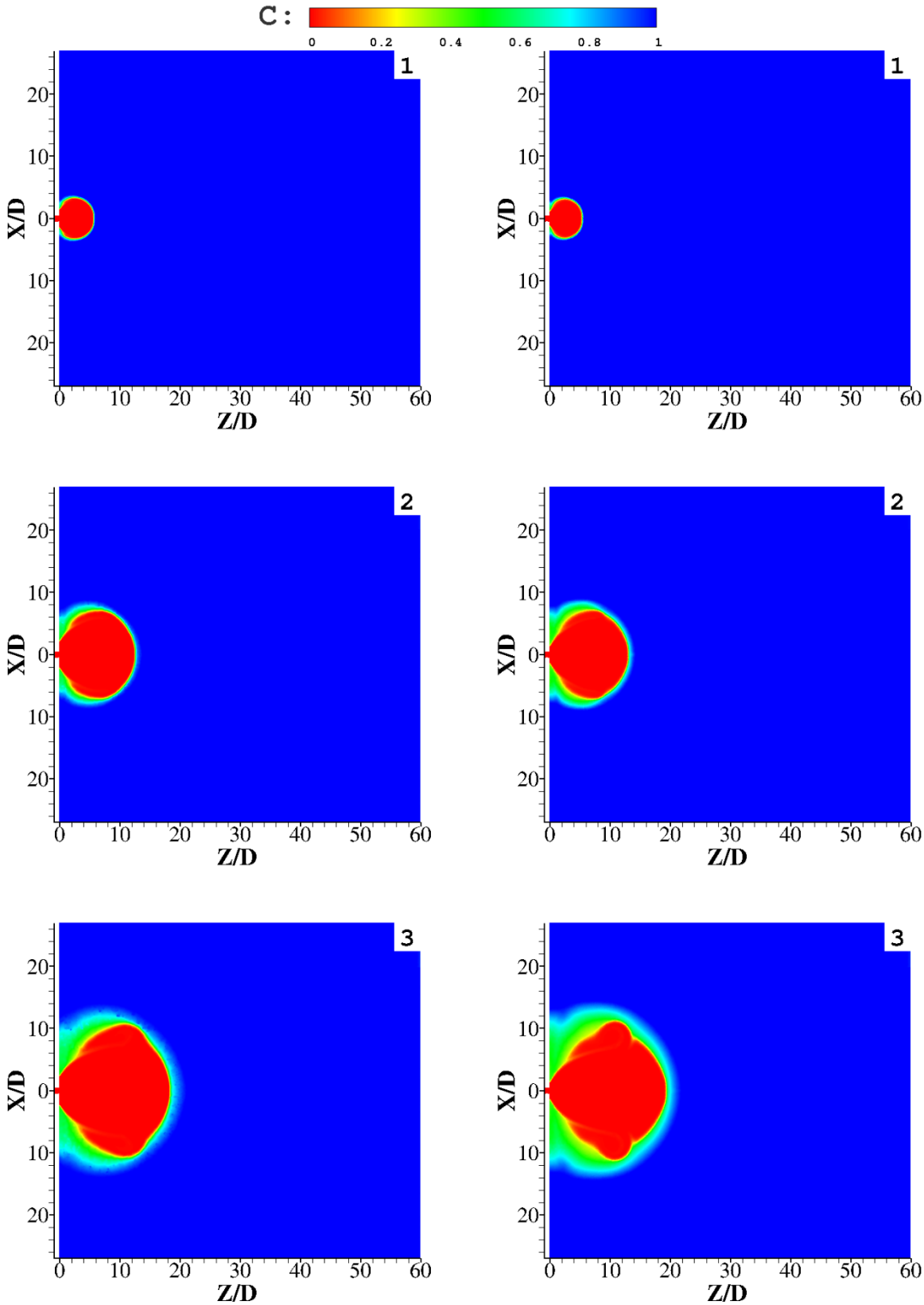

Fig (4. 7): Concentration of hydrogen jet (70 MPa) release from 5mm orifice: LES (left) and inviscid (right) 1) 25, 2) 70, 3)125, 4)160, 5)200 and 6) 250 microsecond

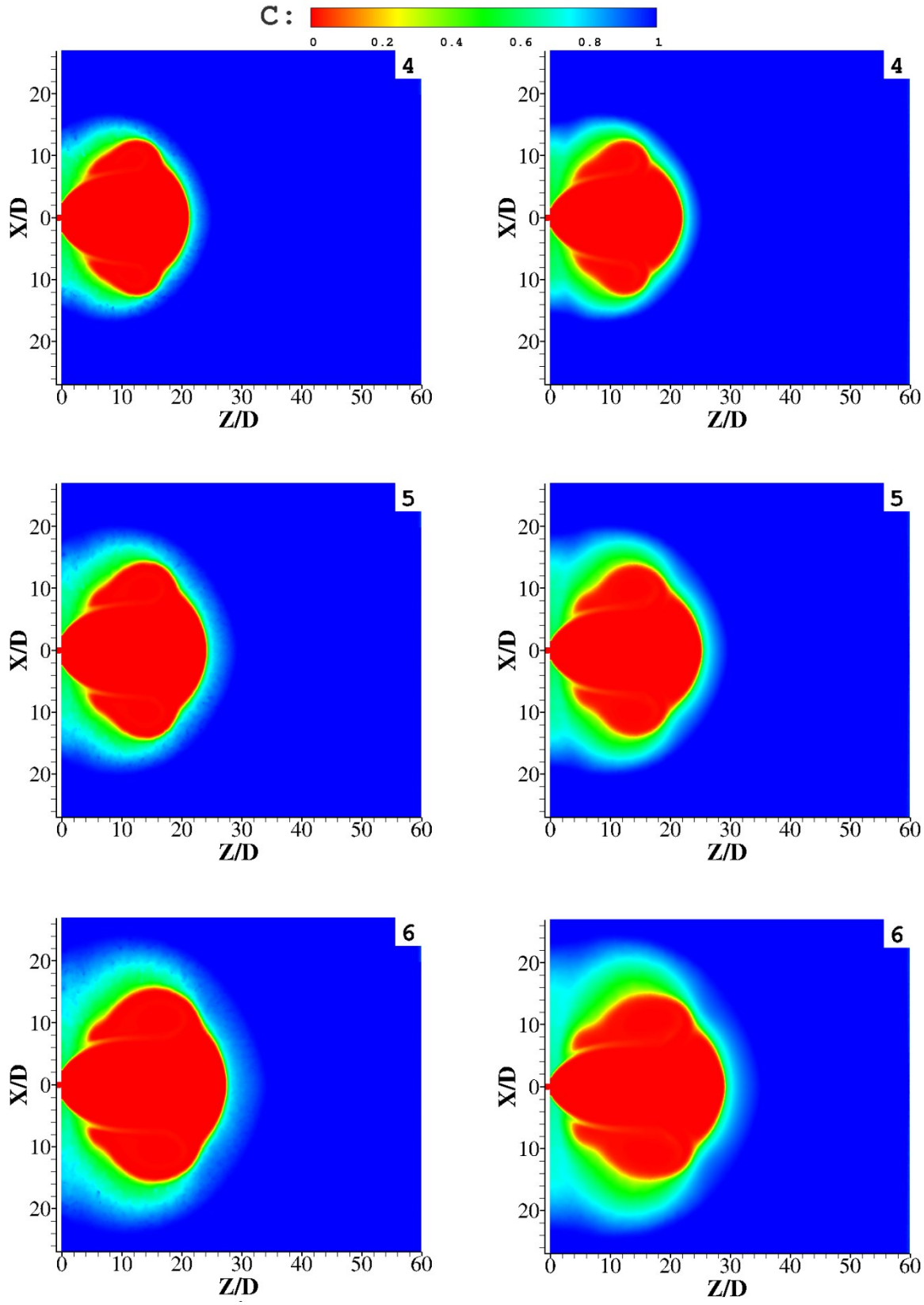

Fig (4.7): Concentration of hydrogen jet (70 MPa) release from 5mm orifice: LES (left) and inviscid (right) 1) 25, 2) 70, 3)125, 4)160, 5)200 and 6) 250 microsecond **(continue)**

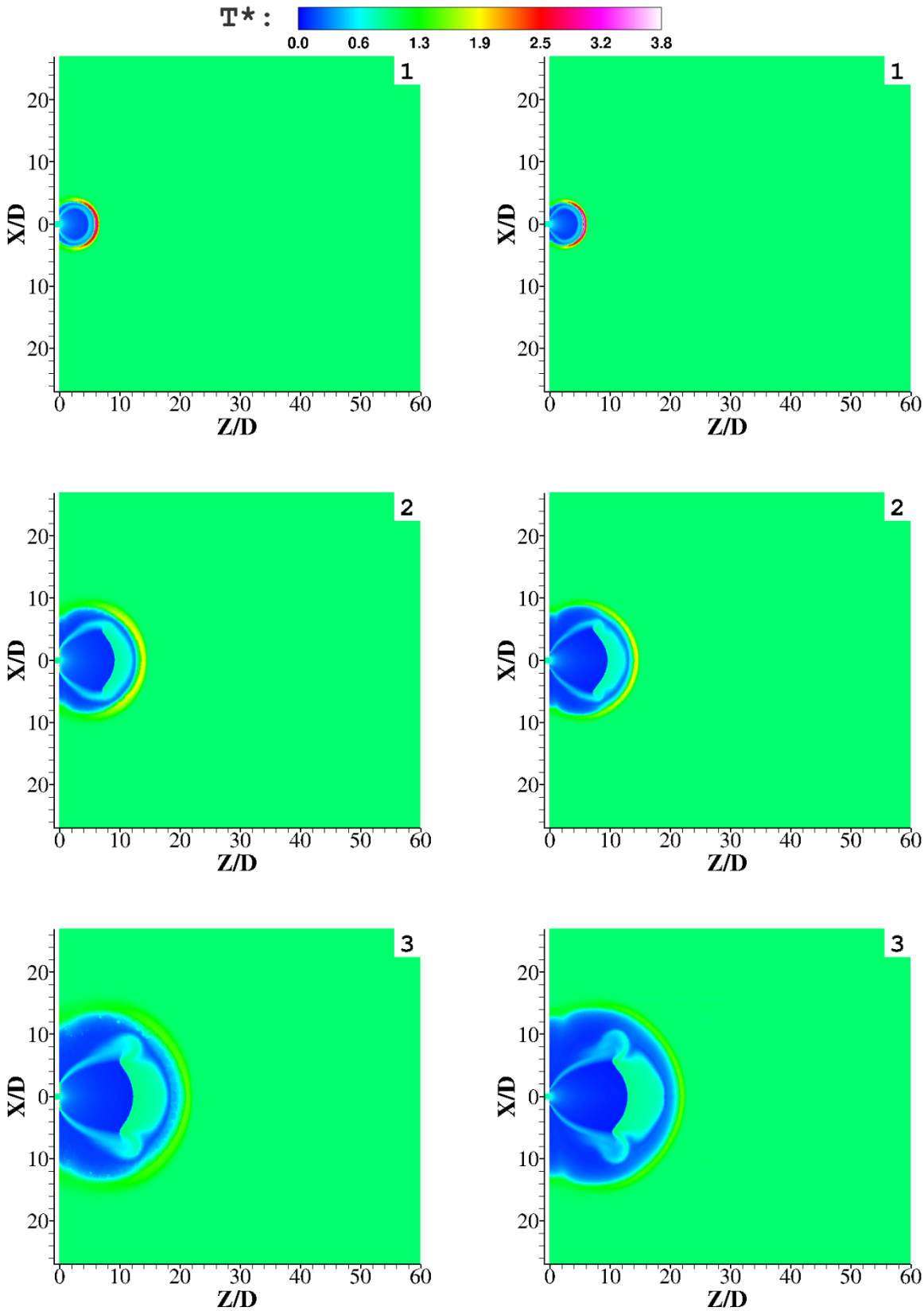

Fig (4. 8): T* of hydrogen jet (70 MPa) release from 5mm orifice: LES (left) and inviscid (right) 1) 25, 2) 70, 3)125, 4)160, 5)200 and 6) 250 microsecond

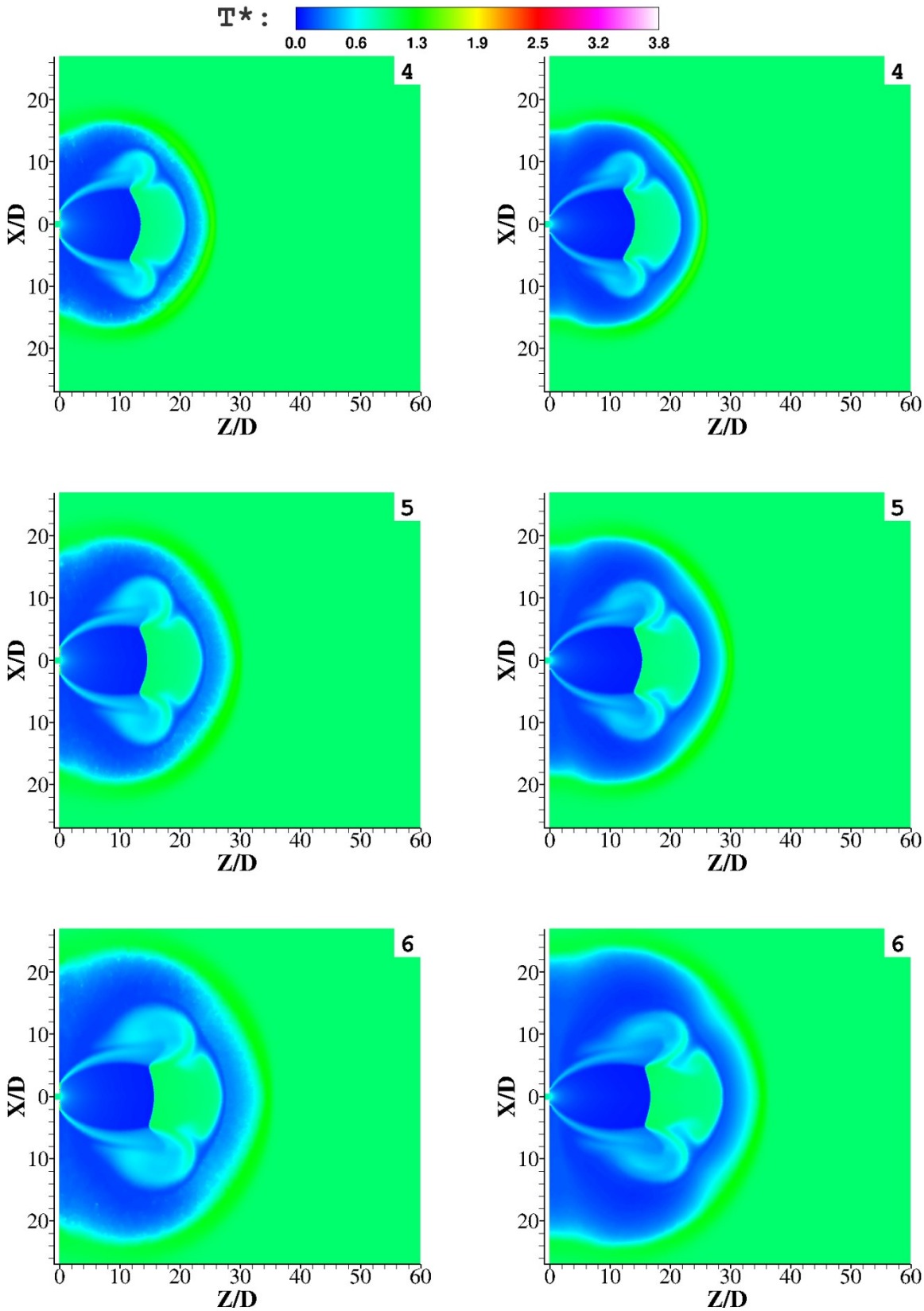

Fig (4.8): T* of hydrogen jet (70 MPa) release from 5mm orifice: LES (left) and inviscid (right) 1) 25, 2) 70, 3)125, 4)160, 5)200 and 6) 250 microsecond **(continue)**

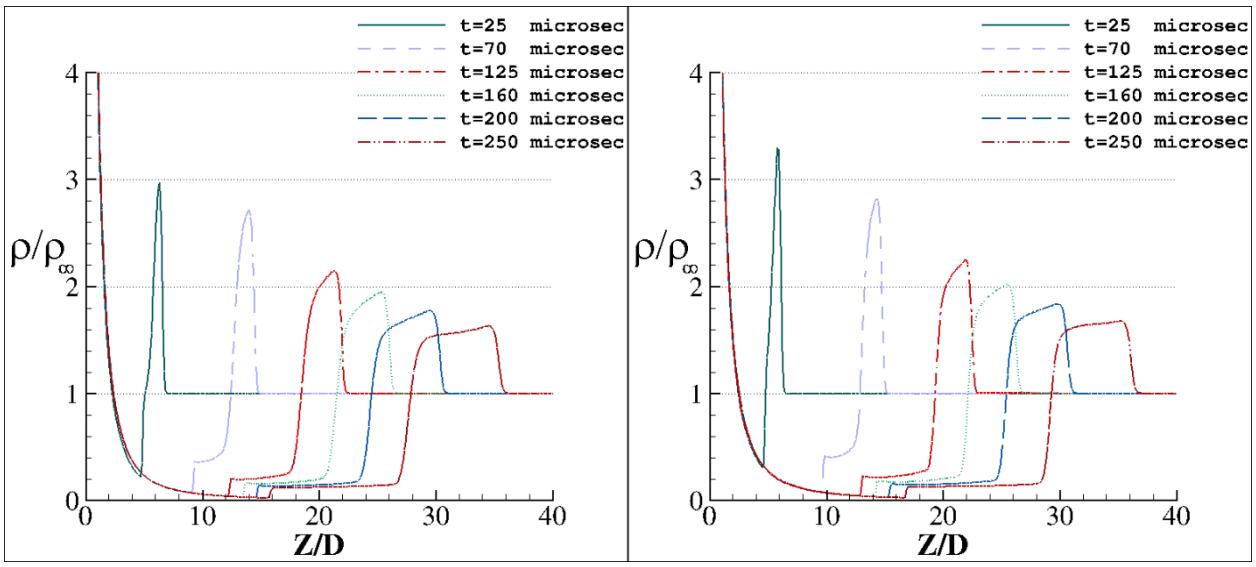

Fig (4. 9): ρ* along centerline, 70 MPa hydrogen jet release from 5mm orifice: LES (left) and inviscid (right) simulation

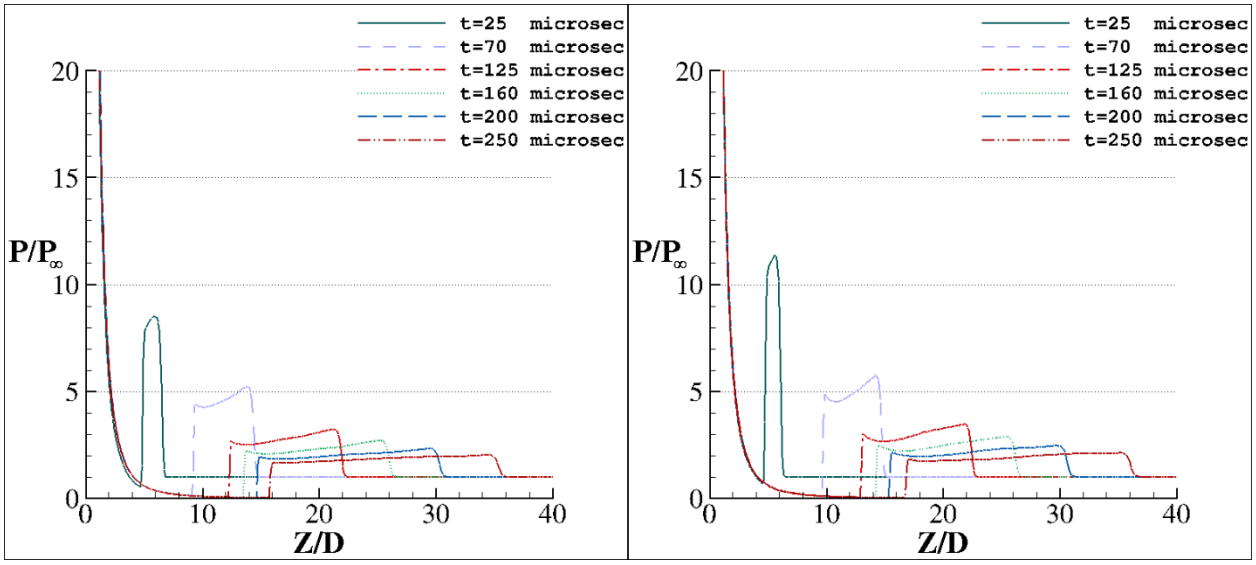

Fig (4. 10): P* along centerline, 70 MPa hydrogen jet release from 5mm orifice: LES (left) and inviscid (right) simulation

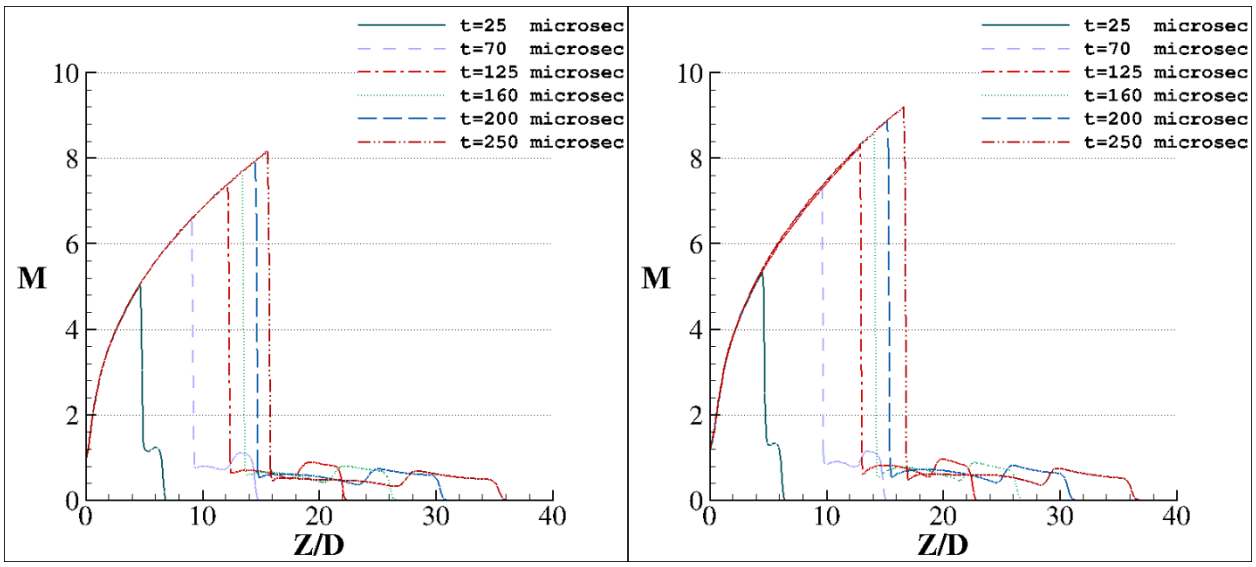

Fig (4. 11): Mach number along centerline, 70 MPa hydrogen jet release from 5mm orifice: LES (left) and inviscid (right) simulation

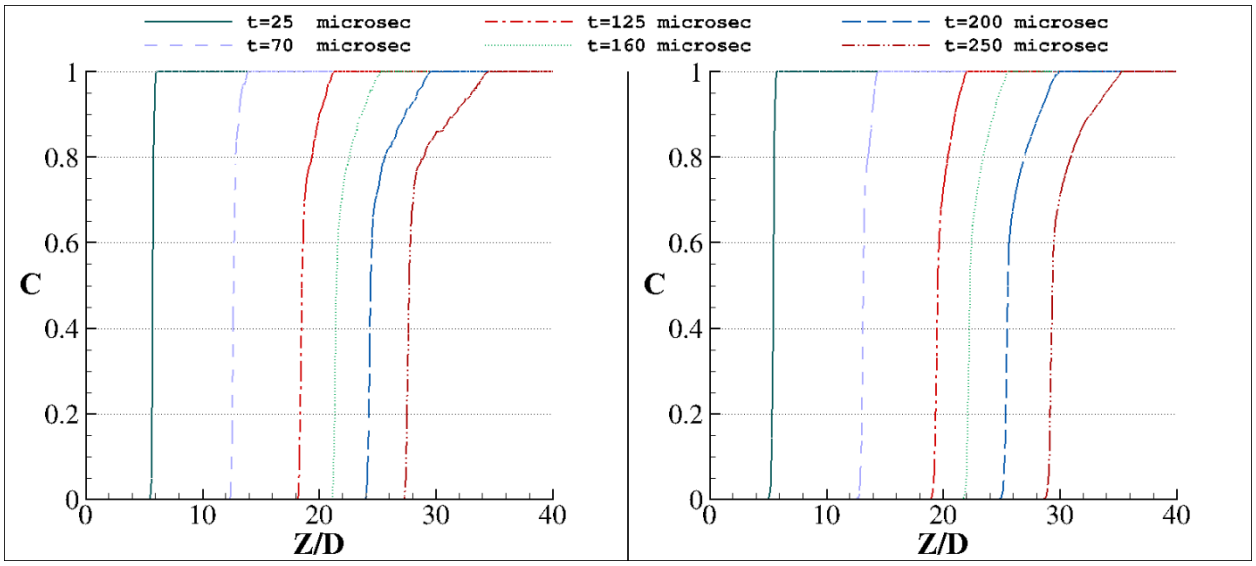

Fig (4. 12): Concentration along centerline, 70 MPa hydrogen jet release from 5mm orifice: LES (left) and inviscid (right) simulation

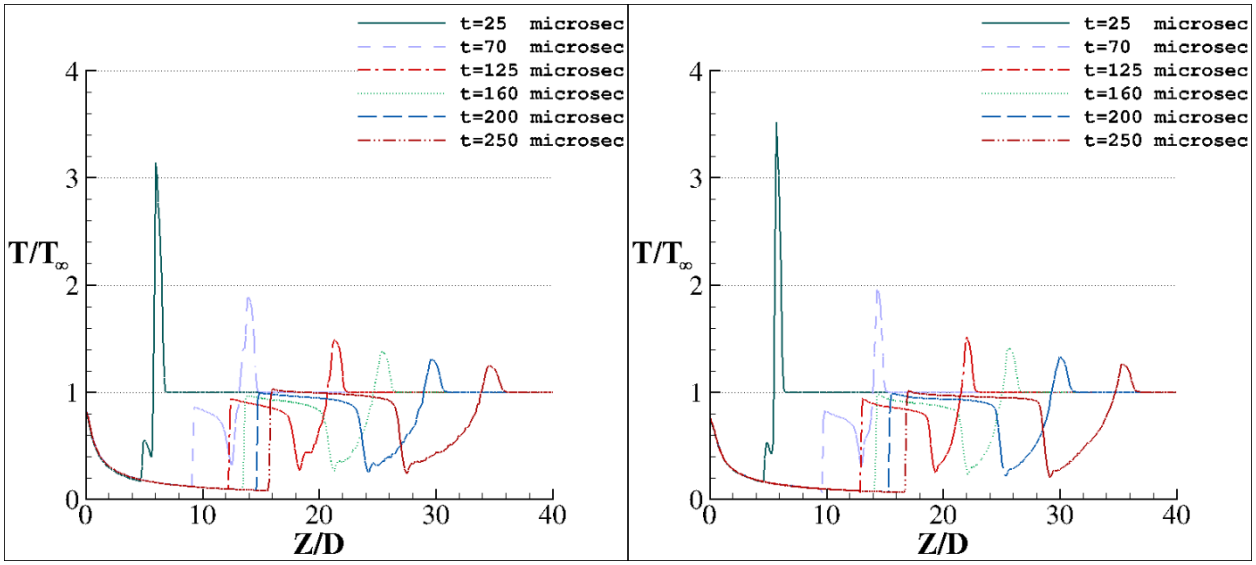

Fig (4. 13): T* along centerline, 70 MPa hydrogen jet release from 5mm orifice: LES (left) and inviscid (right) simulation

Reviewing the results, it seems that the early time jet for the LES and inviscid simulation are very similar. The lead shock has same speed for both simulations. By way of illustration, at 25 microsecond it is located close to 7D from the exit and 36D at 250 microsecond after release for both simulation. The maximum value of density, pressure and Mach number inside the computational field has bigger value in inviscid simulation which shows there is stronger lead shock in this simulation. The hydrogen cloud also has similar behaviour for both simulation. We do not observe more mixing in these earlier stages of release. Reviewing concentration along centerline, the hydrogen cloud behind the lead shock travels at same speed. Considering longer time of simulation, in the inviscid simulation, the hydrogen cloud is a little faster. The turbulent flow has smaller maximum peak temperature which is very important for auto ignition study as this indicated that the inviscid simulation is a worst case scenario. Also, in the radial direction, these two regimes show similar behaviour up to this time.

Fig (4.14) presents the upwinding coefficient for the LES simulation at 250 microsecond. As it is shown, there is a region in front of lead shock where the full-upwinding scheme is applied. Nevertheless, most part of computational field has upwinding parameter less than 0.4 which means that there is very little artificial viscosity added from the upwind term. It should remind that in the LES simulation the second order approximation is imposed all over the domain except a small region near exit area (2D×2D×D)

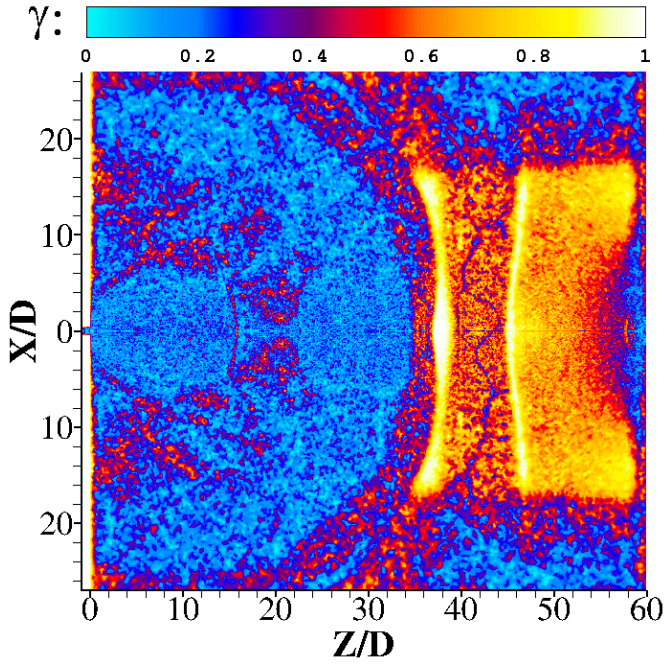

Fig (4. 14): Upwinding parameter, 70 MPa hydrogen jet release from 5mm orifice after 250 microsecond

In this part, the LES simulation is repeated with smaller Smagorinsky subgrid model's constant (C_s). In previous simulations, C_s was 0.001 while it is reduced to 0.0001 in this part. These values are chosen based on [44]. Following, the centerline values of density, pressure, Mach number, concentration and temperature of sonic hydrogen jet simulation with C_s=0.0001 are illustrated in Fig (4.15), compared with different Smagorinsky constant simulation in two different time steps. Clearly, the field solution for both case up to this time are very close. This declare that we have very little turbulence, hence the Smagorinsky constant has very little influence.

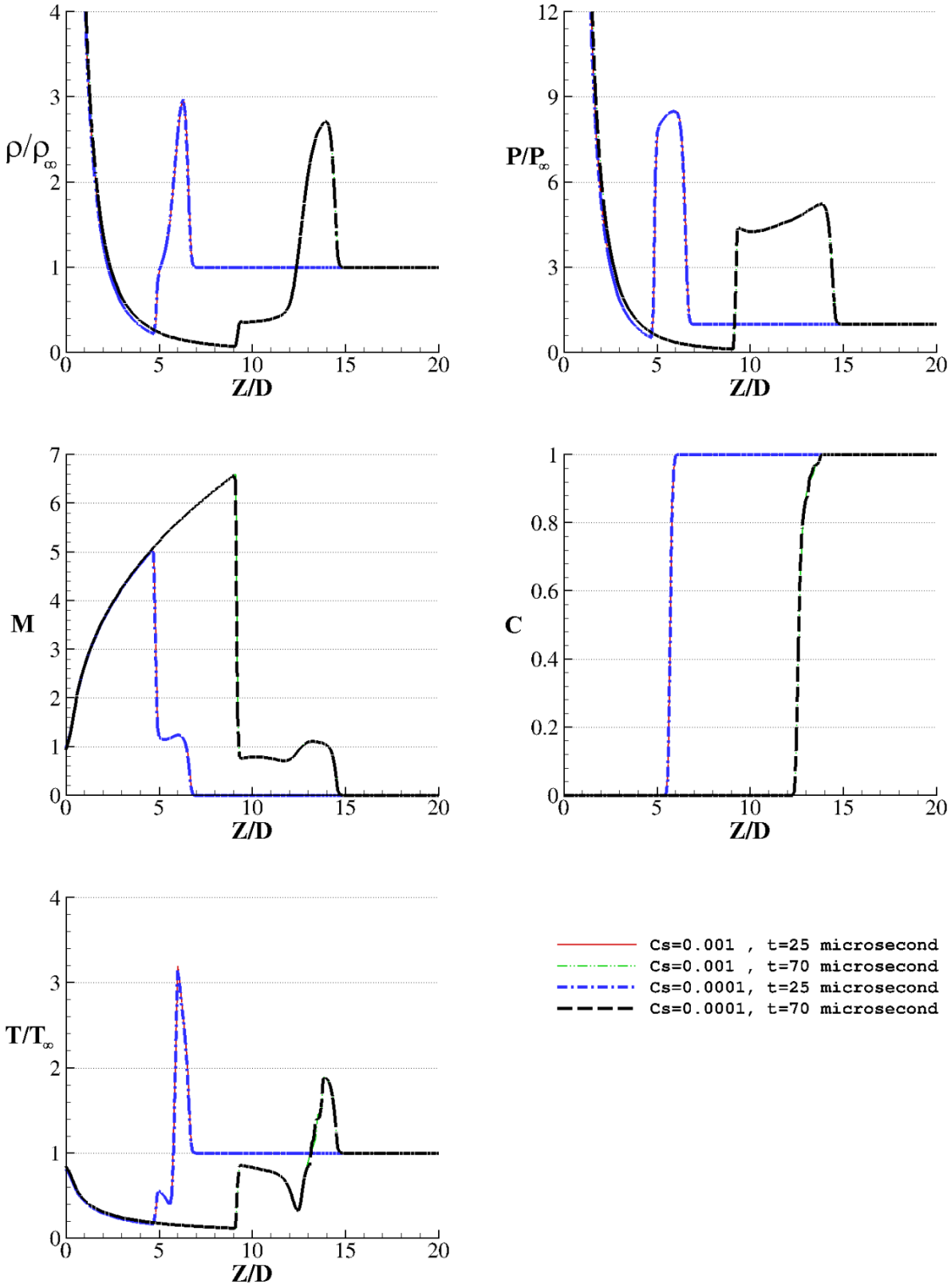

Fig (4. 15): Centerline values of 70 MPa hydrogen jet release from 5mm orifice, LES simulation, Smagorinsky constant comparison

4.2.2 Part two: 1 mm orifice

In this part, the field value and value along centerline of density, pressure, Mach number, concentration and temperature of high pressure (70 MPa) hydrogen jet release from a 1-mm-orifice are presented for the LES simulation at two different times in Fig (4.21) to Fig (4.26). As we can see, in smaller orifice release the flow develops very fast and the lead shock is weaker in comparison with the 5 mm orifice. Although the initial pressure ratio is very high, there is small temperature ratio in computational domain, which reduce the chance of auto ignition and is more conservative. It is quite evident that the viscous forces have very little effect on this flow for the early release.

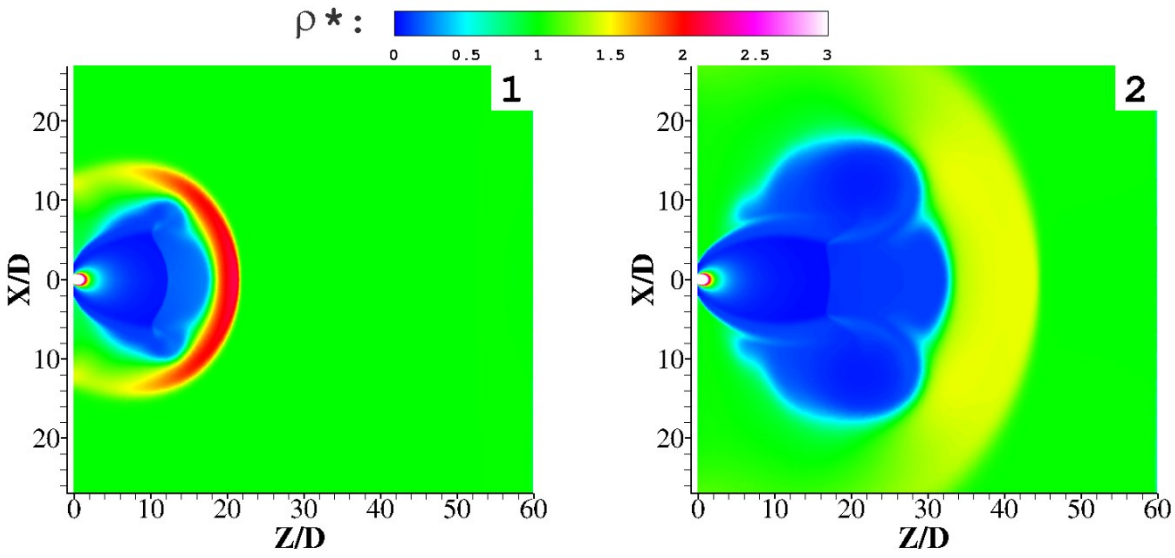

Fig (4. 16): ρ* of hydrogen jet (70 MPa) release from 1mm orifice: LES simulation
1) 25, 2) 70 microsecond

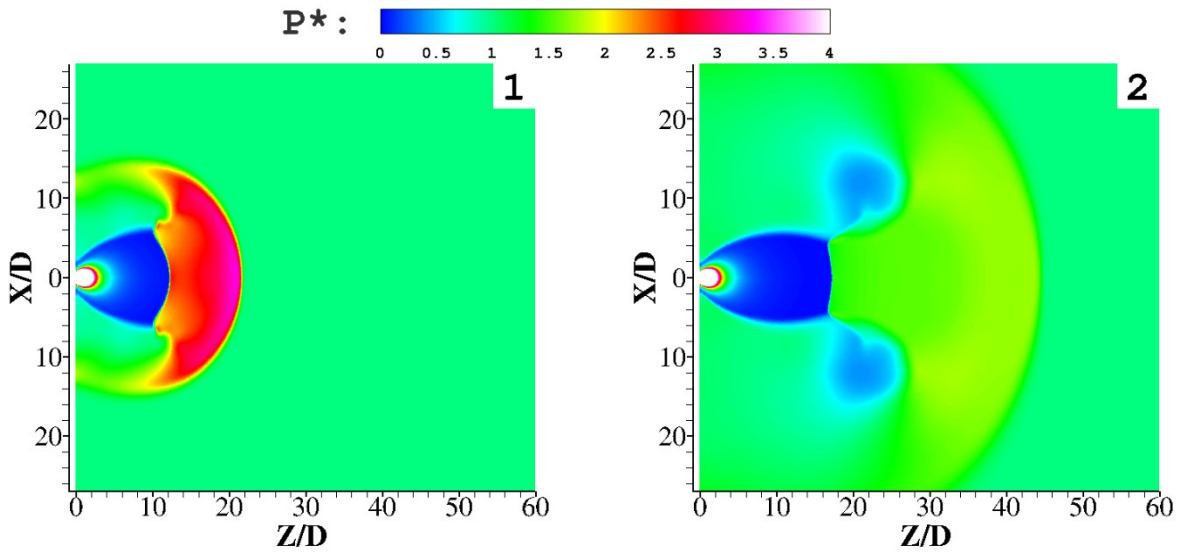

Fig (4. 17): P* of hydrogen jet (70 MPa) release from 1mm orifice: LES simulation

1) 25, 2) 70 microsecond

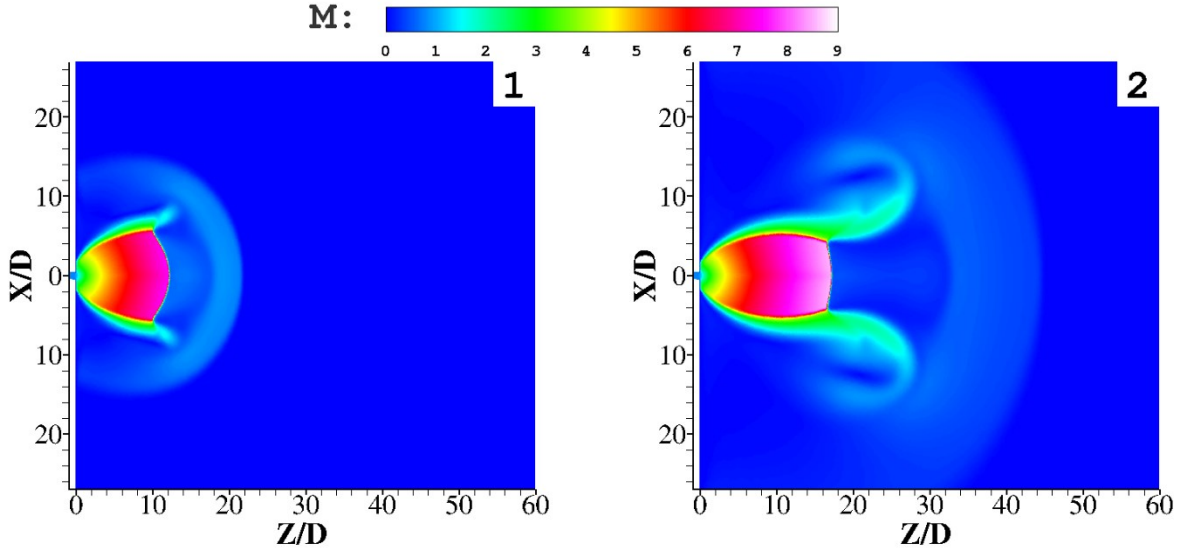

Fig (4. 18): Mach number of hydrogen jet (70 MPa) release from 1mm orifice: LES simulation

1) 25, 2) 70 microsecond

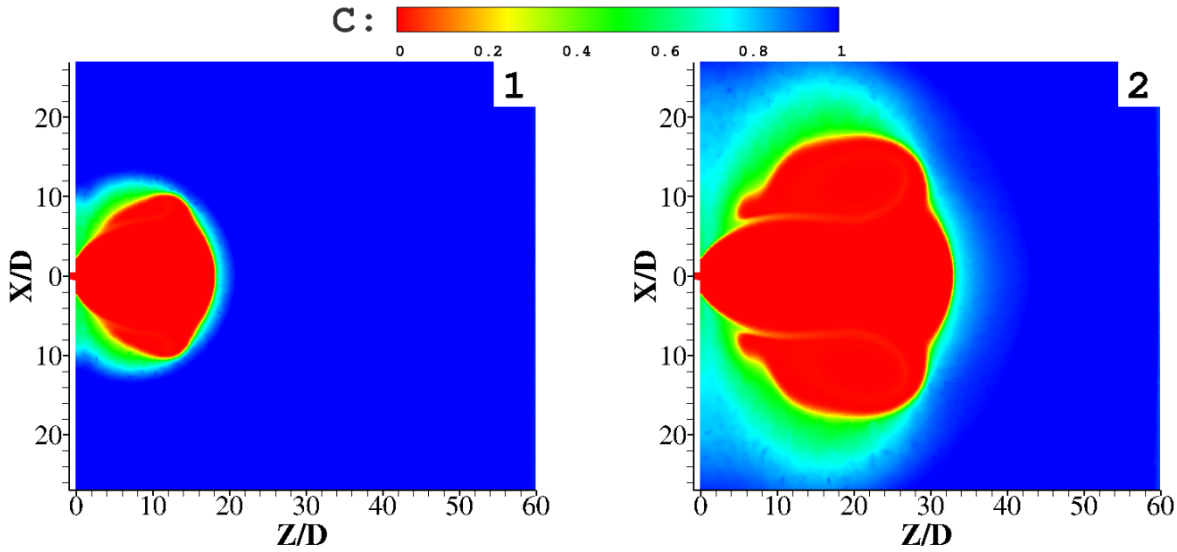

Fig (4. 19): Concentration of hydrogen jet (70 MPa) release from 1mm orifice: LES simulation 1) 25, 2) 70 microsecond

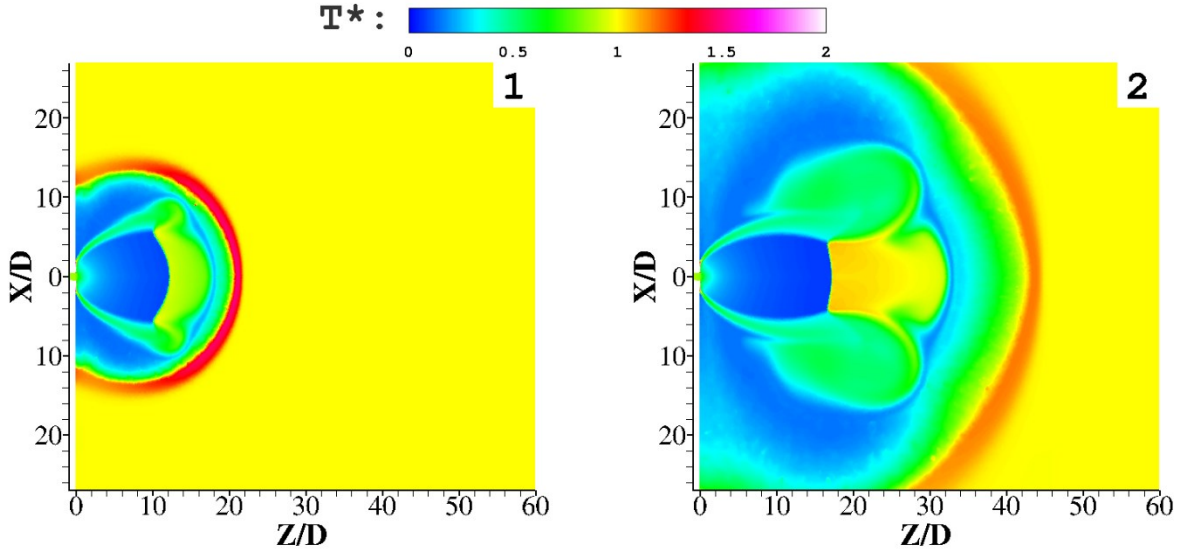

Fig (4. 20): T* of hydrogen jet (70 MPa) release from 1mm orifice: LES simulation 1) 25, 2) 70 microsecond

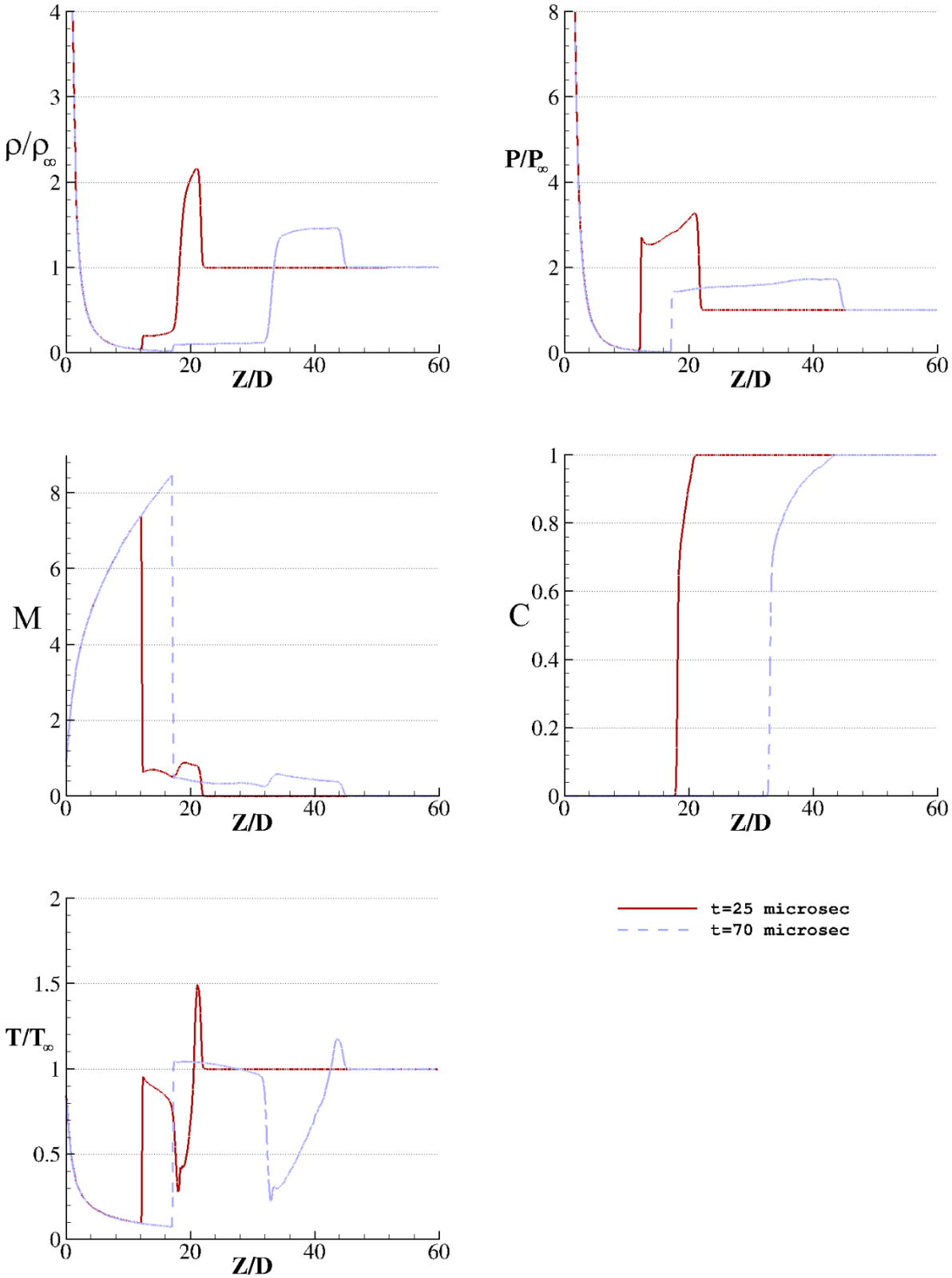

Fig (4. 21): Centerline values of 70 MPa hydrogen jet release from 1mm orifice, LES simulation

Chapter 5

CONCLUSIONS AND FUTURE WORKS

5.1 Conclusions

The turbulence behaviour of highly under expanded hydrogen jet as a real gas is investigated in this research. The novelty of this work is that very high pressure reservoir release with turbulent viscous effects is simulated. An in-house code is developed to simulate this phenomenon with higher order of accuracy while commercial CFD software are incapable to guarantee numerical stability. The LES solver is employed on the compressible code with unstructured tetrahedral Navier-Stokes parallel solver. To minimize the artificial diffusion coming from upwind Roe-MUSCL flux calculation method, a self-adaptive upwinding method was employed. This artificial diffusion amount must be enough to guarantee stability in this high gradient problem while do not adding unrealistic viscosity to the simulation, while the full upwinding method is over-dissipative, preventing sub grid model from delivering the correct LES behavior.

To understand the capability of the developed code, initially, it is used to simulate a subsonic hydrogen jet. In this simulation, the Mach number at the throat is keep around 0.3 and air and hydrogen are assumed to behave as real gases. According to the presented results, good agreement with presented literature [40] is reported, qualitative speaking. The hydrogen cloud radial penetration and vortexes are captured clearly. After that, the turbulence effects reshape the cloud to reach a random shape. The oscillation on concentration of hydrogen is also reported in this simulation. The results showed that the applied turbulence method is working well and the self-adapting upwinding scheme works perfectly with this turbulence scheme.

Furthermore, a 70 MPa hydrogen jet from a 5 mm orifice is simulated by considering viscous effects. To have better insight, the same setup is run for an inviscid flow. In all simulations, hydrogen and air assumed as real gases by applying Abel-Noble equation of state. In the LES simulation, the large number of elements needed on the walls of the release area made it unreasonable to considering no-slip wall boundary condition. Hence, it was decided to assume the interior walls as slip walls. While there is high Reynolds number in that region ($Re_{D=5} = 1.39\times10^{7}$), this assumption can be acceptable. The numerical study shows that in early time the turbulence effects did not affect the hydrogen cloud for 5mm-orifice. There is nevertheless a stronger lead shock and Mach disk in inviscid simulation. In other words, the peak value of Mach number, density and pressure ratio is higher in Euler simulation. Besides, the Euler simulation has bigger hydrogen cloud and has bigger peak temperature in computational field. Hence, it can be concluded that the Euler simulation is more conservative for auto-ignition studies while it shows higher temperature value and bigger amount of hydrogen concentration.

Simulations of the flow release from the 1mm orifice show that the jet developed faster. The maximum temperature and Mach number is smaller in 1 mm orifice in comparison with 5 mm one. In this simulation also, the flow is too convective and the diffusive behaviour did not get the opportunity to appear for the early time of release. The presented results showed that although very fine mesh was employed, it was a course mesh for the LES simulation and finer mesh must be applied for this specific problem.

The presented work demonstrates that the wiggle detector is completely efficient to reduce unnecessary artificial viscosity that is generated from flux calculation. Furthermore, the stability consideration of higher order of accuracy is completely achieved while common commercial CFD tools suffer from this issue.

5.2 Future Work

This subject can be further studied in the following way:

- Since high Reynolds flows can considered as an inviscid flow, it seems that it is affordable to solve Euler equation and ignore viscous in high Reynolds regions. A dynamic coefficient base on resolved medium can be added to control the participation of viscous effects in this case. In other words, a coefficient that can switch the governing equations from Navier-Stokes to Euler one can be provided to reduce computational costs.

- By decreasing the pressure in the reservoir, it could be find out when the viscous/turbulent effects are important in this problem. This is important to identify when the Euler code or the LES code should be used, considering computational cost.
- Based on current results, by applying wall condition the hydrogen cloud will get smaller shape and turbulence effects will have more participation. To have better understanding, it is recommended a fine mesh applied near the walls and no-slip wall condition used for interior walls.
- Sutherland equation has some limitation on temperature. In this simulation there is a small region with high temperature which violate this limitation. But it is better to find out a better correlation to calculate dynamic viscosity. Also, the diffusivity coefficient of hydrogen is strongly depended on temperature and pressure. Although in this work the diffusion term is very small in comparison to convective term, it is recommended that this coefficient is also updated by temperature.

Prandtl number and turbulence Prandtl number are assumed constant in this work. They should be modified to account for the mixture and also considering temperature changes. Prandtl of hydrogen is lower than air.

REFERENCES

[1] Wallace, J. S., “A Comparison of Compressed Hydrogen and CNG Storage”, *International*

Journal Hydrogen Energy, 9(7): 609-611// 1984.

[2] Honda FCX Technical Data: “http://world.honda.com/FuelCell/FCX/tank/”

[3] BMW Hydrogen 7 Technical data: http://www.wired.com/images_blogs/autopia/files/bmw_hydrogen_7.pdf

[4] Schmidt, D., Krause, I I, Schmidtchen, U., “Numerical Simulation of Hydrogen Gas Release Between Buildings”, *International Journal Hydrogen Energy* 24:479-488// 1999.

[5] B. P. Xu, L. El Hima, J. X. Wen, and V. H. Y. Tam, "Numerical study of spontaneous ignition of pressurized hydrogen release into air," *International Journal of Hydrogen Energy,* vol. 34, pp. 5954-5960, 7// 2009.

[6] Wolanski P, Wojcicki S., “Investigation into the mechanism of the diffusion ignition of a combustible gas flowing into an oxidizing atmosphere”, *Proc Combust Inst,* 14:1217e23//1973.

[7] Khaksarfard R , Kameshki M. R., and Paraschivoiu M. , "Numerical simulation of high pressure release and dispersion of hydrogen into air with real gas model," *Shock Waves,* vol. 20, pp. 205-16, 06// 2010.

[8] Pope, S. B., “Ten Questions Concerning the Large-Eddy Simulation of Turbulent Flows”, *New J. of Physics* , Vol. 6, pp. 1-24// 2004

[9] Shirvill LC, Roberts P, Butler CJ, Roberts TA, Royle M., “Characterisation of the hazards from jet releases of hydrogen”, *Proceedings of international conference on hydrogen safety*, Pisa, Italy; Sep 8e10// 2005

[10] F. Ganci, A. Carpignano, N. Mattei, and M. N. Carcassi, "Hydrogen release and atmospheric dispersion: Experimental studies and comparison with parametric simulations," *International Journal of Hydrogen Energy,* vol. 36, pp. 2445-2454, 2// 2011.

[11] E. G. Merilo, M. A. Groethe, J. D. Colton, and S. Chiba, "Experimental study of hydrogen release accidents in a vehicle garage," *International Journal of Hydrogen Energy,* vol. 36, pp. 2436-2444, 2// 2011.

[12] Faris GW, Byer RL. “Tomographic imaging of a supersonic jet”, CLEO ’85. In: Fifth IEEE/OSA conference on lasers and electrooptics. Baltimore, MD, USA; p. 30–1. // 1985

[13] Dillmann A, Wetzel T, Soeller C. “Interferometric measurement and tomography of the density field of supersonic jets”, *Experiments in Fluids* 25(5/6):375–87// 1998.

[14] M. V. Bragin and V. V. Molkov, "Physics of spontaneous ignition of high-pressure hydrogen release and transition to jet fire," *International Journal of Hydrogen Energy,* vol. 36, pp. 2589-2596, 2// 2011.

[15] F. L. Dryer, M. Chaos, Z. Zhao, J. N. Stein, J. Y. Alpert, and C. J. Homer, "Spontaneous ignition of pressurized releases of hydrogen and natural gas into air," *Combustion Science and Technology,* vol. 179, pp. 663-694, 2007.

[16] T. Mogi, K. Dongjoon, H. Shiina, and S. Horiguchi, "Self-ignition and explosion during discharge of high-pressure hydrogen," *Journal of Loss Prevention in the Process Industries,* vol. 21, pp. 199-204, 03/ 2008.

[17] V. V. Golub, D. I. Baklanov, S. V. Golovastov, M. F. Ivanov, I. N. Laskin, A. S. Saveliev*, et al.*, "Mechanisms of high-pressure hydrogen gas self-ignition in tubes," *Journal of Loss Prevention in the Process Industries,* vol. 21, pp. 185-198, 2008.

[18] J. X. Wen, B. P. Xu, and V. H. Y. Tam, "Numerical study on spontaneous ignition of pressurized hydrogen release through a length of tube," *Combustion and Flame,* vol. 156, pp. 2173-2189, 11// 2009.

[19] B. P. Xu, L. El Hima, J. X. Wen, S. Dembele, V. H. Y. Tam, and T. Donchev, "Numerical study on the spontaneous ignition of pressurized hydrogen release through a tube into air," *Journal of Loss Prevention in the Process Industries,* vol. 21, pp. 205-213, 3// 2008.

[20] A. Velikorodny and S. Kudriakov, "Numerical study of the near-field of highly underexpanded turbulent gas jets," *International Journal of Hydrogen Energy,* vol. 37, pp. 17390-17399, 11// 2012.

[21] A. Rona and X. Zhang, "Time accurate numerical study of turbulent supersonic jets," *Journal of Sound and Vibration,* vol. 270, pp. 297-321, 02/06 2004.

[22] F. Péneau, G. Pedro, P. Oshkai, P. Bénard, and N. Djilali, "Transient supersonic release of hydrogen from a high pressure vessel: A computational analysis," *International Journal of Hydrogen Energy,* vol. 34, pp. 5817-5827, 7// 2009.

[23] Cutler, A. D., Diskin, G. S., Drummond, J. P., White, J. A., "Supersonic Coaxial Jet Experiment for Computational Fluid Dynamics Code Validation," AIAA Journal, Vol. 44(3), pp. 585-592//2006.

[24] M. Zbikowski, D. Makarov, and V. Molkov, "LES model of large scale hydrogen–air planar detonations: Verification by the ZND theory," *International Journal of Hydrogen Energy,* vol. 33, pp. 4884-4892, 9// 2008.

[25] W. G. Houf, G. H. Evans, and R. W. Schefer, "Analysis of jet flames and unignited jets from unintended releases of hydrogen," *International Journal of Hydrogen Energy,* vol. 34, pp. 5961-5969, 7// 2009.

[26] J. Zheng, H. Bie, P. Xu, P. Liu, Y. Zhao, H. Chen*, et al.*, "Numerical simulation of high-pressure hydrogen jet flames during bonfire test," *International Journal of Hydrogen Energy,* vol. 37, pp. 783-790, 1// 2012.

[27] Schefer RW, Houf WG, Williams TC, Bourne B, Colton J., "Characterization of high-pressure, underexpanded", hydrogen-jet flames. International Journal of Hydrogen Energy, 32(12):2081e93// 2009.

[28] M. Heitsch, D. Baraldi, and P. Moretto, "Numerical analysis of accidental hydrogen release in a laboratory," *International Journal of Hydrogen Energy,* vol. 35, pp. 4409-4419, 5// 2010.

[29] A. G. Venetsanos, D. Baraldi, P. Adams, P. S. Heggem, and H. Wilkening, "CFD modelling of hydrogen release, dispersion and combustion for automotive scenarios," *Journal of Loss Prevention in the Process Industries,* vol. 21, pp. 162-184, 3// 2008.

[30] S. K. Vudumu and U. O. Koylu, "Detailed simulations of the transient hydrogen mixing, leakage and flammability in air in simple geometries," *International Journal of Hydrogen Energy,* vol. 34, pp. 2824-2833, 3// 2009.

[31] M. F. El-Amin and H. Kanayama, "Boundary layer theory approach to the concentration layer adjacent to the ceiling wall of a hydrogen leakage: Axisymmetric impinging and far regions," *International Journal of Hydrogen Energy,* vol. 34, pp. 1620-1626, 2// 2009.

[32] M. I. Radulescu and C. K. Law, "The transient start of supersonic jets," *Journal of Fluid Mechanics,* vol. 578, pp. 331-369// 2007.

[33] Liu,Y.-F., Tsuboi,N., Sato,H.,Higashino,F.,Hayashi,A.K.: Direct numerical simulation on hydrogen fuel jetting from high pressure tank. 20th International colloquium on the Dynamics of Explosions and Reactive Systems (ICDERS), Montreal, Canada, July 31–August 5, 2005

[34] S. H. Han and D. Chang, "Numerical and experimental study of hydrogen release from a high-pressure vessel," in *2011 2nd International Congress on Computer Applications and Computational Science, CACS 2011, November 15, 2011 - November 17, 2011*, Bali, Indonesia, pp. 489-494// 2012

[35] K. Mohamed and M. Paraschivoiu, "Real gas simulation of hydrogen release from a high-pressure chamber," *International Journal of Hydrogen Energy,* vol. 30, pp. 903-12, 07/ 2005.

[36] Cheng, Z.,Agranat,V., Tchouvelev, A.V. Houf,W., Zhubrin, S.V.: PRD hydrogen release and dispersion; a comparison of CFD results obtained from using ideal and real gas lawproperties. International Conference on Hydrogen Safety, paper 110090, Pisa, Italy, 8–10 September 2005

[37] Andersson, N., Eriksson, L. E., Davidson, L., "Large-Eddy Simulation of Subsonic Turbulent Jets and Their Radiated Sound," *A1AA Journal*, Vol. 43, pp. 1899-1912// 2005.

[38] M. Ciardi, P. Sagaut, M. Klein, and W. N. Dawes, "A dynamic finite volume scheme for large-eddy simulation on unstructured grids," *Journal of Computational Physics,* vol. 210, pp. 632-55, 12/10 2005.

[39] Tajallipour N. , "Large eddy simulations for compressible turbulent jet flows", *PhD thesis*, Concordia University// 2009

[40] B. Chernyavsky, T. C. Wu, F. Peneau, P. Benard, P. Oshkai, and N. Djilali, "Numerical and experimental investigation of buoyant gas release: Application to hydrogen jets," *International Journal of Hydrogen Energy*, vol. 36, pp. 2645-55, 02// 2011.

[41] Wilcox, C. D., "Turbulence modeling for CFD", DCW Industries, Inc., 2nd edition // 1998.

[42] Hydrogen Hazards Assessment Protocol for Components and Systems, National Aeronautics and Space Administration(NASA) https://info.aiaa.org/Standards/PE/HCOS/Shared%20Documents/WSTF-IR-1117-001-08_Hydrogen%20HAP_Current_12-18-08.pdf

[43] Khaksarfard R., "Numerical investigation of hydrogen sonic jet with real gas model", *PhD thesis*, Concordia University// 2011

[44] N. Tajallipour, V. Kumar, and M. Paraschivoiu, "Large-eddy simulation of a compressible free jet flow on unstructured elements," *International Journal of Numerical Methods for Heat and Fluid Flow,* vol. 23, pp. 336-354// 2013